ESA STUDY CONTRACT REPORT

No ESA Study Contract Report will be accepted unless this sheet is inserted at the beginning of each volume of the Report.

ESA CONTRACT No **AO/1-4469/03/NL/SFe**	SUBJECT **BIONICS & SPACE SYSTEMS DESIGN CASE STUDY 1 – MARS WALKER**		CONTRACTOR **UNIVERSITY OF SURREY**
* ESA CR( )No	* STAR CODE	No of volumes 1 This is Volume No 1	CONTRACTOR'S REFERENCE

ABSTRACT:
This document is Case Study 1 Technical Report for the Bionics & Space Systems Design study jointly authored by the University of Surrey (prime), University of Sussex, and EADS Astrium.

It provides a design of a legged robot for Mars Exploration and the investigation into the benefits and detriments of such a system. An out line of the physical design of the vehicle is provided, as well as investigations into the control system and navigation techniques.

Names of authors: Dr. Alex Ellery, Mr. Gregory P. Scott, Dr. Yang Gao, Professor Phil Husbands, Mr. Eric D. Vaughan and Mr. Steven Eckersley.

** NAME OF ESA STUDY MANAGER Dr. Mark Ayre DIV: Advanced Concepts Team DIRECTORATE:	** ESA BUDGET HEADING

This page is left intentionally blank

BIONICS & SPACE SYSTEMS DESIGN
AO/1-4469/03/NL/SFe

Case Study 1
Mars Walker

Version: 3.0

Date: 07 September 2005

Prepared by:

Dr. Alex Ellery and Mr. Gregory P. Scott
Surrey Space Centre
School of Electronics and Physical Sciences
University of Surrey
Guildford
Surrey GU2 7XH
UK
Tel: +44 1483 683882
Fax: +44 1483 689503
Email: a.ellery@surrey.ac.uk

This page is left intentionally blank

List of Contributing Authors

Dr. Alex Ellery Surrey Space Centre School of Electronics and Physical Sciences University of Surrey Guildford Surrey GU2 7XH, UK Tel: +44 1483 683882 Fax: +44 1483 689503 Email: a.ellery@surrey.ac.uk	Mr Gregory P. Scott Surrey Space Centre School of Electronics and Physical Sciences University of Surrey Guildford Surrey GU2 7XH, UK Tel: +44 1483 689278 x3418 Fax: +44 1483 689503 Email: g.scott@surrey.ac.uk
Professor Phil Husbands Department of Infomatics University of Sussex Brighton BN1 9QH, UK Tel: +44 1273 678556 Fax: +44 1273 671320 Email: P.Husbands@sussex.ac.uk	Dr Yang Gao Surrey Space Centre School of Electronics and Physical Sciences University of Surrey Guildford Surrey GU2 7XH, UK Tel: +44 1483 686001 Fax: +44 1483 689503 Email: yang.gao@surrey.ac.uk
Mr Eric D. Vaughan Centre for Computational Neuroscience & Robotics John Maynard Smith Building University of Sussex Brighton BN1 9QG, UK Tel: +44 1273 872949 Fax: +44 1273 678535 Email: E.Vaughan@sussex.ac.uk	Mr. Steven Eckersley Mission Systems Department EADS Astrium Ltd. Gunnels Wood Road Stevenage Hertfordshire SG1 2AS, UK Tel: +44 1438 773301 Email: Steven.ECKERSLEY@astrium.eads.net

List of Applicable Documents

[AD1]	Invitation to Tender	IMT-CTM//SFe/2003.960
[AD2]	Bionics & Space System Design: Statement of Work (Appendix 1)	GSP-03/L27
[AD3]	Draft contract (Appendix 2)	AO/1-4469/03/NL/Sfe
[AD4]	Special Conditions of Tender (Appendix 3)	AO/1-4469/03/NL/Sfe
[AD5]	General Conditions of Tender for ESA Contracts	ESA/C/290 rev 5
[AD6]	Biomimicry – A Review	ESA pdf publication (Mark Ayre)
[AD7]	Bionics & Space Systems Design – Technical Note 1	ESA pdf publication (Alex Ellery)
[AD8]	Bionics & Space Systems Design – Technical Note 2	ESA pdf publication (Mark Ayre)
[AD9]	Bionics & Space Systems Design – Technical Note 3	ESA pdf publication (Alex Ellery)

List of Reference Documents

Allouis, E. (2004). "MarsGen – Mars Terrain Generator" Document KU-MG-DOC-02 V1.0, University of Surrey, Surrey Space Centre, 10 June.

Anderson, J. (1995). *An Introduction to Neural Networks.* The MIT Press, Cambridge, MA.

Apostolopoulos, D. (1996). "Systematic Configuration of Robotic Locomotion." CMU-RI-TR-96-30. The Robotics Institute, Carnegie Mellon University. 26-July.

Apostolopoulos, D. (2001). "Analytical Configuration of Wheeled Robotic Locomotion," Carnegie Melon University, CMU-RI-TR-01-08.

Arvidson, R. *et. al.* (2002). *Journal of Geophysical Research.* **107** (E11): 2.1-2.16.

Ayers, M. (2004). "Thermal Properties of Silica Aerogels", Ernest Orlando Lawrence Berkeley National Laboratory. *http://eande.lbl.gov/ECS/aerogels/satcond.htm.* Viewed: 22 May 2005.

BAE Systems (2002). "RAD6000 Single Board Space Computer in CompactPCI® Form Factor." DoD Release 02-S-1497. June 2002.

BAE Systems (2004). "RAD6000 Space Computers." Publication PUBS-04-C34. August 2004.

Beer, R. D. (1995). "On the dynamics of small continuous-time recurrent neural networks." *Adaptive Behavior* **3**(4):471-511.

Beer, R. D. and Gallagher, J. G. (1992). "Evolving dynamical neural networks for adaptive behavior." *Adaptive Behavior* **1**:92–122.

Beer, R. D., Chiel, H. J., Quinn, R. D., Ritzmann, R. E. (1998). "Biorobotic Approaches to the Study of Motor Systems" *Current Opinion in Neurobiology* **8**(6):777-782.

Beer, R. D., Quinn, R. D., Chiel, H. J., Ritzmann, R. E. (1997) "Biologically Inspired Approaches to Robotics: What can we learn from insects?" *Communications of the ACM*. **40**(3): 31-38.

Beer, R. D., Quinn, R. D., Chiel, H. J., Ritzmann, R. E. (1997). "Biologically Inspired Approaches to Robotics." *Communications of the ACM* **40**:31-38.

Bekker, M. (1959). *Theory of Land Locomotion: Mechanics of Vehicle Mobility.* University of Michigan Press, Ann Arbor, USA.

Bekker, M. (1969). *Introduction to Terrain Vehicle Systems.* University of Michigan Press, Ann Arbor, USA.

Blaesing, B. and Cruse, H. (2004). "Stick insect locomotion in a complex environment: climbing over large gaps." *J. Exp. Biol*. **207**,1273 -128.

Bourke, P. (1997). "Sigmoid Function." *http://astronomy.swin.edu.au/~pbourke/analysis/sigmoid/*

Braitenberg, V. (1984). *Vehicles: Experiments in Synthetic Psychology*, MIT Press.

Brooks, R. (1990). "Elephants don't play chess." *Robotics & Autonomous Systems.* **6**: 3-15

Bucher, D., Akay, T., DiCaprio, R. A., Buschges, A. (2003) "Interjoint Coordination in the Stick Insect Leg-Control System: The Role of Positional Signaling" *Journal of Neurophysiology* **89**:1245-1255.

Burnham, R. (2004). "Spirit hits the jackpot." Astronomy Magazine: *http://www.astronomy.com/asy/default.aspx?c=a&id=2253*. 25 June 2004.

Canadian Press (2005). "New plastic can better convert solar energy." *http://www.ctv.ca/servlet/ArticleNews/story/CTVNews/1105319242587_49?hub=SciTech*. 09-Jan-05. Viewed: 16-Feb-05

Carrier, W. (1991). "Physical properties of the lunar surface," In *Lunar Sourcebook*, ed. Heiken, G. *et. al.*, Cambridge University Press, Cambridge, UK, pp. 522-530.

Chiel, H.J. and Beer, R.D. (1997). "The brain has a body: Adaptive behavior emerges from interactions of nervous system, body and environment." *Trends in Neurosciences* **20**:553-557.

Cliff, D. T., Harvey, I., and Husbands, P. (1993). "Explorations in Evolutionary Robotics." *Adaptive Behaviour* **2(1)**, 71-108.

Collett, M. and Collett, T. (2000). "How do insects use path integration for their navigation?" *Biol Cybern*. **83**(3):245-259.

Collett, M., Collett, T. S., Bisch, S., and Wehner, R. (1998). "Local and global vectors in desert ant navigation." *Nature*, **394**:269-272.

Cornell (2004). "Mars Exploration Rovers – About the MER PanCam." *The Caves of Mars Project.* NIAC Phase II Grant from NASA Institute for Advanced Concepts.

Cruse, H., Dean, J., Durr, V., Kindermann, Th., Schmitz, J., Schumm, M. (2002) "A Decentralized, Biologically Based Network for Autonomous Control of (Hexapod) Walking" In *Neurotechnology for Biomimetic Robots* (ed. Ayers J, Davis J, Rudolph A), Bradford Books, MIT Press, Cambridge, MA, USA, 383-400

Cruse, H., Dean, J., Durr, V., Kindermann, Th., Schmitz, J., Schumm, M. (2000). "Control of Hexapod Walking – A Decentralized Solution Based on Biological Data" *RTO AVT Symposium on Unmanned Vehicles (UV) for Aerial, Ground and Naval Military Operations*. 9-13 October. Ankara, Turkey.

Cruse, H., Schmitz, J., Braun, U., and Schweins, A. (1993). "Control of body height in a stick insect walking on a treadwheel." *J. Exp. Biol*. **181**:141–155

de Garis, H. (1990). "Genetic programming: Evolution of time dependent neural network modules which teach a pair of stick legs to walk." In *Proc. 9th. Eur. Conf. Artificial Intelligence*, Stockholm, Sweden, pp.204–206

Di Natale C., Salimbeni D., Paolesse R., Macagnano A. & D'Amico A. (2000) "Porphryins-based opto-electronic nose for volatile compounds detection" *Sensors & Actuators* **B65:** 220-226

Dickenson, M. H., Farley, C. T., Full, R. J., Koehl, M. A. R., Kram, R., Lehman, S. (2000) How Animals Move: An Integrative View. *Science*. **288**:100-106. 7 April.

Ellery, A. (2000). *An Introduction to Space Robotics.* Praxis Publishing, Chichester.

Ellery, A. (2002). "Vanguard: a new development in experimental astrobiology." UK Astrobiology. April. **43**:2.22-2.24.

Ellery, A. (2004a). "Environment-robot interaction – the basis for mobility in planetary micro-rovers." *Robotics and Autonomous Systems*. Accepted for publication: 12-August-04.

Ellery, A. (2004b). "An engineering approach to the dynamic control of space robotic on-orbit servicers." *Proceedings of the Institution of Mechanical Engineers Part G: Journal of Aerospace Engineering*. **218**.

ESA/ESTEC (2003). "ESA Technology Tree Document: Harmonisation and Strategy." Document IMT-THS/4760/MG/EW/ap. Issue 1, Revision 1. June 2003.

Espenschied, K.S., Quinn, R.D., Beer, R.D. and Chiel, H.J. (1996). "Biologically-based distributed control and local reflexes improve rough terrain locomotion in a hexapod robot." *Robotics and Autonomous Systems*. **18**(1-2): 59-64

Ferrell, C. (1995). "A comparison of three insect-inspired locomotion controllers." *Robotics and Autonomous Systems* **16**(2-4): 135-159.

Fielding, J. (2005). "Massiva: Mars Surface Sampling and Imaging VTOL Aircraft." PhD Thesis. University of Surrey.

Fordahl, M. (2004). "Software on Mars rovers 'space qualified'." *SecurityFocus*. The Associated Press. 23-Jan-04.

Fortescue, P. and Stark, J. (1995). *Spacecraft Systems Engineering*. 2nd Edition. Wiley Publishing

Freund, M. S., Lewis, N. S. (1995). "A Chemically Diverse Conducting Polymer-Based Electronic Nose." *Proc. Natl. Acad. Sci.* U.S.A. **92**: 2652.

Fujiwara, C. (2004). "Metal matrix composites for aerospace structures." In *Metal and Ceramic Matrix Composites*. Eds. Cantor, B., Dunne, F. P. E., Stone, I. C. IOP Publishing Ltd. 52-65.

Gallagher, J., Beer, R., Espenschiel, K., and Quinn, R. (1996). "Application of evolved locomotion controllers to a hexapod robotl." *Robot. Autonomous Syst.*, vol. 19, no. 1, pp. 95–103.

Galt, S., Luk, B. L. and Collie, A. A. (1997). "Evolution of Smooth and Efficient Walking Motions for an 8-Legged Robot." *Proceedings of the 6th European Workshop on Learning Robots.* Brighton, UK.

Golombek, M., and Rapp, D. (1997). "Size-Frequency Distributions of Rocks on Mars and Earth Analog Sites: Implications for Future Landed Missions," *Journal of Geophysics Research.* **102:**3967-3988.

Gomi, T., and Ide, K. (1997). "Emergence of gaits of a legged robot by collaboration through evolution." in *Proceedings of the International Symposium on Artificial Life and Robotics*. Berlin, Germany: Springer-Verlag.

Goodall, K. (2005). "Mars Global Surveyor." *http://mars4.jpl.nasa.gov/mgs/*. Viewed: 01 April 2005.

Gruau, F. (1995). "Automatic definition of modular neural networks." *Adaptive Behavior*. **3(2)**: 151-183.

Gruau, F. and Quatramaran, K. (1997). "Cellular Encoding for Interactive Evolutionary Robotics." In P. Husbands and I. Harvey (Eds.). Fourth European Conference on Artificial Life. The MIT Press/Bradford Books.

Hamilton, C. J. (2001a). "Chronology of Space Exploration." *http://www.solarviews.com/eng/mars.htm*. Viewed: 01 April 2005.

Hamilton, C. J. (2001b) "Project Viking Fact Sheet." *http://www.solarviews.com/eng/vikingfs.htm*. Viewed: 01 April 2005.

Hamilton, C. J. (2003). "View from Lander 2" *http://www.solarviews.com/cap/mars/vlfmos21.htm*. Viewed: 01 April 2005.

Haskin, L. *et. al.*(1997). *Journal of Geophysical Research* **102**:19,293-19,306.

HD Systems (2005). "Mars Rover to Earth: 'Where to now?'" *http://www.machinedesign.com/ASP/strArticleID/56430/strSite/MDSite/viewSelectedArticle.asp*. Viewed: 17 Apr 2005.

Hopfield, J. (1984). "Neurons with graded response have collective computational properties like those of two-state neurons." *Proceedings of the National Academy of Sciences of the USA*, 81:3088 – 3092

Husbands, P. (1994). "Distributed coevolutionary genetic algorithms for multi-criteria and multi-constraint optimisation." In Fogarty, T., editor, *Evolutionary Computing, AISB Workshop Selected Papers*, volume 865 (LNCS), pages 150–165. Springer-Verlag.

Husbands, P. and Harvey, I. (1992). "Evolution versus design: controlling autonomous mobile robots." *Proc. 3rd IEEE Annual Conf. on Artificial Intelligence, Simulation and Planning in High Autonomy Systems*. IEEE Computer Society Press, Los Alimitos, CA, Pp.139-146.

Israel, E. *et. al.* (1997). *Journal of Geophysical Research (Planets)* **102**(D23)**:** 28,705-28,716.

Jakobi, N. (1998a). *Minimal Simulations for Evolutionary Robotics*. PhD thesis, University of Sussex, U.K.

Jakobi, N. (1998b). "Running across the reality gap: Octopod locomotion evolved in a minimal simulation." in *Evolutionary Robotics*, P. Husbands and J.Meyer, Eds. Berlin, Germany: Springer-Verlag, LNCS **1468**.

JPL D-11509 (1996). "Mars Global Surveyor Spacecraft Requirements." Revision A. 10 September 1996.

JPL Image Gallery (2005). "ENose Sensor" *http://technology.jpl.nasa.gov/gallery/index.cfm?page=imageDetail&ItemID=143&catId=8*. Visited: 13-April-2005.

Judd, S. P. D. and Collett, T. S. (1998). "Multiple stored views and landmark guidance in ants." *Nature*, **392**:710-714.

Kieffer, H. H., Jakosky, B. M., Snyder, C. W., Matthews, M. S. eds. (1992) *Mars.* The University of Arizona Press.

Kirchner, F., Spenneberg, D., Linnemann, R. (2002) "A Biologically Inspired Approach Toward Robust Real-World Locomotion in Legged Robots" In *Neurotechnology for Biomimetic Robots* (ed. Ayers J, Davis J, Rudolph A), Bradford Books, MIT Press, Cambridge, MA, USA. 419-448.

Klein, C. A. and Kittivatcharapong, S. (1990). "Optimal Force Distribution for the Legs of a Walking Machine with Friction Cone Constraints." *IEEE Transactions on Robotics and Automation*. **6**(1):73-85.

Kodjabachian, J. and Meyer, J. A. (1998). "Evolution and development of neural networks controlling locomotion, gradient following and obstacle avoidance in artificial insects." *IEEE Trans. Neural Networks*, **9**:796–812.

Kolb, C. *et. al.* (2002). Proc 2nd European Workshop on Exo/Astro-Biology (SP-518), Graz, Austria, 181-184.

Lambrinos D., Möller R., Labhart T., Pfeifer R., Wehner R. (2000). "A mobile robot employing insect strategies for navigation." *Robotics and Autonomous Systems*, **30**:39-64.

Landis, G. A. (1998). "Mars Dust Removal." *AIAA Journal of Propulsion and Power.* **14**(1): 126-128., January.

Landis, G. A., Kerslake, T. W., Jenkins, P.P., Scheiman, D. A. (2004). "Mars Solar Power." *Second International Energy Conversion Engineering Conference*. 16-19 August, AIAA-2004-5555

Lang H. *et. al.* (1999) "Artificial nose based on a micromechanical cantilever array" *Anal Chimica Acta* **393**: 59-65

Lang, H. P., Berger, R., Battiston, F., Ramseyer, J.-P., Meyer, E., Andreoli, C., Brugger, J., Vettiger, P., Despont, M., Mezzacasa, T., Scandella, L., Güntherodt, H.-J., Gerber, Ch. and Gimzewski, J. K. (1998). "A chemical sensor based on a micromechanical cantilever array for the identification of gases and vapors." *Appl. Phys. A*. **66**: S61-S64.

Laszlo, J. F., van de Panne, M., Fiume, E. (1996). "Limit cycle control and its application to the animation of balancing and walking." In *Proc. Int. Conf. Computer Graphics and Interactive Techniques (SIGGRAPH)*, pp. 155–162.

Le, A. T. (1999). Modelling and Control of Tracked Vehicles. PhD Thesis. Department of Mechanical and Mechatronic Engineering. The University of Sydney. 26 January.

Lewis, M. A., Fagg, A. H., Bekey, G. (1994). "Genetic Algorithms for Gait Synthesis in a Hexapod Robot." in Zheng, ed. *Recent Trends in Mobile Robots,* pp. 317-331,

Lewis, M. A., Fagg, A. H., Solidum, A. (1992). "Genetic Programming Approach to the Construction of a Neural Network for Control of a Walking Robot." in *Proceedings of the 1992 IEEE International Conference on Robotics and Automation.* Nice France, pp. 2618-23.

Lombry, T. (2005) "Space Communications with Mars." *http://www.astrosurf.org/lombry/qsl-mars-communication3.htm*. Viewed: 20 Apr 2005.

Lonergan, M. C., Severin, E. J., Doleman, B., J., Grubbs, R. H., Lewis, N. S. (1996). "Array-Based Sensing with Carbon-Polymer Composites." *Chem. Mater.* **8**: 2298.

Lou, X. Y. (2003). "Chapter 5: Flying and Swimming" *MEC407 – Fundamental Biomechanics.* The University of Sheffield, Department of Mechanical Engineering.

Lundstrom, I. and Petersson L. G. (1996). *Journal of Vacuum Science and Technology A.* **14**(3): 1539.

Maas, D. (2004). "Anatomy of a Rover." *http://www.pbs.org/wgbh/nova/mars/rove-nf.html*. Cornell University, NASA, JPL. Dec. 2005.

Mathayomchan, B. and Beer, R.D. (2002). "Center-crossing recurrent neural networks for the evolution of rhythmic behavior." *Neural Computation* **14**:2043-2051.

maxon motor uk ltd (2004). "High Precision Drives and Systems." maxon motor 2004/05 Product Catalogue. Finchampstead, GB-Berkshire.

McDonald, S. A., Konstantatos, G., Shiguo, Z., Cyr, P. W., Klem, E. J. D., Levina, L., Sargent, E. H. (2005) "Solution-processed PbS quantum dot infrared photodetectors and photovoltaics" *Nature* Materials. , vol. 4, no. 2, pp. 138-142, Feb. 2005

McGeer, T. (1990). "Passive walking with knees." *In Proceedings of the IEEE Conference on Robotics and Automation,* volume 2, pages 1640–1645.

McHale, G., and Husbands, P. (2004a) "Quadrupedal locomotion: GasNets, CTRNNs and Hybrid CTRNN/PNNs compared." in J. Pollack *et. al.* (Eds*), Proc. Alife IX*, MIT Press, 106-112.

McHale, G., and Husbands, P. (2004b). "GasNets and other evovalble neural networks applied to bipedal locomotion." in S. Schaal *et. al.* (Eds), *Proc. From Animals to Animats 8: Proceedings of the Eigth International Conference on Simulation of Adaptive Behaviour (SAB'2004),* MIT Press, 163-172.

Merriam-Webster (2005). *Merriam-Webster's Collegiate® Dictionary*, Tenth Edition.

Michalewicz, Z. and Fogel, D. B. (2004). *How to Solve It: Modern Heuristics (2nd ed)*. Springer Verlag.

MicroMo Electronics (2005). "Motor Calculations." *MicroMo Electronics Technical Library: http://www.micromo.com/notestutorials/*. Viewed: 13 April 2005.

Montero, J. N. (2002). "Wireless Networking and Its Impact in Computing Now and in the Future." Bowie State University.

Nolfi, S. and Floreano, D. (2000). *Evolutionary Robotics: The Biology, Intelligence and Technology of Self-Organizing Machines*. MIT Press, Cambridge, Massachusetts.

Ojeda, L., Borenstein, J., Witus, G. (2005). "Terrain Trafficability Characterization with a Mobile Robot." Proc. of the SPIE Defense and Security Conference, Unmanned Ground Vehicle Technology VII, Orlando, FL, 28 March to 01 April.

Parnell, J., Mazzini, A., Honghan, C. (2002). "Fluid Inclusion Studies of Chemosynthetic Carbonates: Strategy for Seeking Life on Mars" *Astrobiology* **2**(1): 43-57.

Patel, N., Scott, G. P., Ellery, A. (2004). "Application of Bekker Theory for Planetary Exploration through Wheeled, Tracked and Legged Vehicle Locomotion." AIAA-2004-6091. Space 2004 Conference and Exhibit. San Diego, California. 28-30-September.

Pearce T (1997a) "Computational parallels between the biological olfactory pathway and its analogue 'the electronic nose': part I. Biological olfaction" *Biosystems* **41**: 43-67

Pearce T (1997b) "Computational parallels between the biological olfactory pathway and its analogue 'the electronic nose': part II. Sensor-based machine olfaction" *Biosystems* **41:** 69-90

Pearce, T. C. *et. al.* (2002). Handbook of Machine Olfaction: Electronic Nose Technology, Wiley-VCH, Weinheim.

Planetary Society (2005). "Mars Exploration Rover Mission." http://*www.planetary.org/mars/mer.html*. Viewed: 20 Apr 2005.

Pratt, J. and Pratt, G. (1999). "Exploiting natural dynamics in the control of a 3d bipedal walking simulation." in *Proceedings of the International Conference on Climbing and Walking Robots (CLAWAR99), Portsmouth, UK*.

PSL Electromagnetics (2005). Product Catalog. Physical Science Laboratory, New Mexico State University. Published: 24-March.

Rawal, S. (2001). "Metal-Matrix Composites for Space Applications." *Journal of Materials*. **53**(4): 14-17.

Reil, T., and Husbands, P. (2002). Evolution of Central pattern Generators for Bipedal Walking in Real-time Physics Environments, *IEEE Trans. Evolutionary Computation 6*(2):10-21.

Richter, L. (2003). *Private communication*.

Ryan, M. A., Homer, M. L., Zhou, H., Manatt, K. and Manfreda, A. (2001). "Toward A Second Generation Electronic Nose at JPL: Sensing Film Optimization Studies." Jet Propulsion Laboratory, California Institute of Technology. *Society of Automotive Engineers.* 2001-01-2308.

Ryan, M. A., Shevade, A. V., Zhou, H., Horner, M. L. (2004). "Polymer-Carbon Black Composite Sensors in an Electronic Nose for Air-Quality Monitoring." *Materials Research Society Bulletin*. October 2004. p. 714-719.

Shedd, W. (2001). "Space Electronics the Radiation Hardened Way." Air Force Research Lab. Reference Document: VS-00-13. September 2001.

Slocum, K. R., Surdu, J. R., Sullivan, J., Rudak, M., Colvin, N., Gates, C. (2003). "Trafficability Analysis Engine." CrossTalk: The Journal of Defense Software Engineering. June 2003. p.28-30.

Smith, R. (2003). "The open dynamics engine user guide." http://opende.sourceforge.net/.

Spectrolab (2002). "26.8% Improved Triple Junction (ITJ) Solar Cells." Spectrolab: Photovoltaic Products. Sylmar, CA, USA. 08 May 2002.

Srinivasan, M. (1998). "Ants match as they march." *Nature*, **392**:660-661.

Srinivasan, M. V., Zhang, S. W., and Bidwell, N. J. (1997). "Visually mediated odometry in honeybees." *Journal of Experimental Biology*, **200**:2513-2522.

Stride, S. (1998). "Frequently Asked Questions." *http://mars.sgi.com/rovercom/rovfaq.html* Viewed: 15 Apr 2005.

Strom, R. G. (2002) "Ancient Oceans and Ice Sheets on Mars." *Science on the Frontiers*. The Research Corporation

Stumpf, M. (2003). "Wind River and NASA – Embedded Development for the Extreme Demands of Space Exploration." Dedicated Systems Magazine. pp. 25-27.

Tarcea, N. *et. al.* (2002). Proc 2nd European Workshop on Exo/Astro-Biology (ESA SP 518), Graz, Austria, 399-402.

Thakoor, S. (2003). "Bio-Inspired Engineering of Exploration Systems." *NASA Tech Briefs: NPO-21142*. May.

US Department of Energy (1998). "Department of Energy Facts: Radioisotope Heater Units (RHUs)." Office of Space and Defence Power Systems. December.

Vaughan, E., Di Paolo, E. A. and Harvey, I., (2004b). "The Tango of a Load Balancing Biped." in *Proceedings of the Seventh International Conference on Climbing and Walking Robots, CLAWAR,* Madrid. Springer-Verlag.

Vaughan, E., Di Paolo, E. A., and Harvey, I. (2004a). "The Evolution of Control and Adaptation in a 3D Powered Passive Dynamic Walker." in J. Pollack *et. al.* (Eds.), *Proceedings of the Ninth International Conference on the Simulation and Synthesis of Living Systems, Artificial Life IX*, 139-145, MIT Press.

Vickerstaff, R. (2003). "First Steps in Evolving Path Integration in Simulation." in Banzhaf, W., Christaller, T., Dittrich, P., Kim, J.T. and Ziegler, J., editors, *7th European Conference on Artificial Life (ECAL 2003)*, pages 209-216. Springer-Verlag, Heidelberg.

Vickerstaff, R. J., and Di Paolo, E. A., (Forthcoming). Building neural models of path integration using artificial evolution. *Journal of Experimental Biology*.

Viking Imaging Team (1978). *The Martian Landscape.* NASA SP-425. Washington, D.C.

Viotti, M. (2005). "Mars Exploration Rover Mission." http://marsrovers.jpl.nasa.gov/home/index.html. Viewed: Mar-Apr.

Wang, A. *et. al.* (2003) *Journal of Geophysical Research* **108** (E1): 5.1-5.18.

Webster, G. (2005). "Mars Reconnaissance Orbiter Mission Status." JPL News Release: 2005-006. Jet Propulsion Laboratory, Pasadena, CA, USA. 07 January 2005.

Wendler, G. (2002) "The Organization of Insect Locomotion Systems and Computer-Based Flight Control in the Tobacco Hawkmoth *Manduca sexta*" In *Neurotechnology for Biomimetic Robots* (ed. Ayers J, Davis J, Rudolph A), Bradford Books, MIT Press, Cambridge, MA, USA. 451-468.

Whittaker, W. (1997) "Icebreaker: A Lunar south Pole Exploring Robot." The Robotics Institute, Carnegie Mellon University. Document: CMU-RI-TR-97-22.

Wilcox, B. *et. al.* (1998). "A Nanorover for Mars." *Space Technology*. **17**(3/4):163-172.

Wolff, S. (2005). "Deep Space Network." http://deepspace.jpl.nasa.gov/dsn/. Viewed: 28-April 2005.

Wong, J. Y. (1989). *Theory of Ground Vehicles*. Wiley, New York, second edition.

Wynn-Williams, D. and Edwards, H. (2000). "Proximal Analysis of Regolith Habitats and Protective Biomolecules in Situ by Laser Raman Spectroscopy: Overview of Terrestrial Antarctic Habitats and Mars Analogs." *Icarus* **144**(2): 486-503.

Yardney Technical Products (2004). Lithion Standard Cell Product Line. *http://www.yardney.com/lithion/*. Viewed: 25-April-05.

Ziegler, C. *et. al.* (1998). "Bioelectronic noses: a status report. Part II" *Biosensors & Bioelectronics* **13**: 539-571

List of Acronyms, Abbreviations, and Terminology

ACT	Advanced Concepts Team
AI	artificial intelligence
AO	announcement of opportunity
AOCS	attitude and orbit control system
BAS	British Antarctic Survey
CBNT	Centre for Biomimetic & Natural Technologies
CCNR	Centre for Computational Neuroscience & Robotics
CDH	command and data handling
EDLS	Entry, Descent, and Landing System
EPFL	Ecole Polytechnique Federale Lausanne
ESTEC	European Space Research & Technology Centre
GOFAI	good old fashioned AI
ITT	invitation to tender
OBDH	onboard data handling
PI	principal investigator
PM	project manager
PRR	preliminary requirements review
SMP	study management plan
SoW	statement of work
SSC	Surrey Space Centre
SSTL	Surrey Satellite Technology, Ltd
TBC	to be confirmed (by the Agency)
TBD	to be determined (by the contractor)
TBS	to be specified (by the Agency)
TN	technical note
TT&C	tracking telemetry and command
WP	work package
WS	workshop

List of Figures

List of Tables

Table of Contents

I. INTRODUCTION AND HISTORY

1. INTRODUCTION

The goal of this project was to design a viable Mars explorer with biomimetic inspiration. The vehicle must have the capability to transport a payload that can aid in the search for life on another planet, as well as the capability to provide proof of biomimetic methods in physical and control system design.

The University of Surrey was focused on the biomimetic vehicle design, while the University of Sussex developed a bioinspired autonomous, learning control system. EADS Astrium provided insight to the system budgets developed at the University of Surrey.

2. MARS CHARACTERISTICS

Mars is the closest terrestrial analogue in the solar system and this makes it of considerable geological, geochemical and geophysical interest. Furthermore, the possibility that life may have emerged on Mars during earlier epochs makes Mars a prime target (in line with the Aurora programme) [Ellery *et. al.* 2002]. After Beagle 2, several Aurora missions will target Mars, including ExoMars and Mars Sample Return (MSR) missions. The Mars environment impacts explorer design in several ways.

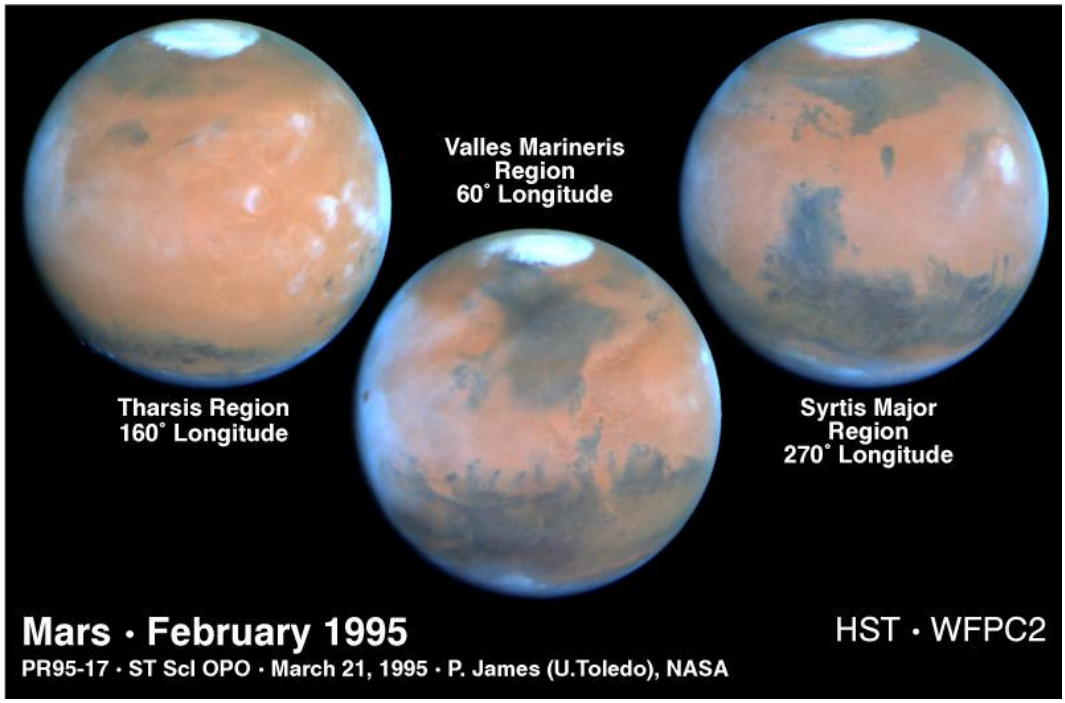

Figure 1 – Mars From All Sides [Hamilton 2001b].

Table 1 – Mars Characteristics [Hamilton 2001b; Kieffer 1992]

Property	Value	Units
Mass	6.42E+23	(kg)
Mass (Earth = 1)	0.10745	
Equatorial radius	3397.2	(km)
Equatorial radius (Earth = 1)	0.53264	
Mean density	3.94	(gm/cm^3)
Mean distance from the Sun	227,940,000	(km)
Mean distance from the Sun (Earth = 1)	1.5237	(AU)
Rotational period	24.6229	(hours)
Rotational period	1.025957	(days)
Orbital period	686.98	(days)
Mean orbital velocity	24.13	(km/sec)
Orbital eccentricity	0.0934	
Tilt of axis	25.19	(degrees)
Orbital inclination	1.85	(degrees)
Equatorial surface gravity	3.72	(m/sec^2)
Equatorial escape velocity	5.02	(km/sec)
Visual geometric albedo	0.15	
Magnitude	-2.01	(Vo)
Minimum surface temperature	-140	(°C)
Mean surface temperature	-63	(°C)
Maximum surface temperature	20	(°C)
Atmospheric pressure	0.007	(bars)
Atmospheric Composition:		
Carbon Dioxide (CO_2)	95.32%	
Nitrogen (N_2)	2.7%	
Argon (Ar)	1.6%	
Oxygen (O_2)	0.13%	
Carbon Monoxide (CO)	0.07%	
Water (H_2O)	0.03%	
Neon (Ne)	0.00025%	
Krypton (Kr)	0.00003%	
Xenon (Xe)	0.000008%	
Ozone (O_3)	0.000003%	

Localised regions of the Martian surface are reasonably well characterised from Viking Lander 1 and 2 and Pathfinder landing sites. The Mars Exploration Rovers (MERs), Spirit and Opportunity, are helping to provide more detail of the surface structure through their search for extraterrestrial life. Mars has a number of different types of soil (drift, crusty-to-cloddy, blocky and rock), which have been measured in terms of soil cohesion and friction angles. There is no data on Martian soil deformation parameters but these can be taken from the German Aerospace Centre (DLR) Mars soil simulant [Richter 2003] or lunar data. This

environment proves to be quite diverse across the surface, requiring the rover to autonomously navigate around obstacles, without the benefit of human intervention or real-time control. Table 1 above shows some of the common properties of Mars; including orbital, atmospheric and surface data while Section III.1 discusses soil properties of different Mars, Lunar, and simulated surfaces.

3. BRIEF HISTORY OF MARS SURFACE EXPLORATION

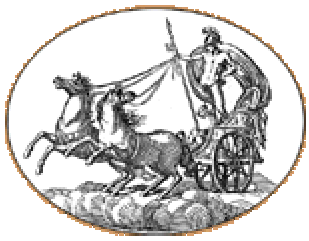

Mars has been of interest to those on Earth for over 1500 years. Babylonian astronomers have made careful observations of the Red Planet dating back as early as 400 BC. The Egyptians were the first to notice the 5 brighter "stars" in the sky that moved differently from the other stars. Mars was given the name Har Decher, Egyptian for The Red One. The Greeks and Romans later named it after their gods of war, Ares and Mars, respectively [Hamilton 2001a].

But more recently, there have been many mission sent by several countries around the world to explore Mars. A brief history of these missions, both successful and unsuccessful, are listed below [Hamilton 2001a]:

Mars 1960A – USSR Mars Probe (October 10, 1960)

Failed to reach Earth orbit.

Mars 1960B – USSR Mars Probe (October 14, 1960)

Failed to reach Earth orbit.

Mars 1962A – USSR Mars Flyby (October 24, 1962)

Spacecraft failed to leave Earth orbit after the final rocket stage exploded.

Mars 1 – USSR Mars Flyby – 893 kg (November 1, 1962)

Communications failed en route.

Mars 1962B – USSR Mars Lander (November 4, 1962)

Failed to leave Earth orbit.

Mariner 3 – USA Mars Flyby – 260 kg (November 5, 1964)

Mars flyby attempt. Solar panels did not open, preventing flyby. Mariner 3 is now in a solar orbit.

Mariner 4 – USA Mars Flyby – 260 kg (November 28, 1964 – December 20, 1967)

Mariner 4 arrived at Mars on July 14, 1965 and passed within 9,920 kilometres of the planet's surface. It returned 22 close-up photos showing a cratered surface. The thin

atmosphere was confirmed to be composed of carbon dioxide in the range of 5-10 mbar. A small intrinsic magnetic field was detected. Mariner 4 is now in a solar orbit.

Zond 2 – USSR Mars Flyby (November 30, 1964)

Contact was lost en route.

Mariner 6 – USA Mars Flyby – 412 kg (February 24, 1969)

Mariner 6 arrived at Mars on February 24, 1969, and passed within 3,437 kilometres of the planet's equatorial region. Mariner 6 and 7 took measurements of the surface and atmospheric temperature, surface molecular composition, and pressure of the atmosphere. In addition, over 200 pictures were taken. Mariner 6 is now in a solar orbit.

Mariner 7 – USA Mars Flyby – 412 kg (March 27, 1969)

Mariner 7 arrived at Mars on August 5, 1969, and passed within 3,551 kilometres of the planet's south pole region. Mariner 6 and 7 took measurements of the surface and atmospheric temperature, surface molecular composition, and pressure of the atmosphere. In addition, over 200 pictures were taken. Mariner 7 is now in a solar orbit.

Mariner 8 – USA Mars Flyby (May 8, 1971)

Failed to reach Earth orbit.

Kosmos 419 – USSR Mars Probe (May 10, 1971)

Failed to leave Earth orbit.

Mars 2 – USSR Mars Orbiter/Soft Lander – 4,650 kg (May 19, 1971)

The Mars 2 lander was released from the orbiter on November 27, 1971. It crashed-landed because its breaking rockets failed - no data was returned and the first human artifact was created on Mars. The orbiter returned data until 1972.

Mars 3 – USSR Mars Orbiter/Soft Lander – 4,643 kg (May 28, 1971)

Mars 3 arrived at Mars on December 2, 1971. The lander was released and became the first successful landing on Mars. It failed after relaying 20 seconds of video data to the orbiter. The Mars 3 orbiter returned data until August, 1972. It made measurements of surface temperature and atmospheric composition.

Mariner 9 – USA Mars Orbiter – 974 kg (May 30, 1971 – 1972)

Mariner 9 arrived at Mars on November 3, 1971 and was placed into orbit on November 24. This was the first US spacecraft to enter an orbit around a planet other than the Moon. At the time of its arrival a huge dust storm was in progress on the planet. Many of the scientific experiments were delayed until the storm had subsided. The first hi-resolution images of the moons Phobos and Deimos were taken. River and channel like features were discovered. Mariner 9 is still in Martian orbit.

Mars 4 – USSR Mars Orbiter – 4,650 kg (July 21, 1973)

Mars 4 arrived at Mars on February, 1974, but failed to go into orbit due to a malfunction of its breaking engine. It flew past the planet with in 2,200 kilometres of the surface. It returned some images and data.

Mars 5 – USSR Mars Orbiter – 4,650 kg (July 25, 1973)

Mars 5 entered into orbit around Mars on February 12, 1974. It acquired imaging data for the Mars 6 and 7 missions.

Mars 6 – USSR Mars Orbiter/Soft Lander – 4,650 kg (August 5, 1973)

On March 12, 1974, Mars 6 entered into orbit and launched its lander. The lander returned atmospheric descent data, but failed on its way down.

Mars 7 – USSR Mars Orbiter/Soft Lander – 4,650 kg (August 9, 1973)

On March 6, 1974, Mars 7 failed to go into orbit about Mars and the lander missed the planet. Carrier and lander are now in a solar orbit.

Viking 1 – USA Mars Orbiter/Lander – 3,399 kg (August 20, 1975 – August 7, 1980)

Viking 1 and 2 were designed after the Mariner spacecraft. They consisted of an orbiter and lander. The orbiter weighed 900 kg and the lander 600 kg. Viking 1 went into orbit about Mars on June 19, 1976. The lander touched down on July 20, 1976 on the western slopes of Chryse Planitia. Both landers had experiments to search for Martian micro-organism. The results of these experiments are still being debated. The landers provided detailed colour panoramic views of the Martian terrain. They also monitored the Martian weather. The orbiters mapped the planet's surface, acquiring over 52,000 images. Viking 1 orbiter was deactivate on August 7, 1980 when it ran out of altitude-control propellant. Viking 1 lander was accidentally shut down on November 13, 1982, and communication was never regained.

Viking 2 – USA Mars Orbiter/Lander – 3,399 kg (September 9, 1975 – July 25, 1978)

Viking 1 and 2 were designed after the Mariner spacecraft. They consisted of an orbiter and lander. The orbiter weighed 900 kg and the lander 600 kg. Viking 2 went into orbit about Mars on July 24, 1976. The lander touched down on August 7, 1976 at Utopia Planitia. Both landers had experiments to search for Martian micro-organism. The results of these experiments are still being debated. The landers provided detailed colour panoramic views of the Martian terrain. They also monitored the Martian weather. The orbiters mapped the planet's surface, acquiring over 52,000 images. Viking 2 orbiter was deactivate on July 25, 1978 when it ran out of altitude-control propellant. Viking 2 lander used Viking 1 orbiter as a communications relay, and had to be shut down at the same time as the orbiter on August 7, 1980.

Phobos 1 – USSR Mars Orbiter/Lander – 5,000 kg (July 7, 1988)

Phobos 1 was sent to investigate the Martian moon Phobos. It was lost en route to Mars through a command error on September 2, 1988.

Phobos 2 – USSR Phobos Flyby/Lander – 5,000 kg (July 12, 1988)

Phobos 2 arrived at Mars and was inserted into orbit on January 30, 1989. The orbiter moved within 800 kilometres of Phobos and then failed. The lander never made it to Phobos.

Mars Observer – USA Mars Orbiter (September 25, 1992)

Communication was lost with Mars Observer on August 21, 1993, just before it was to be inserted into orbit.

Mars Global Surveyor – USA Mars Orbiter (November 7, 1996)

Mars Global Surveyor was inserted into an elliptical capture orbit on 12 September 1997. The spacecraft was initiated due to the loss of the Mars Observer and the basic design is after the Mars Observer. Mars Global Surveyor is designed to orbit Mars over a two-year period and collect data on the surface morphology, topography, composition, gravity, atmospheric dynamics, and magnetic field. This data will be used to investigate the surface processes, geology, distribution of material, internal properties, evolution of the magnetic field, and the weather and climate of Mars.

Mars 96 – Russia Orbiter & Lander (November 16, 1996)

Mars '96 consisted of an orbiter, two landers, and two soil penetrators that were to reach the planet in September 1997. The rocket carrying Mars 96 lifted off successfully, but as it entered orbit the rocket's fourth stage ignited prematurely and sent the probe into a wild tumble. It crashed into the ocean somewhere between the Chilean coast and Easter Island. The spacecraft sank, carrying with it 270 grams of plutonium-238.

Mars Pathfinder – USA Lander & Surface Rover – 264 kg (lander), 10.5 kg (rover) (December 4, 1996 – September 27, 1997)

Mars Pathfinder arrived at Mars on July 4, 1997 and impacted the surface at 16:57 UT (12:57 PM EDT) at a velocity of about 18 m/s. It bounced about 15 meters into the air, bouncing another 15 times and rolling before coming to rest approximately 2.5 minutes after impact and about 1 km from the initial impact site. The landing site was in the Ares Vallis region is at 19.33 N, 33.55 W and was named the Sagan Memorial Station. A six-wheel rover, named Sojourner, rolled onto the Martian surface on July 6 at about 05:40 UT. Mars Pathfinder returned 2.6 billion bits of information, including more than 16,000 images from the lander and 550 images from the rover, as well as more than 15 chemical analyses of rocks and extensive data on winds and other weather factors. The last successful data transmission was on September 27, 1997, the 83rd day of the mission since landing on the surface. This is the second mission in NASA's low-cost Discovery series.

Nozomi (Planet B) – Japan Mars Orbiter (3 July 1998)

Japan's Institute of Space and Astronautical Science (ISAS) launched this probe to study the Martian environment. This will be the first Japanese spacecraft to reach another planet. The spacecraft will encounter Mars in December of 2003.

Mars Climate Orbiter – USA Mars Orbiter (11 December 1998)

The Mars Climate Orbiter, also known as the Mars Surveyor '98 Orbiter, was a companion to the Mars Polar Lander. The mission was to study the Martian weather, climate, and water and carbon dioxide budget. It was destroyed when a navigation error caused it to miss its target altitude at Mars by 80 to 90 kilometres, instead of entering the Martian atmosphere at an altitude of 57 kilometres during the orbit insertion manoeuvre.

Mars Polar Lander – USA Mars Lander (3 January 1999)

The Mars Polar Lander, also known as the Mars Surveyor '98 Lander, was a companion to the Mars Climate Orbiter. It was to touch down on the southern polar layered terrain, between 73 S and 76 S, less than 1000 km from the south pole, near the edge of the carbon dioxide ice cap in Mars' late southern spring. The last telemetry from the spacecraft was sent just prior to atmospheric entry on 3 December 1999. No further signals have been received from the lander, the cause of this loss of communication is not known.

Deep Space 2 (DS2) – USA Mars Penetrators (3 January 1999)

The Deep Space 2 (DS2) project is a New Millennium mission consisting of two probes which were to penetrate the surface of Mars near the south polar layered terrain and send back data on the sub-surface properties. On 3 December 1999 the probes were nearing Mars on a trajectory to enter the atmosphere and bring them to their intended landing site, but contact was never made with either probe and the mission was presumed lost.

2001 Mars Odyssey – USA Mars Orbiter (7 April 2001)

Odyssey was launched from Cape Canaveral in Florida on April 7, 2001 and began its science mapping mission on February 19, 2002. Its objective involves conducting a detailed mineralogical analysis of the planet's surface from orbit and measuring the radiation environment. The mission has as its primary science goals to gather data to help determine whether the environment on Mars was ever conducive to life, to characterize the climate and geology of Mars, and to study potential radiation hazards to possible future astronaut missions. The still-operational spacecraft has been approved for an extended mission through September 2006.

Mars Exploration Rovers – USA Two Mars Rovers (22 May/4 June 2003)

The big science question for the Mars Exploration Rovers is how past water activity on Mars has influenced the red planet's environment over time. While there is no liquid water on the surface of Mars today, the record of past water activity on Mars can be found in the rocks, minerals, and geologic landforms, particularly in those that can only form in the

presence of water. That's why the rovers are specially equipped with tools to study a diverse collection of rocks and soils that may hold clues to past water activity on Mars.

Mars Express – ESA Mars Orbiter and Lander (1 June 2003)

Mars express will remain in orbit around Mars for at least one Martian year, 687 Earth days, which is the nominal mission lifetime. During this time, the point of orbit closest to Mars (pericentre) will move around to give the scientific instruments coverage of the entire Martian surface at all kinds of viewing angles. Beagle 2 was planned to descend to the surface, entering the atmosphere at more than 20,000 km per hour. A heat-resistant shield would have protected it as friction with the upper atmosphere slowed it down. Unfortunately, the Beagle 2 lander was declared lost after it failed to make contact with orbiting spacecraft and Earth-based radio telescopes.

Mars Reconnaissance Orbiter – USA Mars Orbiter (July 2005)

The Mars Reconnaissance Orbiter carries six primary instruments: the High Resolution Imaging Science Experiment, Context Camera, Mars Color Imager, Compact Reconnaissance Imaging Spectrometer for Mars, Mars Climate Sounder and Shallow Radar. All but the imaging spectrometer are currently onboard. That instrument is the last of several that had been installed but were removed so the science teams could replace an electrical component. It will be re-delivered this month. The orbiter will also carry a telecommunications relay package and two engineering demonstrations.

4. IMPLICATIONS TO ESA TECHNOLOGY TREE

The ESA Technology Tree were developed to provide a structured and complete ESA classification of all the technical know-how involved in space activities [ESA/ESTEC 2003]. The ESA Biomimicry Technology Tree categorises technologies with biological inspiration and was assigned a structure largely identical to the ESA Technology Tree [AD8]. There are 26 technology domains used to categorise these technology capabilities. Technical Notes 1 and 3 submitted for this contract cover the details of some technologies within these categories. Technical Note 2 bridges the biomimetic technology applications discussed in Technical Note 1 with those specific to space exploration in Technical Note 3, while making specific reference to the ESA Biomimicry Technology Tree.

This case study, though not covering many of these technologies in specific, does apply some solutions discussed in the previous Technical Notes. The technologies applied in this case study were selected due to their immediate or near-term application to space and their potential to offer the greatest increase in capability above current technology.

Some specific aspects of the ESA Biomimicry Technology Tree covered in this document are as follows:

6100 – Structures.2 – Adaptive Structures

The vehicle legs are designed and controlled to support complex terrain and adapt to the hazards of the Martian surface. See Section VI.2 – Structure.

6200 – Mechanisms.1 – Muscles and Actuators

The vehicle legs are designed to mimic the visco-elasticity of biological muscle through the control of the electric DC motors in each joint. See Sections VI.3.4 – Motors and VI.3.5 – Compliance.

6200 – Mechanisms.2 – Locomotion

The vehicle uses legs as opposed to the wheels used on many exploration rover designs to-date. This biological inspiration provides benefits on the complex terrain of the Martian surface. See Section VI.3 – Locomotion System.

6300 – Behavoiur.2 – Behavioural Artificial Intelligence

The vehicle uses biologically inspired artificial intelligence for behaviour control. See Section VII – Behaviour Control.

6300 – Behaviour.3 – Learning Mechanisms

The vehicle control system is designed to learn from its environment to better plan for future incidents and obstacles. See Section VII – Behaviour Control.

6300 – Control.1 – Reflexive Control

The vehicle control system is designed to respond to changes in the terrain based on obstacles and soil interaction. See Section III – Conditions for Surface Travel on Mars.

6400 – Sensors.3 – Touch

The vehicle uses touch sensors in the feet in order to determine force distribution across the legs and impact with obstacles during locomotion. See Sections VII.4 – Walking and VII.5 – Rough Terrain.

6400 – Sensors.4 – Taste and Smell

One of the vehicle's payloads, the Enose developed by JPL, replicates the way a nose can sense different airborne odours. See Section V.3.2 – Secondary Payload.

6500 – Generational.2 – Genetic Mechanisms

The vehicle control system makes use of genetic algorithms to enhance the locomotion capability. See Section VII – Behaviour Control.

II. FROM BIOLOGY TO ROBOTICS

1. BIOMIMETIC ANALOGUES TO SPACE ROBOTICS

There is little doubt that biological systems are hugely successful in solving problems encountered in their environments. Their success is attributed to the process of natural selection whose primary metric is such success – failure implies extinction. No wonder engineers have begun to examine biological systems to learn how organisms solve problems. Such reverse engineering of biology has met with varying degrees of success for a number of reasons, but renewed impetus has emerged following technological developments and increased scientific understanding. It seems appropriate therefore to examine biological solutions to common biological and engineering problems. According to Mjolsness & Tavormina (2000):

> *…how biological systems store and retrieve information, control development, fabricate structural components, build molecular machines, sense the external environment, reproduce and disperse themselves throughout the environment, engage in error detection, and carry out self-repair can pay big dividends to space exploration.*

This is particularly the case as space exploration missions give way from global reconnaissance to more focussed *in-situ* investigation and exploration requiring enhanced capabilities. Specifically, we are interested in replicating the capabilities of some biological organisms in robotic spacecraft. Fritz *et. al.* (1989) suggested that the primary goal of an intelligent system is survival and self-preservation, and this is the guideline used in applying biological lessons to the engineering of spacecraft.

There are many subsystems that make up the overall design of an interplanetary robotic explorer. Similarly, there are many separate functions of a living organism. Taking a closer look at these systems, both robotic and natural, relationships between the two can be made. Some examples are summarised in Table 2.

The application of biological evolution and development to systems design offers useful lessons in the application of modularity to spacecraft design. Traditional spacecraft design involves developing each subsystem separately and iteratively from scratch (as noted in Table 1), with a team of specialists in that area do the best they can to develop exactly what is required within their specified budget. There is very limited interaction between team members of different subsystems and each subsystem is designed in a mostly self-sufficient way. However, in living organisms, although they can be broken down into different systems (in theory), the interactions between these systems are tightly intertwined.

Table 2 – Biological Analogues to Spacecraft Subsystems Matrix.

Spacecraft Subsystem	Relevant Biological System
Space Systems Engineering	Evolution, embryonic development, animal growth
Propulsion System	Animal locomotion
Human Element	Human-machine interfacing, closed loop ecology
Space Environment	UV protection and oxidant tolerance
Attitude Control System	Animal navigation and vestibular system
Power System	Photosynthesis, ATP energy storage, eating
Thermal Control System	Thermoregulation, psychrophilic, hyperthermophilic extremophile strategies
Command and Data System	Animal ethology, biological neural nets, CPGs
Onboard Control	Learning and behaviour control
Communications system	Animal communication and human languages
Structural / Mechanical System	Bones, muscles, internal structure
Payloads (Sensors)	Senses: sight, hearing, smell, touch, taste
Reliability	Autonomy, self-repair, immune system

For example, solar panels on a spacecraft will provide power to charge batteries. This process can happen without any interaction from other systems, except for attitude control, in order to ensure the solar panels are pointed at the Sun. The rest of the spacecraft's subsystems can do other tasks and not be involved in the process of charging the batteries, whether that be recording images, sensing thermal differences on the planetary surface, or whatever the task is at hand. However, for an insect to "recharge" it requires searching for food (a stretch of the attitude control comparison of the spacecraft), then physically collect and consume this food, which involves a search routine that would impact any other tasks the creature may want to do. This process requires visual, auditory, and olfactory searching as well as complete body locomotion. Therefore, it cannot simultaneously search for food and evade a predator.

Though this seems like it might be advantageous in favour of the spacecraft due to its ability to multitask, the difference is that the creature is a much more efficient system. The spacecraft process is built through modular designs based on heritage through multi-purpose platforms (similar to evolutionary heritage), which are inefficient with respect to the operation of the system as a whole.

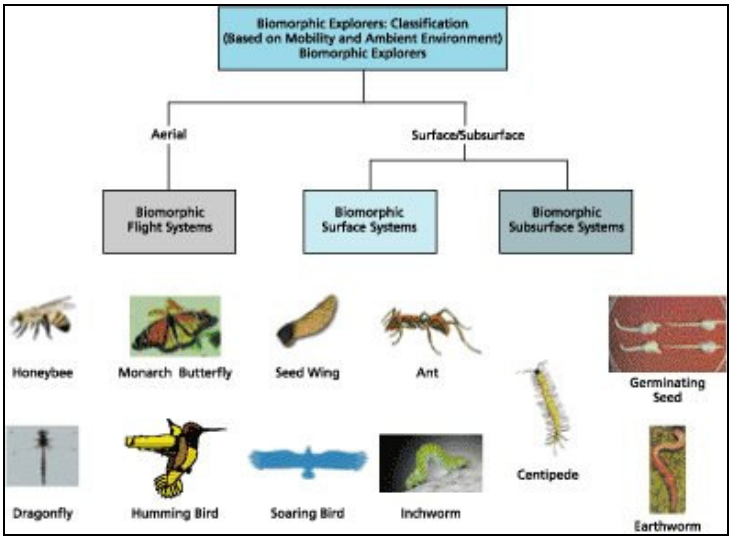

Figure 2 – Examples of Biological Inspiration in Different Mobility Categories [Thakoor 2003].

The biological analogue for propulsion systems is studied in greater detail in this report. Animal locomotion, such as legged locomotion, flight, swimming or burrowing are some examples of propulsion. However, this report concentrates on legged locomotion, specifically a 6-legged (hexapod) vehicle with 3-DOF per leg, similar to many insects

II.1.1. Biomimetic Planetary Rovers

The aim of a biomimetic robotic explorer is to display certain functional aspects of biological systems to gain advantage over standard mechanical designs, such as mobile robotic systems. The exploration of poorly understood planets and moons or the surveillance of hazardous environments is a difficult challenge, where the versatility to deal with and quickly adapt to unknown or unpredictable situations and environmental conditions is critical.

The definition of a number of system performance metrics is essential to provide a fair comparison of biomimetic approaches to traditional approaches to space mission design. For robotic planetary missions, there are a number of parameters currently adopted:

- Mobility in rugged terrain
- Sensing modalities for navigation and high scientific return
- Sample acquisition, manipulation and preparation including drilling
- Communication bandwidth
- Decision-making capabilities, eg. path planning, resource utilisation
- Planetary protection

2. INSECT BEHAVIOUR

Behaviour control involves dividing up the control system into modular task-based behaviours, which are built up from basic locomotion to increasing levels of competence such as obstacle avoidance in incremental fashion. Each task-based behaviour module encapsulates its own perception and actuation functions – each behaviour module requires only task-relevant data to function. Each task module is connected directly to the outside world via sensors and actuators and they operate in parallel. Each behaviour represents an active processing sequence from sensor input to actuator output. The subsumption architecture is a common example of behaviour-based control whereby task-based behaviours operate asynchronously. The control system is built bottom up incrementally and each level of competence includes the lower level as a subset. Each level is implemented and debugged from the bottom up analogous to the evolutionary process of adding layers of greater behavioural complexity to animal brains to provide greater capabilities. Each level specifies a behavioural pattern, which directly links perception to action and are summarised in Table 3.

Table 3 – Levels of Behaviour [Brooks 1990].

Level	Module	Effect
0	Collide, Runaway	remains stationary until a moving obstacle approaches it
1	Wander Randomly, Object Avoidance	generate new headings periodically accepts a force vector input from level 0 and suppresses output from Runaway module
2	Explore	finds a corridor to a specified goal at a distance and moves towards it (likened to exploratory behaviour for the provision of information)
3	Build Cognitive Maps	plan routes between landmarks
4	Monitory Environment	monitors dynamic changes in the environment
5	Identify Objects	identifies objects in the environment and reasons about tasks to be performed on them
6	Plan Tasks	formulates plans to change the state of the world as required
7	Reason About Object Behaviour	reasons about object behaviour in the world and modifies plans accordingly

Through previous studies, it has been shown that insect walking is not controlled only by a hardwired central system such as fixed action patterns or central pattern generators organized in a hierarchical structure. Instead there seems to be a decentralized architecture consisting numerous different and somewhat independent modules that together form a control hierarchy to cooperate in a sensible way. Functional modules performing distinct tasks can be identified on different levels of integration and can be ordered from global to more local [Cruse *et. al.* 2000]:

- Movement of the whole body (control of speed and direction)
- Coordination among legs (gait control)
- Control of different actions by a single leg (stance/swing phase, avoidance reflex, ground contact searching)
- Control of movement of each joint of a single leg performing a given action

- Control of synergistic and antagonistic muscles affecting movement of a single joint

As can be seen, the control of legged locomotion is a hierarchical control problem – this robot will have to successfully integrate all of the above levels to create a fully operational system.

3. INSECT WALKING

An interactive approach to locomotion focuses on the interactions between the muscular, skeletal, nervous, respiratory, and circulatory systems. These systems possess functional properties that emerge only when they interact with each other and the environment. One key challenge in the study of locomotion is to determine how each individual component within a locomotor system operates, while at the same time discovering how they function collectively as an integrated whole [Dickenson *et. al.* 2000].

There are two basic models of legged locomotion. The first is for walking creatures, where the centre of mass "rotates" around the rigid leg, as in an inverted pendulum. This can certainly be seen in humanoid walking if one attempts to walk with very rigid legs. The second model is for running creatures where a non-rigid leg acts as a spring. This creates a spring-mass system where the kinetic and gravitational potential energies are stored as elastic energy during the braking phase of the stride and recovered during the propulsive phase [Dickenson *et. al.* 2000]. This spring-mass model can be considered a form of compliance. This can be visualised in Figure 3.

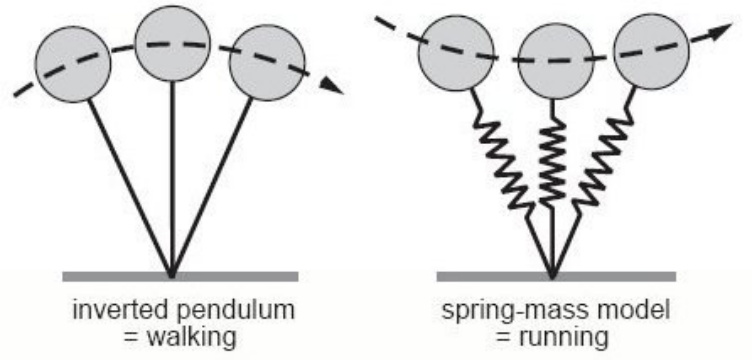

Figure 3 – The Inverted Pendulum and Spring-Mass Models for Walking and Running, Respectively [Dickenson *et. al.* 2000].

The legs of sprawled-posture animals (insects, crabs, spiders, etc.) generate substantial lateral forces while in contact with the ground. The dynamic result of these lateral forces is consistent with the hypothesis that elastic energy storage and recovery may occur within the horizontal plane (orthogonal to the direction of motion). This allows species with sprawled postures to actively alter course by changing the orientation of forces generated by a single leg [Dickenson *et. al.* 2000].

Insects do much more than simply walk across flat horizontal surfaces with a variety of gaits at different speeds. One of the most appealing factors of legged locomotion is the relative ease that insects traverse complicated natural terrains: uneven, slippery and unstable surfaces or

obstacles of varying size or with significant vertical variations, as well as many other non-smooth terrain characteristics [Beer *et. al.* 1997].

However, muscles normally consist of a number of fibres that are individually very weak, but can perform the required tasks collectively. Through control of a set of these muscle fibres, muscles can perform a wide range of tension and contraction speeds and strengths, up to a limit. Without jumping, the only way to increase walking speed is to increase step frequency (which is impacted through tension changes of the muscles). A range of contraction speeds is necessary in order to be able to walk at different speeds [Wendler 2002].

Recent views of behaviour consider the interaction of neural activity, the body, and the environment, as these components have co-evolved naturally within each species over time. Animals and insects must be understood as integrated organisms. Locomotion in animals with multi-jointed limbs requires the coordinated action of several appendages and their segmented limbs. The control of the actual motor output encompasses three levels [Bucher *et. al.* 2003]:

- Intrajoint control
- Interjoint control
- Intersegmental coordination between adjacent limbs

For engineering purposes, bioinspired robots can be built that incorporate aspects of biomechanics and neural control to improve agility and robustness on a given task. However, when studying a natural model, differentiating between incidental details and those essential to performance is a difficult task, i.e. which muscles (or joints or reflexes, etc.) are important for accurate modelling of legged locomotion and which are not [Beer *et. al.* 1998].

II.3.1. Gaits and Leg Movement

When creatures walk, they tend to move in a repetitive way. Under ideal conditions, legs move in a certain order that repeats with every step. This movement is called a gait and every creature uses gaits to traverse terrain. Gaits aid animal locomotion in several ways. First and foremost, they allow for equal pressure distribution along the supporting legs for greater stability across different terrains. This is especially important in the calculation of Drawbar Pull, discussed in more detail in Section III.2. Additionally, gaits aid in obstacle negotiation. Creatures can switch gaits at any time, even use a flexible "free gait" to traverse difficult terrain and surmount obstacles. Increased gait flexibility helps increase the mean free path of a creature, a benefit to legged robotic locomotion that is discussed in more detail in Section III.3.

The wave gait is used at slow speeds of walking in which only one leg is lifted at a time. Faster than the wave gait, the tetrapod gait requires the creature to move two legs at a time, usually legs that are diagonally opposite. The tripod gait is used at high walking speeds, in which the front and back legs on each side of the body step in unison with the middle leg on the opposite side [Beer *et. al.* 1997]. The tripod and tetrapod gaits are shown below in Figure 4.

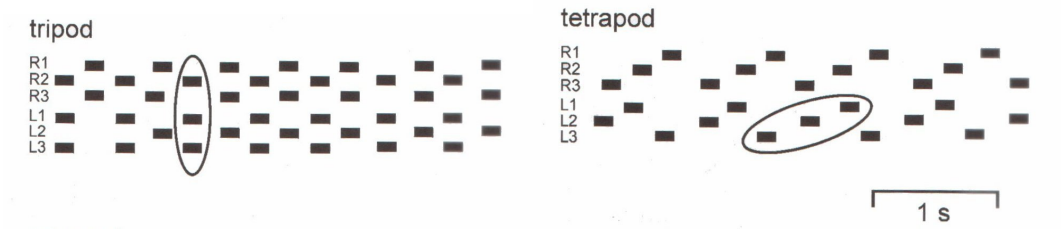

Figure 4 – Tripod and Tetrapod Gaits for a 6-legged Walking Robot, Where the Black Bars Represent the Swing Movement of Each Leg During Locomotion [Cruse *et. al.* 2002].

Changes in gait pattern are executed to achieve the most efficient locomotion based on the loss of leg or change in condition. Unfortunately, most robots are designed to either avoid much of the actual complexity of the real world or to minimize its impact. However, animals in nature evolved to survive under these conditions and often they depend upon or even actively exploit this complexity in their behaviour [Beer *et. al.* 1997].

The movement of each leg can be broken up into two phases. Stance phase is when the leg is providing support and propelling the body. Swing phase is when the leg is lifted from the ground and is swinging forward in order to begin another stance phase. For example, scorpions almost always use the same gait, L4-R3-L2-R1 and R4-L3-R2-L1, as shown in Figure 5a:

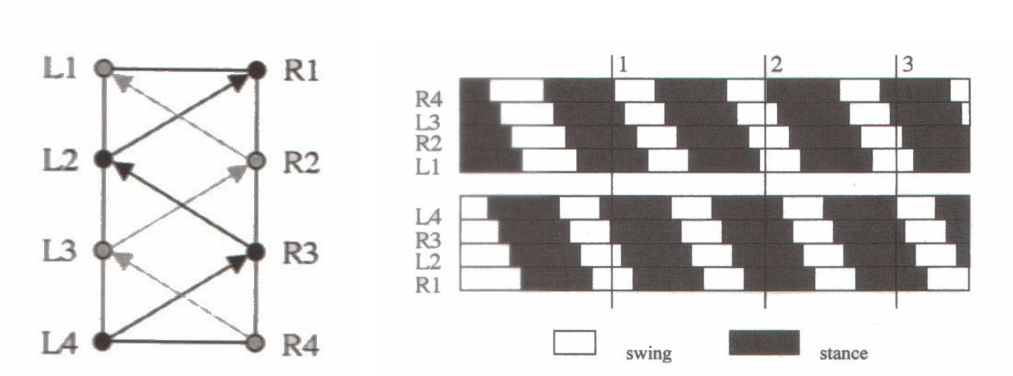

Figure 5 – a) Typical Scorpion Gait Pattern and b) Swing and Stance Pattern [Kirchner, *et. al.* 2002].

This shows that the rear left leg (4th position) starts, followed by the right leg number 3, then left 2, then right 1. This system is repeated on the opposite side starting with right leg number 4 after right leg 1 is placed firmly on the ground [Kirchner *et. al.* 2002].

During locomotion, the robot should be moving in the desired direction without any shift in any other direction. Therefore, the joints of each leg have to harmonize their rotations at every moment of a stance. To do this, a straightforward set of equations of motion must be established based on the free body diagram shown in Figure 6.

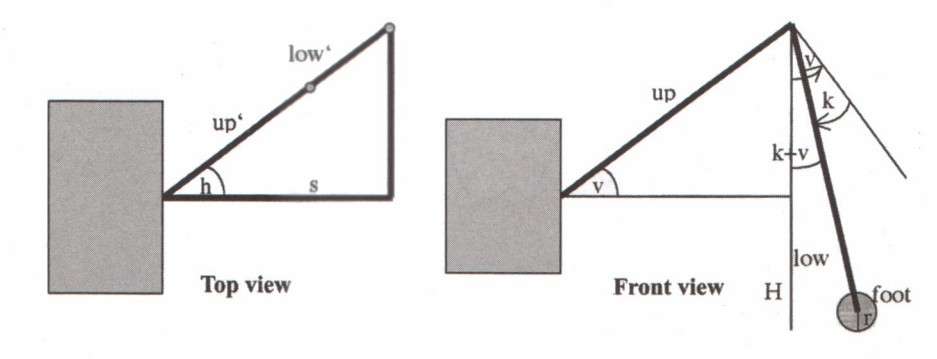

Figure 6 – Free body diagram of the forces, angles, and distances required to determine proper joint angles during locomotion [Kirchner *et. al.* 2002].

II.3.2. Reflex Motion

Reflexes, like recovering from a stumble or a trip, should also integrated into legged vehicles to help provide a significant step towards bio-inspired robotics. Several strategies and reflexes have been incorporated into numerous legged robots in order to help them walk over rough terrain. Some examples include:

- Stepping reflex allowing the robot to compensate for mechanical perturbations it receives while walking on rough terrain. Also, any leg that is sufficiently perturbed will step to a more posturally favourable position [Espenschied 1996].
- Elevator reflex allows the robot to surmount vertical obstacles when impacted during leg-swing motion [Espenschied 1996].
- Searching reflex is triggered when no footholds are available at the end of a swing phase or if support is lost in the stancing leg [Espenschied 1996].

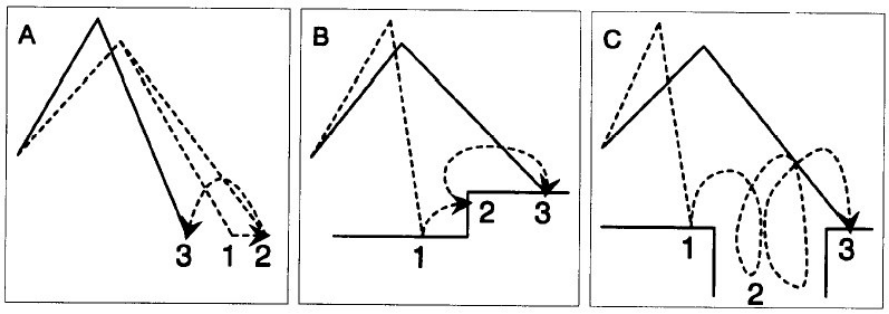

Figure 7 – Stepping, Elevator and Searching Reflexes [Espenschied 1996].

The control of reflexes in real-time is designed to be computationally inexpensive. This is especially important for small walking vehicles that carry their complete data controller and power systems [Ferrell 1995]. Conversely, computationally costly algorithms can be developed for force distribution on the legs of these vehicles whenever two or more parallel kinematic chains are mechanically coupled via the ground [Klein and Kittivatcharapong 1990]. However, this problem can be eliminated in control system programming, because the

kinematic equations to location each leg segment at every point along the step is not necessarily required. A relatively computationally inexpensive and biologically inspired gait controller, coupled with a variety of simple local reflexes found in insects can produce smooth locomotion over complicated terrain without any global knowledge of terrain characteristics [Kirchner *et. al.* 2002].

III. CONDITIONS FOR SURFACE TRAVEL ON MARS

1. SOIL COMPOSITION

An important aspect of designing planetary rovers is consideration of the soil mechanics properties such as soil shear strength, compressive strength, bearing capacity, penetration resistance, etc. Almost all of these parameters are inter-related, the most important of which are related to shear strength and quantified by the Mohr-Coulomb relation. From the effective soil shear stress, rover trafficability and other parameters can be determined. Different soil parameters can make a significant difference to sinkage and compaction, which is why a vehicle must be designed with its environment in mind. A summary of many soils used in this study can be found in Table 4 below.

Table 4 – Planetary and Terrestrial Soil Characteristics [Ellery 2004a]

Soil	Specific Gravity	Soil Cohesion	Friction Angle	Soil Cohesive Modulus *	Soil Frictional Modulus *	Consistency	Deformation Coefficient **
Symbol	g_s	C_o	ϕ	k_c	k_ϕ	k	n
Units		(Pa)	(°)	(N/m^{n+1})	(N/m^{n+2})	(N/m^{n+1})	
DLR soil simulant A	4.24	188	24.8	2370	60300	8400	0.63
DLR soil simulant B	4.24	441	17.8	18773	763600	95133	1.1
VL1 drift	4.29	1600	18	1400	820000	83400	1.0
VL1 blocky	5.97	5500	30.8	1400	820000	83400	1.0
VL2 crusty-cloddy	5.22	1100	34.5	1400	820000	83400	1.0
PL drift	4.36	380	23.1	1400	820000	83400	1.0
PL cloddy	5.70	170	37	1400	820000	83400	1.0
Dry sand	5.67	1040	28	990	1528000	153790	1.1
Sandy loam	5.67	1720	29	5270	1515000	156770	0.7
Clayey soil	5.67	4140	13	13190	692200	82410	0.5
MER-B 'sandy loam'	4.24	4800	20.0	28000	7600000	788000	1.0
MER-B 'slope soil'	4.24	500	20.0	6800	210000	27800	0.8

* as there is no experimental data from VL1, VL2 and PL, lunar values for those soils have been used [Carrier 1991]

** as there is no experimental data from VL1, VL2 and PL, n=1 is assumed for those soils [Carrier 1991]

Soil is the layer of minerals and organic matter, in thickness from centimetres to a metre or more, on the land surface. Its main components are mineral matter, organic matter, moisture, and air [Wikipedia 2005b]. When discussing the planetary surface composition, the words soil and regolith have been commonly used interchangeably. However, technically "soil" contains an organic substance that differs from regolith, which is simply a layer of loose, heterogeneous material covering solid rock and not necessarily organic. Although often used

interchangeably when discussing planetary surfaces and simulated planetary surfaces, it should be noted that there is a difference between them.

Table 5 below shows the chemical composition of Mars soil based on Viking mission experiments, meteorite analyses and estimations made through simulation.

Table 5 – Representative Chemical Composition of Mars Soil (Kieffer *et. al.* 1992).

Soil Composition	%	Soil Comp. Variations	%
SiO	43.0%	CO_3	<2%
Al_2O_3	7.2%	NO_3	?
FE_2O_3	18.0%	H_2O	0-1%
MgO	6.0%		
CaO	5.8%		
TiO_2	0.6%		
K_2O	0.2%		
P_2O_5	0.8%		
MnO	0.5%		
Na_2O	1.3%		
Cr_2O_3	0.2%		
SO_3	7.2%		
Cl	0.6%		
Sum of Above	91.4%		

2. BEKKER THEORY

The primary goals for a planetary rover are the capability to 1) navigate in an unknown, hostile terrain, 2) recognise and negotiate obstacles, 3) deploy scientific instruments and 4) acquire samples from scientific targets. These goals must be attained with minimum mass and volume and tight mobility, power, thermal and communications constraints. For most planetary rovers, the mobility system is characterised by a number of parameters – wheelbase, footprint, drive wheel number, drive wheel torque, wheel design (dimensions, stiffness, grouser placement, construction material, etc.), power requirements, suspension and stability. However, in this report, all wheel-based parameters will obviously be replaced with characteristics of legged vehicles. Performance is generally quantified in terms of vehicle Drawbar Pull (DP – defined as the difference between soil thrust and motion resistance) and power requirements. Motion resistance comprises a number of components – rolling, compaction, bulldozing, materials flexure, and slippage are only a few examples [Bekker 1959, 1969]. Locomotion requires traction to provide forward thrust on the ground and the mobility system must provide robust locomotion with maximum payload capacity for scientific instruments. Trafficability is defined by the capacity of soil to support a vehicle and provide sufficient traction for locomotion. There are two groups of terrain parameters that affect soil trafficability – one group relates to soil strength and the other to ground surface geometry [Apostolopoulos 2001].

III.2.1. Soil Properties and Dynamics

The Bekker analysis provides the basis for determining the theoretical performance of a vehicle traversing on a particular terrain. Based on the definitions expressed above, formulae were developed to determine the properties of any soil and its interaction with forces it encounters. The equations expressed below have been modified from those originally developed by Bekker in the 1950's for large tractor/tank-sized vehicles to fit legged planetary explorers that are orders of magnitude smaller.

III.2.1.1. Viking Lander 2 Properties

For this design, Viking Lander 2 site was selected and in the Bekker analysis, only VL2 data was analysed. Additional regolith properties are taken from Lunar data, as it is expected to have very similar soil properties to Martian soil.

Table 6 – Viking Lander 2 Site Soil Properties

Soil Properties	Symbol	Value	Units
Specific Gravity	g_s	5.22	
Soil Cohesion	C_o	1100	Pa
Soil Cohesive Modulus	k_c	1400	N / m^(n+1)*
Soil Frictional Modulus	k_f	820000	N / m^(n+2)*
Soil Deformation Exponent	n_k	1	
Internal Friction Angle	ϕ	34.5	°
Gravity	g	3.72	m/s^2
Max Slope	θ	40	°
Min Slope	θ	0	°
Shear Deformation Slip Modulus	κ	0.005	m
Coefficient of Friction	μ	0.687280959	
Coefficient of Surface Adhesion	ω	10	N / m^2
Poisson's Ratio	v	0.3	

III.2.1.2. Soil Shear Strength

Soil shear strength measures the point at which a soil will shift under force. It is characterised by the Mohr-Coulomb Law such that the shear stress parallel to the plane of failure will be given as [Ojeda *et. al.* 2005]:

$$\tau = C_0 + \sigma \tan \phi \qquad (1)$$

where:

τ = *soil shear strength*
C_0 = *soil cohesion*
σ = *applied stress* = $\frac{A}{W}$
A = *footprint area*
W = *vehicle weight*
ϕ = *internal friction angle*

As shown in the design in further sections, the mass of the vehicle is approximately 23 kg, which equates to 85.56 N on 3.72 m/s^2 gravity on Mars. With a footprint area of 0.00152 m^2 per leg, the normal stress on the VL2 soil during a step in the tripod gait (with 3 legs stepping simultaneously) is 18.7 kPa, which leads to a maximum soil shear stress of 14.0 kPa under that load.

III.2.1.3. Soil Thrust and Slip

The soil thrust provides the tractive effort of the vehicle against the soil. When the force exerted by legs pushes on the soil at an angle to provide movement of the vehicle, the resulting force from the soil is called the soil thrust. The maximum thrust available to a vehicle from the soil can be found using a modified Bernstein-Bekker equation [Bekker 1959; Bekker 1969]. The maximum soil thrust for a legged vehicle with 'n' legs is given by:

$$H_0 = n\left(AC_0 + W\tan\phi\right) \qquad (2)$$

where:

H_0 = *maximum soil thrust*
n = *number of legs on the vehicle*

For the 6-legged vehicle in this design, a maximum soil thrust when walking in a tripod gait on VL2 soil is found to be 362.8 N.

However, soil thrust is modified by the slip of the foot against the soil, given in a relation to its shear deformation modulus. For a legged vehicle, this loss is the difference between the vehicle's translational velocity and leg rotation in the velocity direction. At low velocity we can compute the soil thrust [Apostolopoulos 2001] as:

$$H = H_0\left(1 - e^{-sl/\kappa}\right) \qquad (3)$$

where:

s = *slip*
l = *footprint-to-ground contact length*
κ = *shear deformation modulus*

The shear deformation modulus (κ) is a measure of the amount of shear deformation that a soil can sustain before shear failure. The value of κ may be represented by the distance

between the vertical axis and the point of intersection of the tangent to the shear curve at the origin and the horizontal line representing the maximum shear stress τ_{max}, as shown in Figure 8. Wong (1989) shows that, experimental data show that κ varies from 0.6 cm for clay at maximum compaction, 1 cm for firm sand, 2.5 cm for loose sand, and is in the range from 2.5 cm to 5 cm for undisturbed, fresh snow [Le 1999]. For Mars regolith, the shear deformation modulus for lunar regolith (1.8 cm) was used [Whittaker 1997].

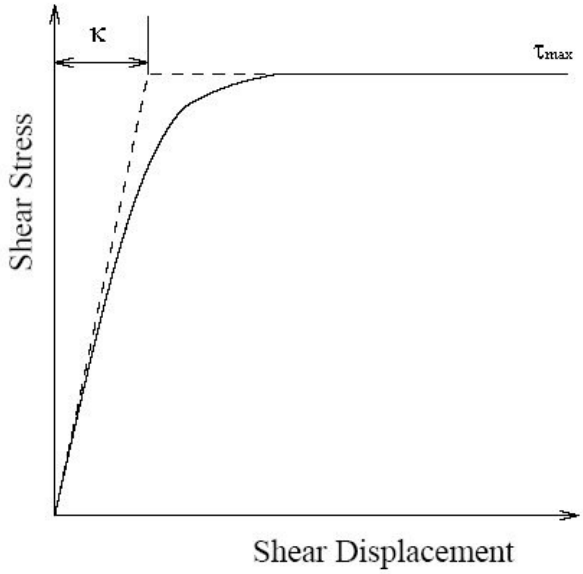

Figure 8 – Determination of Shear Deformation Modulus (κ) [Le 1999]

Slip is an internal resistance and leads to considerable power losses, therefore it is advantageous to maximise footprint-to-ground length (l) to minimise the power losses. Accurate modelling of slippage is extremely difficult, as slip is a function of tractive force and is dependent on vehicle velocity. The following relation is linear only for the low speeds to be encountered on planetary missions.

$$s = \frac{\omega W}{k_t l^2} \qquad (4)$$

where:

ω = *coefficient of surface adhesion (10 N/m^2)*
k_t = *tangential stiffness of leg (4,000 kN/m^2)*

When the soil-vehicle interaction values above are calculated, a slip of 0.11 N/m^2 is determined. This slip applied to the maximum soil thrust produces a final soil thrust of 277.0 N during tripod gait locomotion on VL2 soil.

III.2.1.4. Grousers

The addition of a grouser-like tread to the foot of a legged vehicle will also impact traction on inclined or rugged surfaces, however, the impact will be minimal when traversing standard soils on level terrain. Grousers are also expected to benefit high-speed running, as the force exerted by the legs is in more of a horizontal direction. However, this study only concentrates on slow-speed walking for planetary exploration and therefore has not been investigated.

III.2.2. Motion Resistances

Acting in opposition to the soil thrust are resistances to motion. Such a resistance is dominated by soil compaction and bulldozing of the soil – it can absorb between 5-35% of gross motor power depending on the soil and vehicle speed.

III.2.2.1. Soil Compaction due to Sinkage

The dominant source of resistance for legged vehicles is compaction resistance (R_c) due to the low footprint-to-ground contact area that the feet of a legged vehicle have. The most effective means to reduce compaction resistance is to increase the footprint size. Soil compaction resistance for a legged vehicle is determined through the following function

$$R_c = n\left(\frac{k}{n_k + 1}\right) z^{n_k+1} \qquad (5)$$

where:

R_c = *compaction resistance*
z = *sinkage*
n_k = *soil deformation exponent (1 for the Moon and Mars)*
k = *soil consistency* ($k = k_c + bk_\phi$)
k_c = *soil cohesive modulus (1,400 N/m$^{n_k+1}$ for the Moon and Mars)*
b = *footprint-to-ground contact width*
k_ϕ = *soil frictional modulus (820,000 N/m$^{n_k+2}$ for the Moon and Mars)*

Sinkage and compaction resistance decrease with increasing footprint size as well as the number of legs in contact with the ground, as the dispersion of the full vehicle mass across a larger surface area will keep the vehicle above the surface. Sinkage can also vary significantly in different soils. The sinkage equation for an n-legged vehicle is given by [Apostolopoulos 1996]:

$$z = \frac{1}{n}\left(\frac{3W}{(3 - n_k)k\sqrt{2d}}\right)^{2/(2n_k+1)} \qquad (6)$$

where:

d = distance from hip joint to foot to simulate wheel radius

For a walking vehicle, the determination of sinkage varies considerably, even in a single vehicle during different phases of locomotion. When a 6-legged vehicle is standing on all 6 legs, the weight of the vehicle is distributed across all of the legs. However, in walking with a tetrapod or tripod gait, 2 or 3 legs are lifted simultaneously, changing the weight distribution. Additionally, legs that "simultaneously" touch the ground at each step may actually touch at different times due to reflexes, slope in the terrain or stepping on scattered rocks, which also impacts sinkage. Although several variations exist, a tripod gait (with a minimum of 3 legs in contact with the ground at any time) was used to determine vehicle sinkage. Using the above equations under these circumstances, the robot detailed in Section VI sinks 1.2 cm when walking with a tripod gait. This sinkage leads to a compaction resistance of 15.5 N which will impact DrawBar Pull, as shown in Section III.2.3.

III.2.2.2. Bulldozing

Bulldozing occurs significantly in wheeled and tracked vehicles. It is the measurement of the effect of regolith pushed in front of a rotating wheel or track as it moves along. However, bulldozing resistance (R_b) is insignificant for legged vehicles because of the vertical lifting motion of each leg instead of horizontal rolling of wheels and tracks. Therefore, bulldozing resistance is 0 N for legged vehicles.

III.2.2.3. Gravitational

The rover experiences gravitational resistance (R_g) while negotiating the slopes. The maximum slopes that must be negotiable on Mars are the inner slopes of craters such as the aptly named Endurance Crater that may reach up to 35-40^o [Burnham 2004].

$$R_g = W \sin\theta \qquad (7)$$

Wheeled vehicles are generally limited to gradients < 25^o due to wheel slippage. Recently, all 6 wheels of the Mars Opportunity rover became stuck in the Martian sand while traversing a sand ripple on a relatively flat surface. This notes that even on a relatively flat terrain, surprises within the small hills created by ripples of soil can greatly impact the terrain negotiation capability of a vehicle. Legged vehicles can traverse much larger gradients because the vertical movement of each leg when walking is already compensating for gravity in the lifting motion. Also, footprints are discrete allowing for specific placement of each step to better position the centre of gravity to increase terrain traversibility. The maximum gradient of a walking rover is limited only by the centre of gravity of the vehicle when it is outside of the polygon area bounded by all standing legs. This has been emphasised in the past in the design of wheel-walking vehicles to increase slope negotiation capability. Therefore, the previous equation is important to be included in the overall motion resistances of a legged rover. For the rover designed in this project, a maximum gravitational resistance on a 40^o slope is 4.6 N.

III.2.2.4. Other Resistances

There are many other resistances that could be considered in these calculations. However, for the scale of the rover's mass investigated in this research, they are of limited impact to the overall resistance of the system and not included in the analysis.

III.2.3. Drawbar Pull

Drawbar pull is the difference between soil thrust and motion resistance and it defines the most important value in the development of a vehicle's locomotion system: trafficability. Trafficability defines the ability (or inability) of a vehicle to traverse over a specified terrain [Slocum *et. al.* 2003]. In heavy machinery, it is a value used to determine pulling or towing power of a tractor, but in smaller mobile robotics, it simply defines the vehicle's ability to traverse a specific terrain. In order for a vehicle to negotiate terrain, it must have a positive drawbar pull [Apostolopoulos 1996].

$$DP = H - R = H - \left(R_c + R_b + R_g + R_{other}\right) = H - R_c - R_g \qquad (8)$$

where:

DP = drawbar pull
H = soil thrust
R = sum of the resistances expressed above

The total drawbar pull of the 6-legged vehicle when using the tripod walking gait was determined to be 256.8 N in the VL2 soil. Positive values of drawbar pull indicates that the Martian terrain is traversable by a legged micro-rover vehicle. Analysis for the upcoming ESA ExoMars mission shows that a simulated 220 kg ExoMars rolling rover with 6 wheels has a drawbar pull of 378.8 N at the VL2 site. To produce nearly as much drawbar pull from a walking vehicle 1/10th the size shows that the development of walking vehicles for Mars exploration would be a great asset to mass-constrained Mars missions. Table 7 summarises the calculations completed in this section to determine the overall drawbar pull of tripod gait locomotion of this vehicle on Mars.

Table 7 – Calculations Leading to Drawbar Pull Determination

Bekker Calculations	Symbol	Value	Units
Sinkage (Standing 1 Leg)	z	0.0235303	m
Sinkage (per leg when standing on 6)	z	0.003921717	m
Sinkage (Tripod Step)	z	0.01176515	m
Slip (at low speeds)	s	0.110485537	N / m^2
Load (Standing 1 Leg)	P	56269.82203	Pa {N/m^2}
Load (per leg when standing on 6)	P	9378.303671	Pa {N/m^2}
Load (Tripod Step)	P	28134.91101	Pa {N/m^2}
Modulus of Elasticity	E	473492.6768	Pa {N/m^2}
Soil Consistency	k	37480	N / m^(n_k+1)*
Soil Deformation Modulus	k	851818.1818	N / m^(n_k+2)*
Bulk Modulus	K	394577.2307	Pa {N/m^2}
Shear Modulus	G	182112.568	Pa {N/m^2}
Applied Stress (Tripod)	σ	18756.60734	Pa {N/m^2}
Contact Pressure (Tripod)	p	10021.76871	Pa {N/m^2}
Maximum Shear Stress (Tripod)	τ	13991.05907	Pa {N/m^2}
Max Tractive Thrust	H_o	362.8580565	N
Soil Thrust	H	276.9774157	N
Resistance (Compaction – Standing 1 Leg)	R_c	62.25521935	N
Resistance (Compaction – Tripod Step)	R_c	15.56380484	N
Resistance (Compaction – per leg when standing on 6)	R_c	0.288218608	N
Resistance (Max Gravitational)	R_g	4.583075657	N
Resistance (Max Gravitational)	R_g	0	N
DrawBar Pull (Min)	DP	210.1391207	N
DrawBar Pull (Tripod)	**DP**	**256.8305352**	**N**
DrawBar Pull (Max)	DP	276.6891971	N

3. ROCK DISTRIBUTION

In general, the Martian surface is very rocky with rocks over 3 cm in diameter occupying up to 16% of areal coverage. However, the problem of reliance on such statistical models was exemplified by Sojourner's difficulties in traversing the rock garden which had an areal coverage of 24.6% of rocks over 3 cm diameter. However, rock coverage can also be low, as found at the MER sites. Based on scientific attraction to sites where water once flowed, rock distribution is expected to be high. The Martian rock distribution model is based on Golombek and Rapp (1997) where the number of rocks for Viking Landers 1 and 2 (VL1 and VL2, respectively) sites are given by an exponential law:

$$N(D) = Le^{-sD} \qquad (9)$$

where:

D = rock diameter
L = cumulative number of rocks of all sizes/m²
$L_{VL1} = 5.61$, $L_{VL2} = 6.84$
s = relationship between rock frequency and size
$s_{VL1} = 12.05$, $s_{VL2} = 8.30$

Table 8 below shows this equation evaluated for varying rock diameters across the VL1 and VL2 sites.

Table 8 – Number of Rocks of Varying Diameters up to 3 Metres.

Rock Diameter	Number of Rocks per Square Metre at VL1	Number of Rocks per Square Metre at VL2	Ratio of VL2 to VL1
D	N(D)	N(D)	
(m)			
0.03	3.908097644	5.332327018	1.364430345
0.06	2.722500391	4.156975355	1.526896146
0.075	2.272318599	3.670352592	1.615245588
0.1	1.681272117	2.982577118	1.774000227
0.13	1.171225597	2.325157391	1.985234438
0.2	0.503863803	1.300550624	2.5811551
0.22	0.39595715	1.101626508	2.782186174
0.25	0.275835865	0.858805964	3.113467361
0.3	0.15100395	0.567104171	3.755558511
0.325	0.111726732	0.460836359	4.124674106
0.4	0.045254676	0.247285369	5.464305391
0.5	0.013562464	0.107828609	7.95051743
0.58	0.005172241	0.05550888	10.73207598
0.6	0.004064562	0.047018588	11.5679346
0.75	0.000666847	0.013538575	20.3023575
0.8	0.00036506	0.008940066	24.48931775
1	3.2788E-05	0.001699855	51.84388607
2	1.91631E-10	4.22443E-07	2204.458131
3	1.12E-15	1.04984E-10	93735.94495

The rock coverage density for Viking Lander sites 1 and 2 is given by a similar relation:

$$\rho(D) = Ke^{-qD} \qquad (10)$$

where:

K = cumulative fractional area covered by rocks of all sizes
K_{VL1} = 0.069, K_{VL2} = 0.176
q = relationship between area coverage and rock size
q_{VL1} = 4.08, q_{VL2} = 2.73

This model represents the most accurate, predictive model available with a 96% correlation with actual Mars data of rock size distribution [Golombek & Rapp 1997]. This exponential law computes the frequency distribution of rocks according to rock diameter for both VL1 and VL2 sites. Table 9 below shows this equation evaluated for varying rock diameters across the VL1 and VL2 sites.

Table 9 – Rock Coverage Densities for Rocks of Varying Diameters up to 3 Metres.

Rock Diameter	Rock Coverage Density at VL1	Rock Coverage Density at VL2	Ratio of VL2 to VL1
D	ρ(D)	ρ(D)	
(m)			
0.03	0.061050812	0.16216008	2.656149428
0.06	0.054017416	0.149408475	2.765931562
0.075	0.050810677	0.143413777	2.822512626
0.1	0.045883543	0.133952331	2.919398175
0.13	0.040597501	0.123418867	3.040060725
0.2	0.030511587	0.101950153	3.341358599
0.22	0.028120715	0.096532911	3.432804242
0.25	0.024881051	0.088941958	3.574686537
0.3	0.020289561	0.077593526	3.824307826
0.325	0.018322073	0.072474443	3.95558099
0.4	0.013492129	0.059055873	4.377060982
0.5	0.008971981	0.044946999	5.009707301
0.58	0.006473433	0.036128571	5.581053124
0.6	0.005966178	0.034208837	5.733794285
0.75	0.003235251	0.022714057	7.020802238
0.8	0.002638225	0.019815887	7.511066681
1	0.001166615	0.011478595	9.839230339
2	1.97245E-05	0.000748626	37.95409831
3	3.33491E-07	4.88248E-05	146.4051078

The average rock height from the VL1 and VL2 sites are found from the same model:

$$H(D) = M*D+0.008 \qquad (11)$$

where:

M_{VL1} = 0.365 and M_{VL2} = 0.506

Table 10 below shows this equation evaluated for varying rock diameters across the VL1 and VL2 sites.

Table 10 – Exposed Rock Height for Rock Diameters up to 3 metres.

Rock Diameter	Rock Height at VL1	Rock Height at VL2	Ratio of VL2 to VL1
D	H(D)	H(D)	
(m)	(m)	(m)	
0.03	0.01895	0.02318	1.223218997
0.06	0.0299	0.03836	1.282943144
0.075	0.035375	0.04595	1.298939929
0.1	0.0445	0.0586	1.316853933
0.13	0.05545	0.07378	1.330568079
0.2	0.081	0.1092	1.348148148
0.22	0.0883	0.11932	1.351302378
0.25	0.09925	0.1345	1.355163728
0.3	0.1175	0.1598	1.36
0.325	0.126625	0.17245	1.36189536
0.4	0.154	0.2104	1.366233766
0.5	0.1905	0.261	1.37007874
0.58	0.2197	0.30148	1.372234866
0.6	0.227	0.3116	1.372687225
0.75	0.28175	0.3875	1.375332742
0.8	0.3	0.4128	1.376
1	0.373	0.514	1.378016086
2	0.738	1.02	1.382113821
3	1.103	1.526	1.383499547

With the new MER data coming, these models can be tested once again. It is expected that the results will show that the models hold, but the L, s, K, q and M coefficients will change as the rock distribution is quite different at the MER sites than previous landing sites [Allouis 2004].

A single row is selected in each of the tables above to highlight the 20 cm rock diameter values. These values show that using the equations above, the following conclusions can be made:

- There are over 2.5 times as many rocks per square metre at VL2 than at VL1.
- The rock coverage density at VL2 is more than 3 times as great as at VL1 of rocks of the same diameter.
- The exposed height of rocks at VL2 is 1.3 times greater than at VL1.

Together these three metrics all show that the terrain at VL2 is a more challenging environment for a vehicle to traverse than the terrain at VL1. This one of the reasons why the

VL2 site was chosen for this vehicle, to show the benefits of a legged walking system and its capability of traversing more challenging terrains.

An example of a surface simulated with rock distribution parameters of the VL2 site is shown below in Figure 9.

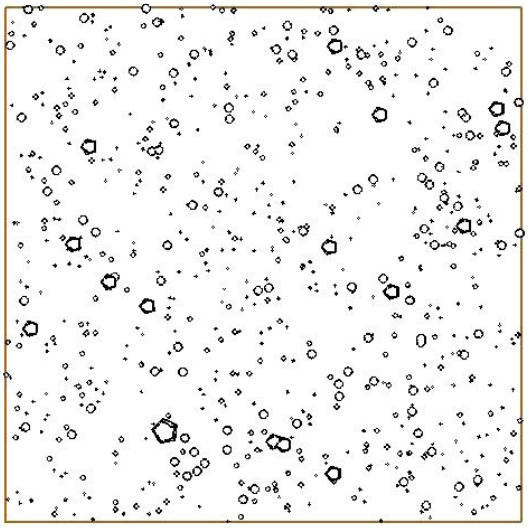

Figure 9 – Simulated Landing Site Based on Viking 2 Rock Distribution [Ellery 2004a].

4. MEAN FREE PATH (MFP)

One of the most important aspects of mean free path (MFP) is that it defines the intelligence requirements of the robot's navigation system. This is the expected straight-line path distance that a vehicle can traverse over a given terrain before a heading change is required due to the incidence of an insurmountable obstacle [Wilcox *et. al.* 1997]. This can be modelled according to the rock distribution laws explained above. A larger MFP means that the rocks are distributed over a greater area, thereby reducing the requirement for steering changes for obstacle avoidance. By reducing this requirement for deviations from straight-line paths, the vehicle can traverse terrain easier and faster with less dependence on an autonomous control system. With a moderate MFP, a reasonable number of heading changes are required due to larger, less distributed obstacles, which would then require a robust and advanced the autonomous navigation system in order to accurately negotiate the terrain. Significantly small MFP would mean the terrain is effectively non-traversable due to insurmountable obstacles located very close together.

The rock frequency distribution may be utilised to compute the MFP – rocks of diameter D. Rocks are assumed to be distributed randomly according to a Poisson distribution. MFP may be defined as the product of the areal coverage of the rover's trajectory of (x+D/2) and the areal density of rocks of diameter D [Wilcox *et. al.* 1998]. For rocks larger than D_0:

$$\int_{D_0}^{\infty} (x + \tfrac{D}{2})(r + D)\rho(D)\, dD = 1 \qquad (12)$$

where:

x = mean free path distance
r = vehicle thorax diagonal

In order to compute the MFP of a vehicle, account must be taken of its obstacle negotiation capability. The solution for MFP is given by:

$$x = \frac{1 - (r/2)\int_{D_0}^{\infty} D\rho(D)dD - (1/2)\int_{D_0}^{\infty} D^2\rho(D)dD}{r\int_{D_0}^{\infty} \rho(d)dD + \int_{d_0}^{\infty} D\rho(D)dD} \qquad (13)$$

Using this equation above, the current baseline ExoMars rover mean free path was calculated to be 18.2 metres for a simulated VL2 site rock distribution, based on single point turning. This means it would travel on average 18.2 metres before a heading change is required to avoid an insurmountable obstacle. Given that ExoMars is expected to travel 100 metres/day, MFP thus has an important impact on the level of autonomy required between the once daily communication windows.

The walking robot designed in detail below has a minimum ground clearance of 20 cm when "crouched" and a maximum clearance of 50 cm when standing as tall as possible. However, for an average step, the ground clearance is 34 cm. Under the same conditions as the ExoMars analysis above, this means that without including climbing capability (as this can significantly increase the obstacle height a walking vehicle can traverse), a MFP of 49.2 metres was determined. This is over twice the mean free path as the ExoMars vehicle, a wheeled vehicle that is designed to be 10 times the size of this walking vehicle.

IV. SYSTEM REQUIREMENTS

1. LANDING SITE SELECTION

The landing site selection must fulfil two criteria:

1) It must be able to traverse terrain where a previously existing riverbed once was.

2) It must provide a valid scientific case for its selection to fulfil the payload requirements.

2. VEHICLE LIFETIME

The vehicle will be designed with a minimum lifetime of 90 operational Martian days (sols) on the surface.

3. LOCOMOTION SYSTEM

The vehicle must be designed to traverse a total distance of 1 km over rocky terrain throughout the entirety of the mission. Over the required 90-sol vehicle lifetime, this provides the expectation that the vehicle will travel 11 metres per sol. However, realising that the vehicle will be required to stop for scientific experimentation for a significant portion of its operational lifetime, a 30 metre per sol capability will be required to ensure meeting or exceeding the 1 km total travel distance requirement.

4. MASS REQUIREMENTS

The vehicle must fit within the micro-rover class (5-30 kg) of planetary rovers.

5. POWER

Power must be provided to all payloads and systems such that only minimal experiments and communications are online while the vehicle is in motion. The vehicle will not provide power to the locomotion system while conducting experiments with the primary payload.

6. PAYLOADS

IV.6.1. Primary Payload

The primary payload will need to provide experimental data to support the search for signs of extraterrestrial life, extinct or living, on the surface of Mars.

IV.6.2. Secondary Payload

The secondary payload must supplement the primary payload in the search for signs of biological / organic life on the surface of Mars.

7. THERMAL

All systems must be able to sustain operability during transit to Mars and during operations on the surface at the selected landing site. Mars atmospheric temperatures at the surface range between -140°C and +20°C while ground temperatures range from -99°C to +22°C.

8. COMMUNICATIONS

The communications system onboard the rover will need to be designed in two parts. High volume data transfer will be relayed through the Mars Global Surveyor spacecraft. The relay payload interface requirements are identical to those stated in the applicable MBR and MOC Interface Control Documents [JPL 1996]. Additionally, the transmission of location and emergency data as well as the receiving command data will be through X-band transmission directly from Earth ground stations.

9. COMMAND AND DATA HANDLING

Onboard data processing must be provided to analyse payload data as well as provide image compression for onboard cameras.

Onboard data storage must be sufficient to contain essential data collected in the event of a 4-day communication delay, as in the case with ESA's Beagle 2 spacecraft.

Onboard control must be able to sustain loss of command data reception for at least a 4-day situation and proceed as nominal, as in the case with ESA's Beagle 2 spacecraft.

V. MISSION PROFILE

1. MISSION OBJECTIVES

The main purpose of this mission is the investigation into the current or previous existence of biological life on Mars.

2. LANDING SITE SELECTION

Landing site selection is one of the key factors in the design of a robotic vehicle for Mars exploration. Investigation into canyon and cliff-side terrains are not of interest in this design, as a very specific vehicle will be required for such missions. Instead, relatively level areas (though reasonably steep in some areas would be traversable, with a slope no greater than approximately 30^{o}) with heavy coverage of larger rocks will be identified.

Localised regions of the Martian surface are reasonably well characterised from Viking Lander 1 and 2 and Pathfinder Landing sites. Its rock distribution with size has been modelled statistically by Golombek & Rapp (1997) providing a well-defined reference terrain environment. This data will provide the basis for the application of Bekker theory to determine tractive capabilities of legged vehicles on this terrain. [Bekker 1959, 1969]. In particular the problem of autonomous navigation across Martian rock-fields – such rock field statistical distribution with size may be modelled using an exponential function [Golombek & Rapp 1997].

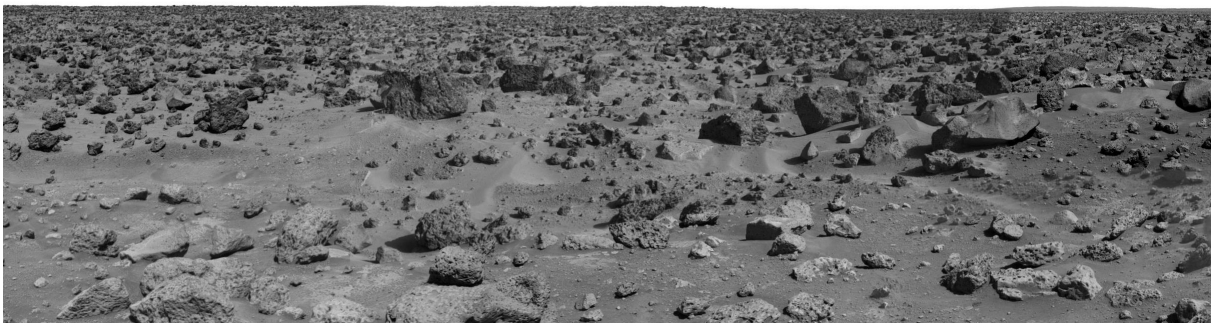

Figure 10 – Viking Lander 2 Panoramic Site Image [NASA/JPL].

The Viking Lander 2 site in Utopia Planitia has more and larger rocks than does the Viking Lander 1 site in Chryse Planitia. The rocks around Utopia Planitia are probably ejecta from impact craters near the VL2 site, while Chryse Planitia (the VL1 site) is more likely the location of outflow channels carved by flowing water [Strom 2002]. Many of the rocks are angular and are thought to be only slightly altered by the action of wind and other forms of erosion. Drifts of sand and dust are smaller and less noticeable at the VL2 site. The overall red colouring of the Martian terrain is due to the presence of oxidized iron in the regolith. The pink colour of the sky is caused by extremely fine red dust that is suspended in Mars' thin atmosphere [Viking 1978].

Based on rock distribution data collected during previous Mars missions, the Viking Lander 2 site is the most heavily covered region on Mars where detailed terrain and soil data exists. Therefore, VL2 was selected as the ideal landing site for a legged vehicle of this magnitude. Details of the rock distribution values can be found in Section III.3.

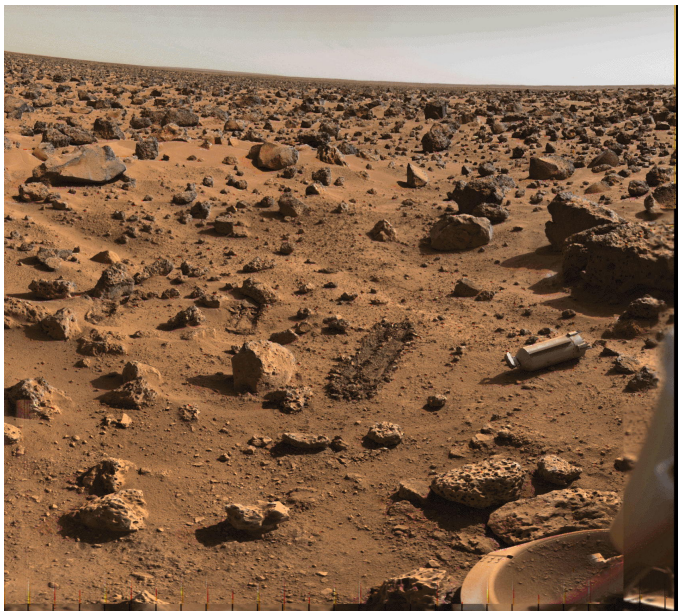

Figure 11 – Viking Lander 2 Site Image [NASA/JPL].

Considerations that must be taken into account based on this landing site include solar constraints, safe landing requirements, rock distribution, and navigation capabilities. Although three of these areas will be reviewed, it is assumed that "safe" landing of a mobile platform can be attained at VL2, as shown in entry, descent, and landing system (EDLS) simulation work not discussed here [Allouis 2004].

V.2.1. Additional VL2 Region Environment Data

The Viking landers continuously monitored weather at the landing sites after landing. Weather in the Martian midsummer was repetitious, but in other seasons it became variable and more interesting. Cyclic variations appeared in weather patterns (probably the passage of alternating cyclones and anticyclones). Temperatures at the VL2 landing site during midwinter dust storms varied as little as 4°C on some days. The lowest predawn temperature was -120°C, about the frost point of carbon dioxide. A thin layer of water frost covered the ground around Viking Lander 2 each winter. A thin layer of water ice is also left behind after the melting of CO_2 ice [Strom 2002].

Barometric pressure varies at each landing site on a semi-annual basis because carbon dioxide, the major constituent of the atmosphere, freezes out to form polar caps at each pole. The carbon dioxide forms a cover of snow and then evaporates again with the coming of

spring in each hemisphere. When the southern cap was largest, the mean daily pressure observed by Viking Lander 2 was as low as 7.3 millibars; at other times of the year it was as high as 10.8 millibars. For comparison, the surface pressure on Earth at sea level is about 1,000 millibars [Kieffer 1992].

Martian winds generally blow more slowly than originally expected. Scientists had expected them to reach speeds of several hundred metres per second from observing global dust storms, but neither lander recorded gusts anywhere near that. During the Viking missions, the average wind velocities were measured at considerably lower values, ~2 m/s at night and ~6-8 m/s during the day. Maximum downslope winds of up to 30 m/s are predicted at the lower altitudes of steep slopes near dawn due to thermal heating of the atmosphere near the soil [Kieffer 1992]. The orbiters observed more than a dozen small dust storms. During the first southern summer, two global dust storms occurred, about four Earth months apart. Both storms obscured the Sun at the landing sites for a time and hid most of the planet's surface from the orbiters' cameras. These winds are of particular interest for solar cell sizing, as dust settling on solar cells will reduce their effectiveness over time. Analysis shows that Martian winds are not strong enough to remove settled dust from solar panels [Landis 1998].

3. MISSION PAYLOAD AND SCIENTIFIC OBJECTIVES

V.3.1. Primary Payload

The search for life elsewhere other than Earth may be considered to be one of the most scientifically important questions of the 21st century. Although the nature of extraterrestrial life (if it exists or has existed in the past) is unknown, there are certain physical and structural constraints that dictate certain aspects of its nature. Most importantly, biomolecules associated with energy transduction require the ability to store electronic energy thereby dictating aspects of their physical molecular structure. The Raman technique is ideally suited for the identification and characterisation of biomolecules, and has such been selected as the primary payload.

V.3.1.1. The Raman spectrometer

Raman spectroscopy provides real-time in-situ high-resolution spectra of the molecular structure and chemical species of solid, liquid (including aqueous) or gaseous samples without the need for sample preparation. Raman spectroscopy detects the vibrational states of molecules which are dependent on the molecular structure. It can be used to detect analytes in single bacterial cells and fluid inclusions in minerals [Parnell *et. al.* 2002]. Raman spectroscopy is non-destructive and non-intrusive. Near-infrared (NIR) wavelengths are required for Raman spectroscopy as optical wavelengths tend to excite biomolecules (autofluorescence), swamping the Raman signal (though fluorescence is useful for epifluorescence microscopy). Unlike infrared absorption spectroscopy, Raman spectroscopy is unaffected by water so it is also suitable for aqueous solutions (eg. water pollution investigation), ice cores and mineral fluid inclusions. Raman spectra are less cluttered than

infrared absorption spectra making peak overlap much less likely and enabling easier identification of samples. Raman spectroscopy is based on the Raman effect such that a small fraction ~10^{-6}-10^{-8} of incident radiation scattered by certain molecules is shifted to different wavelengths, the spectrum of the shift depending on the chemical structure of the molecules generating the scattering. The difference in wavelength (wavelength shift) between incident and scattered radiation is due to the molecular vibration changes in the sample – these usually correspond to infrared absorption energy intensities.

The Raman scattered radiation is of two types: Stokes scattering and anti-Stokes scattering. For comparison, Rayleigh scattering represents elastic collisions between the incident photon and the molecule so that Rayleigh scattering has the same wavelength as the incident radiation – it comprises the vast majority of the scattered radiation. Stokes lines are shifted to longer wavelengths than the Rayleigh peak while anti-Stokes lines are shifted to shorter wavelengths than the Rayleigh peak. The difference in wavelength is due to inelastic collisions with an associated energy loss/gain of $\pm\Delta E$ (i.e. energy of first vibrational level of the ground state). The shift pattern either side of the Rayleigh peak are identical except that the anti-Stokes lines are less intense than the Stokes lines, so only the Stokes lines are usually used. The Raman shifts are independent of the wavelength of the excitation source so the Rayleigh lines are normalised to zero with the Raman spectral lines being relative representing an absolute fingerprint of the sample. The ratio of anti-Stokes and Stokes intensities is directly proportional to the temperature of the sample as a larger fraction of molecules will be in the first vibrationally excited state at higher temperatures. Raman spectroscopy is more useful than infrared spectroscopy for organic compounds, eg. Raman spectroscopy yields an intense 1600 cm^{-1} peak for double bond stretch vibration for olefins, which is not detectable using infrared spectroscopy.

The Raman band (200-4000 cm^{-1}) covers the vibration modes of most biomolecules (including CH stretch near 3000 cm^{-1}) and those of metal oxides in minerals including manganese oxide of terrestrial rock varnishes with broad Raman features at 590 cm^{-1} and 640 cm^{-1} that are characteristic biotic activity [Israel *et. al.* 1997]. Antarctic cyanobacteria require special strategies for survival in extreme environments of Antarctica – such strategies may also be expected in any putative former micro-organisms that might have inhabited Mars in the past (or even currently) [Wynn-Williams and Edwards 2000].

All biological energy acquisition mechanisms are based on molecular electron transfer reactions in a biological pigment linked to proton movement across cell membranes (redox couple) for energy storage in adenosine triphosphates (ATP). Photosynthetic pigments, which are aromatic ring structures such as the red pigment of bacteriorhodopsin found in halobacteria, are readily detected by Raman spectroscopy. Dry conditions in Antarctica invoke the secretion of water-replacement molecules to protect the microorganisms. To reduce their exposure to UVB and UVC solar flux whilst accessing photosynthetic active radiation (PAR) wavelengths, such microorganisms use protective biomolecules such as scytonemin, β-carotene, parietin, rhizocarpic acid and calcin. Indeed, the ratio of parietin and β-carotene may be used to assess changes in the environment. Scytonemin, a cyanobacterial

biomarker, is particularly long-lived in sediment and has a characteristic Raman band at 1590 cm^{-1}.

Biofilm deposits typically contain high concentrations of photosynthetic and UV-protective pigments with their distinctive functional molecular structures. These pigments give Raman bands between 1000-1700 cm^{-1} while structural organics give bands between 2750-3000 cm^{-1}. Cell membrane products are similarly detectable by Raman spectroscopy – porphyrins, carotenoids, isoprenoids and hopanoids. Hopanoids are indicative of eubacteria, and carotenoids of green and purple sulphur bacteria – 2α-methyl hopanes are indicative of cyanobacteria specifically. Indeed, hopanoid derivatives have been detected in relict stromatolite deposits from 2.5 billion year old cherts by Raman spectroscopy. Isoprenoids are characteristic of archaeobacteria indicating that non-photosynthetic organisms are also detectable by Raman spectroscopy. None of these biomolecules are known to form abiotically. Furthermore, the production of hydrated calcium oxalates by cyanobacterial colonies under stressed conditions may be indicative of their use as water storage mechanisms.

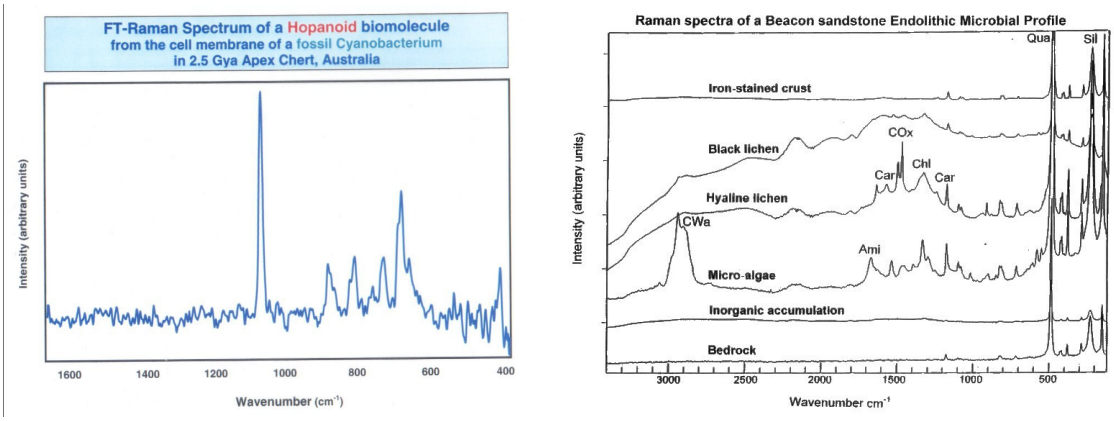

Figure 12 – a) Raman spectrum of hopanoid from 2.5 Gy old chert deposit and b) Raman spectrum from Antarctic endolithic organisms indicating the diversity of information generated from Raman.

Visible wavelength Raman spectroscopy is highly suited to the identification of inorganic compounds such as minerals [Haskins *et. al.* 1997; Wang *et. al.* 2003] – most mineral Raman spectra lie in the range 100-1700 cm^{-1} with most oxides and sulphides below 600 cm^{-1}. Most rock-forming minerals have characteristic Raman spectra, eg. calcite ($CaCO_3$) which can indicate aqueous deposition (1083 and 280 cm^{-1}), and hydrated species (due to OH stretch at 3000-3800 cm^{-1}). The number and intensities of peaks in this range depend on the incidence of OH groups and their context [Tarcea *et. al.* 2002].

Of particular interest for Mars application is detection at NIR of bands of hyroxylated minerals at ~1400 nm and 2200-2400 nm. Key absorptions at ~530 nm and 650 nm allows discriminated between Fe minerals including haematite (α-Fe_2O_3), maghemite (γ-Fe_2O_3) or goethite (α-FeOOH) and lepidocrocite (γ-FeOOH). However, infrared Raman is inferior to optical Raman for mineralogy due to its reduced resolution but between 500-100 cm^{-1}, there

are useful mineralogical bands, eg quartz, silica, haematite, etc. The expected peroxide and superoxide ions within the Martian surface layers are also Raman active (as in catalysis research) [Kolb *et. al.* 2002].

V.3.1.2. Benefits of Raman

Space and planetary environments impose severe constraints on the design of any scientific instrumentation. These constraints include requirements for low mass, low power consumption, low volume, low mechanical complexity, robustness to mechanical launch, flight and landing loads, robustness to extreme temperature variations from high temperature (in space) and in particular low temperatures (in space and on planetary surfaces), robustness to severe radiation exposure (during flight in particular). Raman spectroscopy is compatible with glass, quartz or sapphire sensor head windows and lenses. This differentiates Raman from infrared absorption spectroscopy which requires crystalline halides like NaCl rather than glass for its optical components. Any flight version of any scientific instrument will require design to conform to these constraints and a full suite of testing including vibro-acoustic testing, thermal cycling testing, radiation testing, etc.

The great advantage of Raman is the separability between the sensor head and Raman filters at one end of the fibre optic and the transmitter/detector and associated optics and electronics at the other. The instrument will be accommodated on the rover with the sensor head integrated into a drilling mechanism such as a ground-penetrating mole. In general, it is desirable to employ a movable scanning mirror to move the Raman laser beam over the sample site. Additionally, Raman spectrometry does not require sample preparation. The sensor head can simply be placed in front of the sample to be tested.

V.3.1.3. Raman Spectrometer Hardware

A Raman spectrometer comprises five components: a laser source of radiant energy, fibre optic coupling system, a radiation-detecting spectrometer, signal conditioning electronics, and a readout system.

In this project, the Raman spectrometer electronics will be built into the rover body. There will be two fibre optic sensor heads, each mounted to an extension built below the knee joint of the front legs. For science, the front legs can act as 3-DOF robotic arms and position the Raman sensor head as needed. It would use InGaAs detectors and wavelength stabilised/line narrowed NIR fibre-pigtailed laser diodes and have a maximum mass of 1 kg and maximum power consumption of 5 W [eg. Arvidson *et. al.* 2002].

Table 11 – Raman Spectrometer Payload Characteristics

	Min	Max	Units
Type	InGaAs		
Mass	1.00		(kg)
Power	5.00		(W)
Volume	0.002		(m^3)
Rate	2		(scans/s)
Single Image Scan	4000	10000	(scans/image)
Image Time	2000	5000	(s)
Image Time	33.33	83.33	(min)
Image Time	0.56	1.39	(hr)

V.3.2. Secondary Payload

Chemical sensing is the most fundamental of biological sensing modalities, common to almost all life forms, and is exhibited by single celled microbes for finding food (attractant) and avoiding poisons (repellent). Odour in particular is such a sensing modality. There is also the ubiquitous scientific sensor onboard planetary spacecraft that attempts to determine the elementary composition of planetary atmospheres and soil, i.e. the gas chromatograph-mass spectrometer.

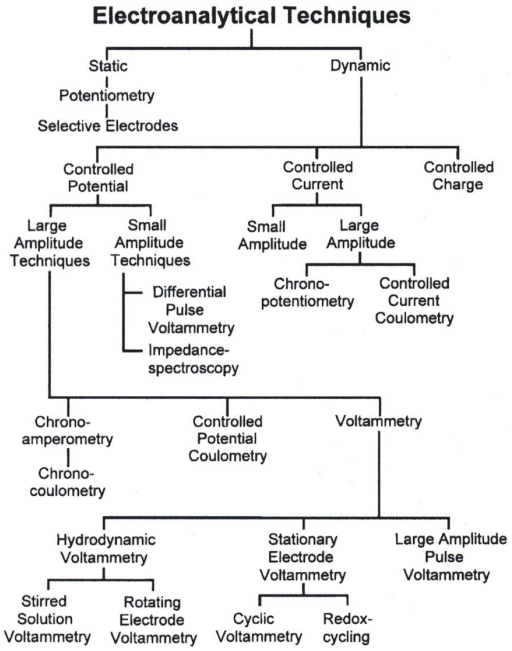

Figure 13 – Techniques for chemical/biochemical sensing [Ziegler et. al. 1998].

Taste and smell are chemical senses – taste is in fact augmented by smell indicating the partial fusion of these senses in the brain. The chemiresistor is the simplest of chemical sensors in which the resistance of a thin film material may be measured. Metal oxides have limited utility in terms of their specificity, high temperature operation up to ~500^{o}C, and requirement for ambient O_2. Conducting polymers may be used as chemical sensors – intrinsic conducting polymers are conductive without doping and extrinsic conductors are made conductive by impregnating with carbon black. Extrinsic conducting polymers are more versatile due to the wide range of polymers that can be used and they are almost entirely reversible. Chemical sensors made from different conductivity polymers embedded with carbon black particles provide an array of large bandwidth. Gas absorption causes swelling of the polymer, which lowers the conductivity. They are particularly suited to deployment as polymer coatings for surface acoustic wave sensors. Chemosensory cells of high sensitivity are the basis for the electronic nose. Given that most odours comprise an array of chemicals, the pattern of activation allows discrimination of a wide variety of smells [Freund & Lewis 1995].

V.3.2.1. The electronic nose

Electronic noses possess arrays of sensors, each sensor producing an electronic output as a function of sensor-specific chemical interactions. The combined electronic signals from the array give a characteristic pattern which can be correlated with a given odour or set of volatile compounds. The strength of the signal reflects the concentrations of each set of compounds. One difficulty is the degree of selectivity which suggests that a range of relatively unselective sensors should be employed with different responses to a range of gases – such an approach would require the use of neural networks trained to deconvolve the data. This makes such sensors suited to neural network processing and classification [Pearce 1997b].

There are two types of acoustic wave sensors that are sensitive to mass – the quartz crystal microbalance (QCM) and the surface acoustic wave (SAW) detector. Both devices are based on the generation of acoustic waves in piezoelectric materials by the application of metal electrodes either side of the crystal. A change in mass causes a shift in the frequency/velocity of the acoustic waves. Applying a thing film coating turns such devices into chemical sensors. Resonance occurs due to constructive interference between waves when the crystal thickness equals multiples of the acoustic half-wavelength [Lang *et. al.* 1999].

Bulk acoustic wave (BAW) devices have been proposed but SAW devices offer much greater flexibility. SAW devices are constructed from a piezoelectric substrate – typically $LiTaO_3$ or $LiNbO_3$ – with metallised electronics including reflector gratings implanted on the surface. The reflector gratings act as mirrors for the SAW and the electrode strip width and spacing are $< \lambda/4$ and determine the limit of sensitivity currently ~0.3 μm. Operating the SAW at high frequencies increases its sensitivity.

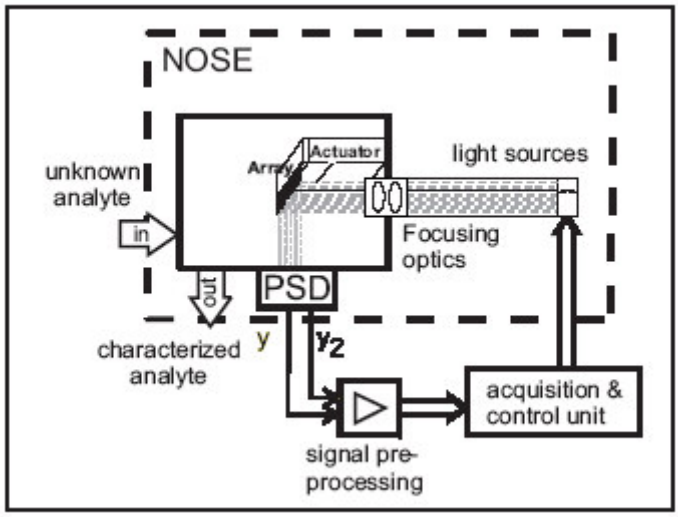

Figure 14 – Electronic Nose Schematic [Lang *et. al.* 1999].

An electronic nose based on a micromechanical array of Si cantilevers has been developed in which the cantilevers are sensitised with a number of different coatings such as metals, monolayers and polymers [Lang *et. al.* 1999]. The chemical reaction is thus transduced to mechanical deflection of the specific cantilever. Each cantilever was 500 μ in length, 0.8 μ in thickness and 100 μ in width with a spring constant of 0.02 N/m. Uncoated cantilevers provide references. Mass change from the accumulation of a small sample at the apex of the cantilever coated with a selective sensor will alter the resonant frequency of the cantilever, typically ~50 kHz.

An array of such devices with individually coated cantilevers provides the basis for a wide range of sensitivities. The cantilevers are sequentially read-out optically by recording the position of an incident light beam reflected from the cantilever by a photodetector array. A lock-in amplifier processes the oscillatory response of the cantilever deflection. A cantilever coating of zeolite ZSM-5, which absorbs water selectively provides the basis for a water sensor.

V.3.2.2. Microchip Design

The advantage of such array devices in process control or online chemical and physical analysis is not only their small size (~1 mm^3) but also their low cost and insensitivity to external disturbances. This allows disposable sensor arrays to be integrated seamlessly into silicon technology for applications such as biochemical analysis or drug testing. Such devices operate in various media with high speed and sensitivity, and offer applications, for example, to oenology or fragrance design [Lang *et. al.* 1998].

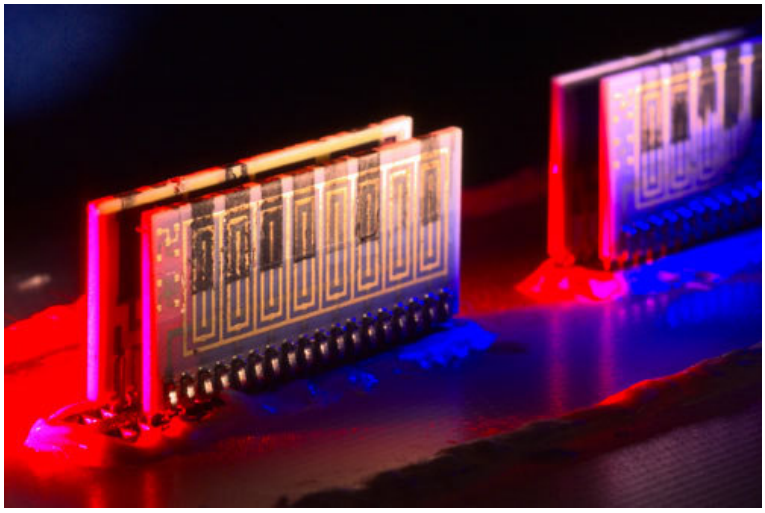

Figure 15 – Electronic Nose Microchip [JPL 2005].

Different polymers respond differently, so each chemical species may yield a unique electrical fingerprint. Using a greater variety of sensors yields a greater diversity of discrimination among a wide variety of chemicals. A 5-10 sensor head is reckoned to provide good results.

V.3.2.3. JPL ENose

The JPL ENose is a low power, miniature device which has the capability to distinguish among, identify and quantify 10 common contaminants which may be present as a spill or leak in the recirculated breathing air of the Space Shuttle or International Space Station. It has as its basis an array of conductometric chemical sensors made from polymer/carbon composite sensing films developed at Caltech [Freund 1995; Lonergan 1996]. It is an array of 32 sensors, coated with 16 polymers/carbon composites. The polymers were selected by analyzing polymer responses to the target compounds and selecting those which gave the most distinct fingerprints for the target analytes. The JPL development model was used in a flight experiment on the Space Shuttle flight STS-95 (October-November 1998) to determine whether it could be used as a continuous air quality monitor [Ryan 2004].

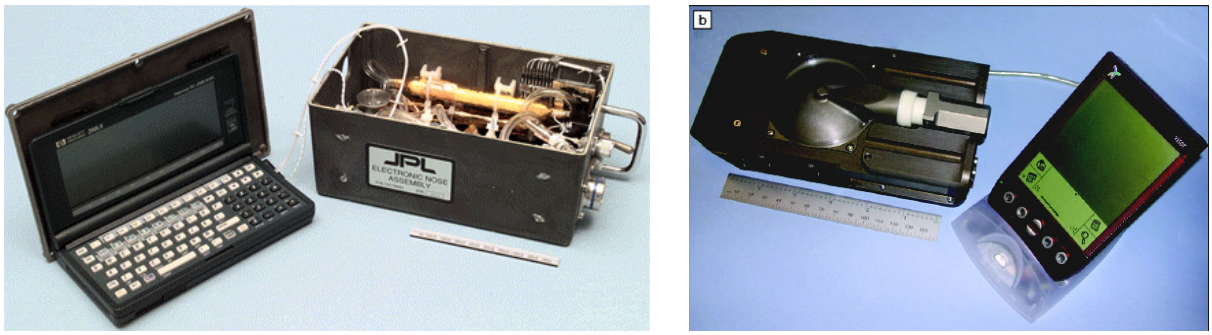

Figure 16 – a) JPL's First Generation Enose and b) JPL's Second Generation Enose [Ryan 2004].

The first and second generation JPL-developed Enoses are shown in Figure 16. The first generation device was used in the STS-95 flight experiment and has a volume of nearly 2 L, a mass of 1.4 kg (including the HP200 LX computer used for control and data acquisition) and uses an average 1.5 W of power. The mass and volume were determined primarily by the spaceflight-qualified container required for the device to be used in an experiment and can be reduced by a factor of 4 with no modifications to the sensor head or the electronics and minor modifications to the pneumatic system [Pearce *et. al.* 2002]. However, the walker rover will use the second generation hardware which weighs only 0.75 kg, takes up 0.001 m^3 in volume, and uses 1.5 W of power during the less than 100 seconds of operation [Ryan 2004]. Table 12 shows a breakdown of the Enose payload characteristics.

Table 12 – Enose Payload Experiment Characteristics

	Value		Units
Type	InGaAs		
Mass	1.00		(kg)
Power	5.00		(W)
Volume	0.002		(m^3)
Rate	2		(scans/s)
	Min	Max	Units
Single Image Scan	4000	10000	(scans/image)
Image Time	2000	5000	(s)
Image Time	33.33	83.33	(min)
Image Time	0.56	1.39	(hr)

VI. VEHICLE DESIGN

1. SYSTEM OVERVIEW

VI.1.1. Vehicle Mass Classification

Robotic explorers come in all shapes and sizes. Large macro-rovers of the order of 1 tonne are typified by the Russian Lunakhods that each drove many kilometres across the Moon's surface in the 1970s. Mini-rovers of mass around 100 kg are typified by the Athena-class and Marsokhod-class rovers and are generally designed with a high degree of autonomy for ranges of several kilometres. This is the class under which NASA's MERs fall, both weighing in at 185 kg. Micro-rovers with mass between 5-30 kg tend to have a moderate degree of autonomy for ranges up to 1 km. The Sojourner rover was a micro-rover with dimensions of 63 cm (length) x 28 cm (height) x 48 cm (width) and a mass of 11.5 kg. Nano-rovers of mass ~1 kg are a new innovation with limited ranges of < 10 m and limited capabilities, typically being tethered to a lander which supplies power and data transfer. Most of the European effort has focussed recently on nano-rover concepts to the exclusion of all other rover concepts until recent investigations into the ExoMars mini-rover. Nano-rovers are limited to tightly local exploration only and act as extensions to robot arms from the lander.

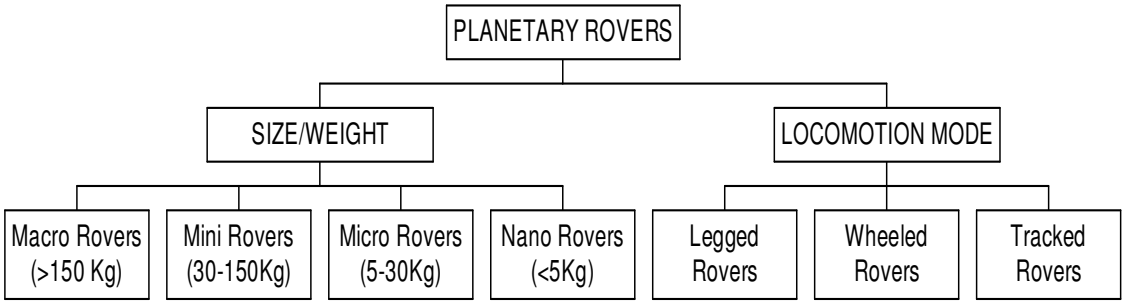

Figure 17 – Planetary Rover Classifications [Patel *et. al.* 2004].

Based on the definitions in Figure 17, the team is designing a micro-rover class walking vehicle for Mars exploration. In trying to keep the design mass near 20 kg, the team was highly constrained due to the masses of the structure, scientific payloads, and especially the motors at each leg joint.

The interest in keeping the mass in this region is several-fold. First, a less massive vehicle will require a lighter entry-descent-landing system, allowing additional payloads to be launched with this vehicle. Also, in comparison to the Sojourner rover, a legged vehicle should be able to traverse greater terrains than could be achieved by a vehicle of similar size, therefore eliminating the need for a significantly larger vehicle. And, as the vehicle gets larger, the motors required to lift the vehicle and payload will also need to increase. As motors are already quite heavy, this could easily drive the overall system mass outside of the micro-rover class. Additionally, it was expected that these motors would require as much if

not more power than Sojourner, therefore the mass-heavy batteries would need to be at least the same size.

VI.1.2. Operational Modes

- Movement – the most power-intensive operational mode for the vehicle.
- Locomotion Warm-up – brings the motors and boards into operating temperature range.
- Primary Payload Operations – though little power is needed, this needs to be accomplished without interruption from other operations.
- Power Recharge – batteries are charged based on their charging profile, likely requiring constant (though minimal) power from the solar array throughout the course of the day.
- Transmit Data – this power-intensive mode will need to be accomplished when the vehicle is not moving.
- Daytime Active Heating/Cooling – all areas of the system are thermally monitored and modifications to heat are made as needed.
- Night-time Active Heating – temperatures drop very low at night on the surface of Mars and systems will need to be kept within their survival or operating thermal ranges.
- Sleep – minimal power is needed for onboard systems in this mode, as most systems are shut down at night.

2. STRUCTURE

Rover electronics will be housed in a separate, heated electronics box (dubbed the warm electronics box or WEB by JPL), the shell of which is built from the same aluminium. The WEB will also make up the main body, or thorax, of the rover. Mounted on top of the robot thorax (or, more accurately, the top panel of the thorax itself, with minor extensions) will be the solar array, providing means of real-time power and battery recharge. The interior of the WEB will contain all rover electronics, batteries, and payloads. Within the box, aerogel will be used to help retain heat energy to keep the equipment within thermal operating constraints.

The dimensions of the two Mars rover designs (Sojourner and the MERs) as well as an in-house legged robot kit, simulation rover, and the final design rover parameters are shown in Table 13.

Table 13 – Properties of existing wheeled explorers, prototype kit, simulation, and the final Walker design parameters.

	Sojourner	MER Total (WEB)	Leg Kit Prototype	Sussex Simulation	Walker Design Parameters
Mass (kg)	16	185	2	20	23
Length (m)	0.63	1.6 (0.86)	0.25	1.0	0.7
Width (m)	0.48	2.3 (0.55)	0.125	0.25	0.5
L/W or W/L	1.31	1.56 (1.43)	2.0	4.0	1.4
Thickness (m)	0.15	0.36	0.045	0.14	0.15
Height (m)	0.28	1.5	0.055 – 0.15	?	0.23 – 0.4
Clearance (m)	0.13	0.3	0.025 – 0.12	?	0.08 – 0.25

The WEB will be built from a metal-matrix aluminium composite made of P100 pitch-based graphite composite hot-pressed into aluminium 6061 alloy (further referred to in this text as simply aluminium) [Fujiwara 2004]. The dimensions of the WEB were selected based on the expected electronics, hardware and payload that it would be enclosing. The dimensions are similar to Sojourner, as the Walker is in the same rover mass category and the expected equipment that it will carry will be somewhat similar. Additionally, the 1.4 length-to-width ratio is similar to previous Mars missions, and is important in the design of the EDLS.

The WEB is lightweight and strong enough to withstand the forces applied to it throughout the mission and was specifically designed for space applications, with structural details noted in Table 14 [Rawal 2001].

Table 14 – Continuous-Fibre Reinforced MCC P100/6061 Aluminium Composite (0^o) Properties [Rawal 2001].

GENERAL	
Volume Percent Reinforcement	42.2
Density, ρ (gm/cm^3)	2.5
Poisson Ratio ν_{xy}	0.295
Specific Heat C_p (J/kg-K)	812
LONGITUDINAL STRENGTH	
Young's Modulus (x) (GPa)	342.5
Ultimate Tensile Strength (x) (MPa)	905
Thermal Conductivity K_x (W/m-K)	320
CTE_x (10^{-6} /K*)	-0.49
TRANSVERSE STRENGTH	
Young's Modulus (y) (GPa)	35.4
Ultimate Tensile Strength (y) (MPa)	25
Thermal Conductivity K_y (W/m-K)	72

A simple structural analysis was performed to determine the structural stability of the body of the rover during landing, since this is where the vehicle would receive the strongest forces applied to it. The analysis assumes a maximum deceleration of 50 times Martian gravity is protected for in the structural design and an upright landing of the vehicle (i.e. landing flat as though in walking position, with the legs folded atop during landing). At 50 Gs, the 23 kg vehicle must sustain nearly 5000 N of impact force.

Using Euler theory to determine the buckling force of the rectangular body of the vehicle:

$$F_{cr} = \frac{\pi^2 EI}{L_e^{\,2}} \qquad (14)$$

where:

F_{cr} = critical buckling load of the wall
E = Young's Modulus in the longitudinal direction, as shown in Table 14
I = moment of inertia of the rectangle where: $I = \left(\frac{bd^3}{12}\right)_{outer} - \left(\frac{bd^3}{12}\right)_{inner}$
b = rectangle width (width of the vehicle)
d = rectangle thickness (length of the vehicle)
L_e = effective length of the rectangle (thickness of the vehicle)

The material properties of the alloy located in Table 14 and the walker design dimensions in Table 13 are both used in the above equation along with the vehicle WEB wall thickness of 2 millimetres. Additionally, the vehicle body is considered to be a guided-free system in the

structural analysis of this example. The guided side of the body is bolted to the landing system, which is in direct contact with the ground where it could slip in any direction except through the terrain (the impact crater distance the vehicle makes upon landing is considered negligible in this stress analysis). The free side would be the top of the rover, which is not attached to anything and thereby a free system. In a guided-free system, the effective length is twice that of the actual length of the leg, therefore L_e is twice the height of the vehicle: 0.3 m.

With this information, the buckling force of the body of the vehicle was found to be 6.78E+09 N. The impact force of the vehicle on the ground when landing perfectly vertically is found to be 4.49E+03 N. Although this analysis shows that the vehicle would survive landing in this specific situation, a more advanced structural analysis would need to be performed in order to ensure that the structure would survive landing at all impact angles. However, a full engineering design of the vehicle must first be completed in order to properly accomplish this analysis.

3. LOCOMOTION SYSTEM

To date many advances have been made in all aspects of legged robotics. Biomimetic robots based on dozens of living creatures now exist that have remarkable detail in mechanics, artificial intelligence, and bioelectronics. Man-made materials used in some of these creatures mimic real muscle and some devices are used that accurately reflect the sensory capabilities of all sorts of creatures.

It is not the intention of this project to attempt to fully model an artificial muscle, as this technology is still at an immature state of development and certainly not qualified for space applications at this point. Instead, it is the intention of this project to extract the principles of animal locomotion and adapt them to the control of electric motors for driving the legs for the development of an efficient walking Mars explorer. As with the control of any appendage, there are two primary parts: the joint and the link. Joint compliance is dominant in locomotion, as link compliance is a property of robustness to load failure and so a structural property not directly related to locomotion (though certainly important in high-loading situations such as jumping). Some vertebrates do incorporate flexible links in their legs to aid in sprawled-leg locomotion, but joint compliance is considered significantly more important in the development of legged robotics for space exploration.

Through this project, adaptations to muscle compliance will be incorporated into electric motors. Analysis is presented here into the way a legged vehicle can benefit from joint compliance models such as a spring-mass-damper model and the sigmoid function model to simulate biological muscle visco-elastic properties. The vehicle used in this design is a hexapod (6-legged) walker with 3 degrees-of-freedom (DOF) in each leg, modelled as an offset 2-DOF hip and a 1-DOF knee, as shown in Figure 18. A permanent magnet direct current (DC) motor actuates each DOF and data from different sensors (angular position and velocity, joint torque as estimated from motor currents, and foot force sensors) will provide feedback to the system for control purposes.

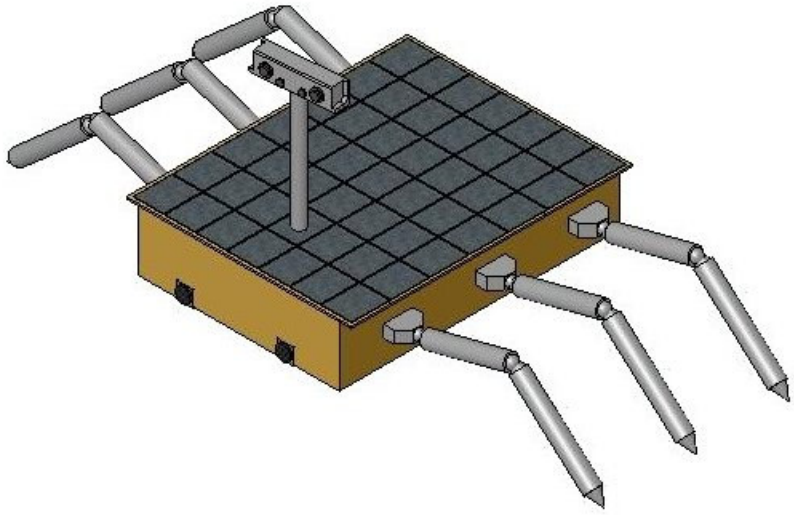

Figure 18 – Full View of the Walker Designed in this Project and Created in SolidWorks.

VI.3.1. Locomotion Expectations

Through the 90-day mission lifetime, the rover is designed to travel 1 km from its initial landing spot. This involves an expected travel distance of no more than 30 metres per day. Mathematically, over the course of 90 days, this means the vehicle could travel 2700 m, nearly 3 times the mission design distance. However, the rover will not be travelling 30 m every day, as sometimes primary payload experiments, data transfer to earth, or targets closer than 30 m apart (among other things) will require time and power that cannot be used for locomotion. These additional tasks and operational modes are described in Section VI.1.2.

VI.3.2. Leg Design

The leg design is based on terrestrial legged robotics projects, with specific account taken to the requirements for a space-rated walking robot, the most significant of which being the difference in gravity between Earth and Mars. Each leg was designed in 3 segments from cylindrical aluminium tube with an inner radius of 2 cm and wall thickness of 0.002 m. The first segment is at the hip, extending 5 cm from the thorax, only far enough away from the body to provide partial housing for the motor and gearing while the rest of the motor is enclosed in the WEB. This joint controls the forward-backward movement of the entire leg. The second segment, known as the femur and is 20 cm long. This length was selected to be just long enough to contain a single motor for vertical movement of the entire leg at the hip joint. The third segment, the tibia, is the longest segment measuring 25 cm and provides housing for a single motor for bending of the knee joint. This motor controls the vertical movement of the tibia. Several different feet designs were also briefly investigated. Though cylindrical feet are shown in Figure 19, it was decided that the feet should be left as the

cylindrical tibia, capped to prevent soil from packing into the foot. This design was used when modelling the soil interaction with the leg during walking.

As shown in Figure 19, the legs will be folded overtop of the thorax, when initially stowed in landing position. This will allow for minimal stresses on the legs during landing impact and gives the legs a chance to be "stretched" when the vehicle "wakes up" to allow for system testing before weight is applied to the legs.

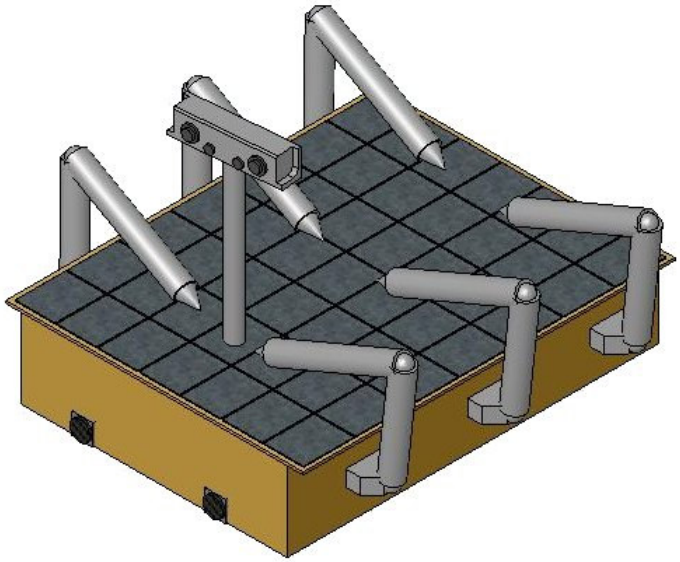

Figure 19 – Walker Vehicle with Legs Folded in Stowed Position for Landing.

VI.3.3. Structural Analysis

A structural analysis was performed on the legs of the vehicle to ensure they could withstand the walking forces applied to them throughout the duration of the mission. Using Euler theory to determine the buckling stress of the leg:

$$\sigma_{cr} = \frac{\pi^2 E}{\left(L_e / k\right)^2} \qquad (15)$$

where:

σ_{cr} = *critical buckling stress of the leg*
$k = \sqrt{I / A}$
I = moment of inertia of the cylinder where: $I = \frac{\pi}{4}\left((r_{outer})^4 - (r_{inner})^4\right)$
A = area of the cylinder cross-section $A = \pi\left((r_{outer})^2 - (r_{inner})^2\right)$
r = leg radius
L_e = *effective length of the leg*

Analysis was done as though a single leg could be required to sustain the weight of the entire system. With regards to buckling stress, the weakest segment of the leg is the tibia, as it is the longest section and is the farthest away from the centre of mass, thereby encountering the most stress. Additionally, the leg is considered to be a guided-free system, where the guided side would be the one in contact with the ground, as it could slip in any direction except through the terrain, and the free side would be the body of the rover, as it is free to move in any direction when "balanced" on a single leg. In a guided-free system, the effective length is twice that of the actual length of the leg, making L_e = 0.4 m.

The results show that a single leg can withstand a maximum stress of 2.9 GPa. With only a single leg supporting the entire vehicle weight, a normal stress of 3.4E+05 Pa can be expected. However, in practice there would always be at least 3 legs in contact with the ground at all times to support the vehicle, thereby reducing this value significantly.

VI.3.4. Motors

The DC motor is an electromechanical driven by an input voltage. The input voltage is applied to the armature coil, which applies a magnetic field to the motor, turning the output shaft. A diagram of this system can be seen in Figure 20.

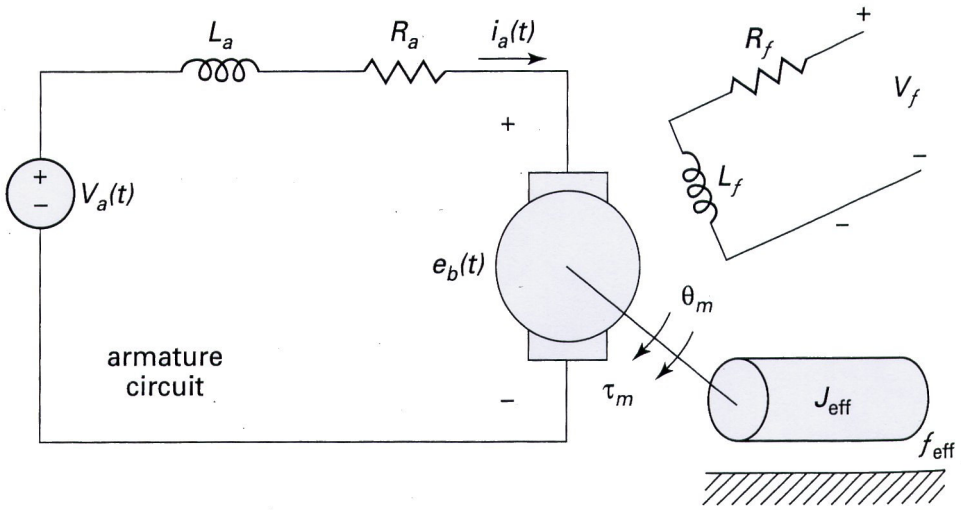

Figure 20 – DC Motor Equivalent Circuit [Ellery 2000].

Equations used to determine the total torque at the motor shaft are noted below in both mechanical and electrical terms (Ellery 2000):

$$\tau = K_t \frac{V_i - L_i \frac{di}{dt} K_b \dot{\theta}_m}{R_i} = \tau_m + \tau_l' = J_{eff} \ddot{\theta}_m + b_{eff} \dot{\theta}_m \qquad (16)$$

where:

t = *torque*
K_t = *motor torque constant*
V_i = *applied control voltage*
L_i = *armature coil inductance*
i = *armature current*
K_b = *motor electromechanical torque constant*
R_i = *armature coil resistance*
τ_m *and* τ_l' = *torque at the motor shaft and at the load*
$\ddot{\theta}_m$ *and* $\dot{\theta}_m$ = *acceleration and velocity of the motor shaft*
J_{eff} = *effective combined inertia in the system*
b_{eff} = *effective viscous friction dampening coefficient*

The motors selected to control each of the joints on the vehicle are all the same. This helps to simplify the system design and reduces distinct testing costs through working with 18 copies of a single piece of hardware. The motors must also be able to fit within the 4 cm inner diameter of the leg segment tubing while providing the required torque Each motor assembly consists of the Maxon RE-25 motor, with Maxon GP 86:1 planetary gearhead, Maxon GS 4:3 spur gearhead, and HD Systems 25SHF 50:1 harmonic drive (to reduce backlash) [maxon 2004; HD Systems 2005]. This complete motor assembly produces an output of 0.17 rpm with

a 5371:1 gear ratio. Table 15 shows the motor and gearing used and their gearing ratios in order to determine the total gear ratio and rotation speed of the overall system.

Table 15 – Motor and Gearing Selections [maxon 2004; HD Systems 2005]

	Brand	Size	Length	Mass	Ratio In	Ratio Out	RPM	rad/s
			(m)	(kg)			(rpm)	(rad/s)
Motor	Maxon RE	25	0.0702	0.13	1.00	1	9550.00	1000.07
Planetary Gearhead	Maxon GP	32A	0.043	0.194	86.00	1	111.05	11.63
Spur Gearhead	Maxon GS	20A	0.019	0.012	1.33	1	83.31	8.72
Harmonic Drive	HD Systems	25 SHF	0.037	0.01	50.00	1	1.67	0.17
Total			**0.1692**	**0.346**	**5731.9**	**1**	**1.67**	**0.17**

This motor assembly will need to turn a worm gear to offset the power along the shaft perpendicularly to move the leg segment.

In designing the leg, it is important to know the maximum torque on each joint throughout a single step. Although it is visibly obvious that the most torque will be required to lift the body of the rover when making contact with the ground, the equations used to determine this free body system are [Ellery 2004b]:

$$\tau = \frac{c_i m_t}{n_{contact}} \tag{17}$$

where:

$$c_i = \sum_{j=0}^{i-1} \frac{m_j}{m_T} r_i + \sum_{j=i+1}^{n} \frac{m_j}{m_T} s_i \tag{18}$$

and:

$n_{contact}$ = *number of legs exerting force on the ground during the step cycle*
n = *number of links in the system*
i = *link number*
τ = *torque*
c_i = *connection barycentre for link i*
m_i = *mass of the link*
m_t = *total system mass*
r_i = *inbound radius from centre of mass of the link centre*
s_i = *outbound radius from the centre of mass of the link centre*

The method used to determine the system torque involves determining the torques around the barycentre (centre of mass) of each segment of the leg based on the lengths and masses of the sections of the leg on each side of the barycentre. The value $n_{contact}$ is determined based on the gait pattern used, such as during the wave gate, where $n_{contact}$ is 1. However, during tetrapod and tripod gate walking, the value is 2 and 3, respectively, because that is the number of legs

moving simultaneously in the pattern. Although wave gait will be used initially while the system "learns" how to traverse the new and strange terrain, it is expected that tetrapod gait locomotion will eventually be used more actively.

To determine the power required based on the torque of a motor, the following equation is used [MicroMo 2005]:

$$P = 1.002(\tau\omega) \qquad (19)$$

where:

P = rotational mechanical power (W)
1.002 = conversation factor
τ = torque (N-m)
ω = motor angular velocity (rad/sec)

Using the equations above during tetrapod gait locomotion, Table 16 was created to determine that a total of 11.4 N-m is required to move a single leg through a full step cycle.

Table 16 – Barycentre Torque/Power Calculations

Link No.	Link Length	Link Mass	Max. Dist. Cent.	Cumulative Mass	r_i	s_i	c_i	T / step	P / step
	(m)	(kg)	(m)	(kg)	(m)	(m)	(m)	(N-m)	(W)
0	0.25	15.979	0.000	15.979	0.000	0.625	0.035	0.425	0.074
1	0.05	0.378	0.275	16.357	0.275	0.350	0.196	2.369	0.414
2	0.2	0.475	0.400	16.831	0.400	0.225	0.276	3.328	0.582
3	0.25	0.507	0.625	17.338	0.625	0.000	0.436	5.260	0.920
						Totals:		**11.382**	**1.990**

A safety margin was incorporated in that each motor may need to provide torque equivalent to the entire leg torque requirements at any time. In the case of link number 3, this is just over a factor of 2. For the motor system described above, it requires less than 2 W of input power to produce the needed 11.4 N-m of torque to move the leg.

Through simple trigonometry the average length of a leg during a step and the step length created from rotating that leg through a 90° hip rotation to provide forward movement can be calculated as follows:

$$l_{leg} = l_{femur} + \alpha l_{tibia} \qquad (20)$$

$$l_{step} = \sqrt{2(l_{leg})^2} \qquad (21)$$

where:

l = length of extended leg during a step, length of leg segment or step length
α = average angle between femur and tibia during step (45°)

With an average step length of 0.53 m, it would require the rover to take more than 56 steps to cover the mission required 30 m per day. The 11.4 N of torque required per step can be produced on these motors with nearly 2 W of power, thereby 112 W of power is required for the 56 steps to move the vehicle the required distance per day. As two legs are moved simultaneously in a tetrapod gait, this means that 224 W of power is required for vehicle locomotion per day. These values are summarised in Table 17.

Table 17 – Total Power Required for Walking in Tetrapod Gait

Leg Characteristics	Value	Units
Ave Leg Extension	0.376776695	(m)
Ave Step Length	0.532842712	(m)
Ave Hip-Ground Length	0.45	(m)
Steps / Day	56.30179281	
Torque / Step / Leg	11.392	(N-m)
Power / Step / Leg	1.991595253	(W)
Power / Day / Leg	112.1303833	(W)
Power / Day / Tetrapod	224.2607666	(W)

VI.3.5. Compliance

Compliance is the ability of an object to yield elastically when a force is applied [Merriam-Webster 2005]. The mechanics of a robotic leg and the equations required to move a leg from one place to another are well known. However, the investigation of compliance within that system has been far less studied. There exist numerous models in the subject of compliance ranging from joint to segment modelling and controlled through hardware or software.

Passive and active compliance provides stability of the robot to conform to terrain containing height disparities proportional to its size [Kirchner *et. al.* 2002] using:

- Springs built into the linear joints of each leg
- Spring-like proportional feedback position control at each revolute joint
- Reduction of joint stiffness in response to increased loads
- Distribution of vertical load among the supporting legs.

Rather than attempt to fully model an artificial muscle or flexible materials to simulate leg segments, it is the intention of this research to extract the principles of animal locomotion and adapt them to the control of electric motors for driving the legs. The example of artificial muscles will certainly be an avenue to examine in the future, but are currently still in an immature state of development and do not have the heritage expected in most space-rated vehicles.

Instead, joint compliance through control system development will be explored, as the investigation of compliance within an electric motor has been far less studied. For example,

the overall motor torque with and without the effects of compliance can be determined through adding a feed-forward compliance factor into the control loop. This project examines two joint compliance models in detail.

First, the feed-forward compliance function to model a simple spring-mass-damper system, such as Hooke's Law, is a simple replacement of displacement with the difference between joint equilibrium position and the deflection from equilibrium. Second, a more complex nonlinear sigmoid function is used to help a system converge to a desired output by limiting extreme deflections. It is expected that these models will emulate muscle compliance through feed-forward control of the joint motors. There also exist numerous biological muscle models, but this research project will concentrate on the above two examples, leaving more advanced biological muscle models to be investigated in the future.

To add compliance (D^*) to the motor system discussed in Section VI.3.4, the following PD motor control equation is used [Ellery 2004]:

$$\ddot{\theta}_i = \ddot{\theta}^d + \left[K_v\left(\dot{\theta}^d - \dot{\theta}\right) + K_p\left(\theta^d - \theta\right)\right] + D^* \qquad (22)$$

where:

$\ddot{\theta}_i$ = *motor acceleration with error and compliance considered*
$\ddot{\theta}^d$ = *motor acceleration without error or compliance considered*
K_v = *velocity feedback gain to minimise overshoot*
K_p = *position feedback gain to reduce steady-state error*
$\left(\dot{\theta}^d - \dot{\theta}\right)$ *and* $\left(\theta^d - \theta\right)$ = *velocity and position error*

The overall motor torque with the effects of compliance modelled can be determined through adding a feed-forward compliance factor to the torque equation discussed in Section VI.3.4:

$$\tau = \tau_m + \tau_l' + D^* = J_{eff}\ddot{\theta}_m + b_{eff}\dot{\theta}_m + D^* \qquad (23)$$

where:

D^* = *compliance factor*

Hooke's Law

Hooke's Law is the linear proportional relationship between the distance a spring is stretched and the output force given by the energy stored in the spring. The constitutive law of the spring is given by the following equation:

$$F = k \cdot x \qquad (24)$$

where:

F = *force*
k = *spring constant*
x = *displacement*

The feed-forward compliance function to model Hooke's Law is a simple replacement of displacement with the difference between joint equilibrium position vibration and the deflection from equilibrium. Compliance using Hooke's Law can be determined through the following equation which shows that when $\delta = \theta$, there is no spring effect on the system.

$$D^* = k(\theta - \delta) \qquad (25)$$

where:

θ = *distance*
δ = *displacement error*

Investigation will be done into determining the spring constant that is appropriate for different conditions, i.e. different soils, different mass loading, pressure distributions, etc. It is expected that different spring constants will be required under different conditions. It may be appropriate to explore altering the spring constant adaptively.

Sigmoid Function

The sigmoid function is used to help a system converge to a desired output. Mathematically speaking, it is simply a special case logistic function or curve that is asymptotically bounded on both extremes of the equation [Wikipedia 2005a]. The sigmoid function has a near-linear slope between the region where it becomes asymptotic or convergent on the desired results and is achieved using the exponential function.

The sigmoid function is used in neural networks as a non-linear transfer function that helps make outputs reachable. The non-linearity is significant. If the transfer function were linear, each of the inputs would be multiplied by the same proportion, which could cause the entire system to "drift" [Anderson 1995].

The sigmoid function: $f(x) = \dfrac{1}{1+e^{-ax}}$ is graphed below for different values of a:

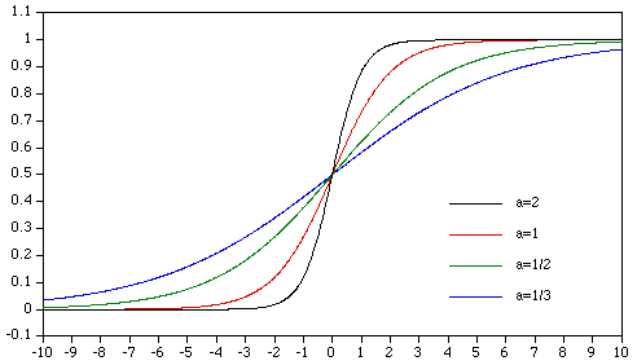

Figure 21 – Sigmoid Function Charted for Various Values of *a* [Bourke 1997].

This helps to visualize how variations of *a* will affect the sigmoid curve. This value can be modified to better fit the desired compliance model for sharp or gradual joint variation. This function arises in many dynamical systems because it is the solution to a first order differential equation [Bourke 1997]:

$$\frac{dx}{dt} = kx - ax^2 \qquad (26)$$

where:

$\frac{dx}{dt}$ = *change in distance over time*

a = *constant to determine the slope of the sigmoid function line*

To use the sigmoid function to determine the compliance model, the equations need to incorporate joint equilibrium position and deflection, as in Hooke's Law. Determination of the feed-forward function using the example sigmoid function described above is found through simple substation of position:

$$\frac{d(\theta-\delta)}{dt} = k(\theta-\delta) - a(\theta-\delta)^2 \qquad (27)$$

$$D^* = \frac{1}{1+e^{-a(\theta-\delta)}} \qquad (28)$$

The compliance factor determined through the function above can be customised through the slope constant to produce extreme or gradual response in the feed-forward model. As shown in Figure 21, a higher value of *a* will produce a more rapid response in the control of the joint motors. Through testing after the completion of the entire control system, it can be determined what the optimal value of this constant would be to provide the greatest benefit to a compliant leg design.

Additional Compliance Models

The compliance models described above are certainly not the only ways to simulate compliance, though each does provide a different approach to modelling compliance around a joint. For example, Hill (1953) hypothesized specific relationships between the force generated by a muscle and the speed at which a stimulated muscle contracts under a given load. A stimulated muscle may contract to 1/3 its size at a particular speed. When that muscle is attached to a load, the speed and size to which it contracts decreases. In other words, as the load increases, the muscle cannot lift the load as far. There are numerous visco-elastic models that have been developed based on Hill's force-velocity concept, but will not be examined in this study.

Additionally, there are ways to model compliance beyond the joint. Vertebrates supplement muscle/joint compliance through a flexible spinal column, which twists with each step to provide a more fluid movement. This also assists in ensuring accurate ground contact of the foot and additional reflex capabilities with each step. Furthermore, compliance within the leg structure exists in nature. Many arthropods have elastic energy-storage mechanisms such as unique material properties within the leg, such as the rubbery protein called resilin, that allow it to bend under their own weight before returning to its resting position [Lou 2003]. This helps to add spring-like movement into each step and aids in agile. However, in the investigation of compliance involved with this project, it was decided to limit the topic of compliance to those models involving the joint alone as these are expected to be dominant.

Though the complex interconnected field of compliance is understood in nature, at this stage only one aspect of compliance is investigated at a time. However, once an accurate model of compliance has been developed for joint control, the addition of the impacts of compliance in these areas should certainly be investigated.

Compliance Summary

The investigation into the comparison between compliant and non-compliant models will require a fully operational control system for the walking robot designed here in this report. Once the control system is developed, both analytical modelling and experimental assessment will be required to accurately resolve this question.

Based on the research done through the design of this robot, it is expected that each of the compliance models discussed above will show an improvement over the non-compliant model. The metrics used to determine this will be drawbar pull, mean free path determination, and obstacle negotiation capability. The incorporation of muscle-like behaviours into electric motors should enable legged robots to better cope with the loose regolith and the obstacles found on Mars. This will be determined based on the measurement of the forward tractive effort of the vehicle (drawbar pull), mean free path determination, and obstacle negotiation. Although joint compliance is expected to benefit legged explorers, for planetary environment deployment, this will likely yield a complex trade-off between performance enhancement and resource availability (i.e. power).

4. POWER

Several primary power system options were investigated by the team. First, the use of nuclear RTGs was discussed, but given a short mission lifetime, the long-life benefits of RTGs would certainly not be exploited and was therefore considered unnecessary. Additionally, the landing of a nuclear device on another celestial body may not be well received by the world population.

An investigation into future technologies was also done. One consideration was to use paintable solar cells, which involves the combination of minute particles called quantum dots with a polymer to make a plastic that can detect infrared energy. This polymer could be painted to a surface to collect energy and pass it into the electrical system of any device (McDonald 2005). However, such a new up-and-coming technology certainly does not have the heritage to be considered a realistic space application at this time, so the use of future technologies was discarded from this study.

Instead, the use of batteries and solar arrays was selected for this project as discussed below.

VI.4.1. Solar Arrays

The primary use of power during the mission is driving the motors during the locomotion phase of the mission. The energy required to do this will come directly from the solar arrays.

The solar cells selected for this rover are triple-junction based on the GaInP/GaAs/Ge cell technology; the same technology was used on the MER missions. Technical information the triple-junction solar cell used in this design can be found in Table 18 along with a diagram of what the cell looks like in Figure 22.

Table 18 – Properties of the Triple-Junction Solar Cells Used in this Design [Spectrolab 2002]

Cell Properties	Value	Units
Structure	GaInP2/GaAs/Ge	
Space : Ground Diff.	1.5	%
Cell Height	0.02	(m)
Cell Width	0.04	(m)
Cell Surface Area	0.0008	(m^2)
Mass	0.85	(kg/m^2)
Mass / Cell	0.00068	(kg)
Power	135.3	(mW/cm^2)
Power	1353	(W/m^2)
Power / Cell	1.0824	(W)
Voltage	2.23	(V)
Average Load	16.1	(mA/cm^2)
Average Load	161	(A/m^2)
Average Load / Cell	0.1288	(A)
Efficiency	26.5	%

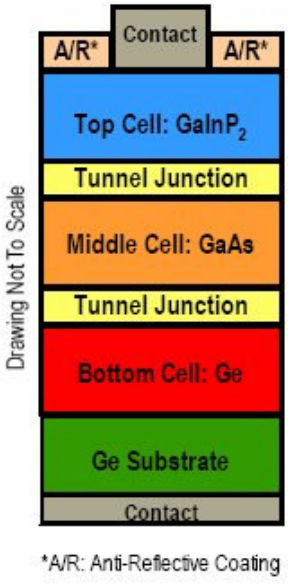

Figure 22 – GaInP2/GaAs/Ge Triple-Junction Solar Array Schematic [Spectrolab 2002].

As discussed in Section VI.3.4, the wave gait will be initially used until a point at which the tetrapod gait will be used. When walking, an average of 120 W per leg is required for locomotion, meaning tetrapod gait locomotion requires 240 W to move both legs simultaneously.

As shown in Table 13, the rover is 70 cm long and 50 cm wide. This gives a top surface area of 0.35 m^2. Since the first segment of the 2 cm radius legs extends 5 cm from each side of the

thorax, that leaves 3 cm that the array can extend past each side of the thorax while still allowing the femur segment to go vertical when the legs fold overtop in stowed position. This provides an additional 0.042 m^2 surface area to the maximum array size allowed, totalling 0.392 m^2. It can be assumed that nearly 75% of the surface area of the solar array is covered by solar cells while the additional 25% incorporates the surface are taken up by connectors and open space between the solar cells.

For an array of this size, 360 0.02 x 0.04 cm cells can be fit into that area. Based on Spectrolab solar cell properties shown in Table 18 [Spectrolab 2002], nearly 390 W of power can be provided through these 360 cells at the beginning of the mission, without the incorporation of losses over time.

There are numerous situations that cause reduction in solar cell capabilities from tested values on Earth in clean-room environments. Some examples of this are [Landis 2004]:

- Distance of Mars from Sun (lower solar intensity than Earth)
- Suspended atmospheric dust (modifies solar spectrum and reduces intensity)
- Low operating temperatures (reduces efficiency)
- Dust deposits on arrays (reduces intensity)

Although most of these losses are included in cell properties in the table above, degradation due to dust deposits on the arrays is not. Dust deposits on the solar arrays during the Pathfinder mission were measured to account for a loss of 0.28% per sol over the first month (though long-term degradation is expected to be half that) [Landis 2004]. Given that maximum efficiency loss over the 90-day mission, it accounts for nearly 25% worst-case losses. Therefore, the 390 W provided by the 360 cells at the beginning of the mission will provide only 290 W at the end of the mission.

Based on the power requirements of moving the leg during locomotion (as shown in Section VI.3.4), 2 W of power is required to turn a single motor for one step and 224 W is required for tetrapod locomotion to move the vehicle 30 m. However, at the end of the mission, after a worst-case loss of 25% solar array efficiency, 280.8 W of power is required for tetrapod locomotion, as shown in Table 19

Table 19 – Walker Array Values

Walker Array	Value	Units
Cells Needed	259.17	
Cells Needed / Leg	129.58	
Array Area Needed	0.424096073	(m^2)
Array Width	0.53	(m)
Array Length	0.80018127	(m)
Loss / day	0.28	%
Max Power Per Leg (Start of Mission)	112.13	(W)
Max Power Per Leg (End of Mission)	140.39	(W)
Max Power (Walking) (Start of Mission)	224.26	(W)
Max Power (Walking) (End of Mission)	280.77	(W)

This provides an additional 10 W of power for performing non-locomotion-based tasks while walking without requiring extra power from the onboard batteries. There are several things that will be simultaneously requiring power while the vehicle is walking, such as data acquisition, image taking and processing, communications, and payload experimentation. As the mission gets close to this power-critical end of mission timeframe, the vehicle can go back to wave gait locomotion, thereby requiring only 140.4 W of power for locomotion and allowing nearly 150 W of power to non-locomotion-based tasks.

VI.4.2. Batteries

Electrical power is a precious commodity on Mars, and even more so during the Mars night where the rover relies solely on the batteries for power. Therefore, supplemental power is important. During daylight hours, the batteries will supplement power to the system to fulfil requirements above the nominal wattage provided by the arrays. At night, the batteries will provide power for data communications, control box heating, and scientific payloads as needed.

The lithium-ion batteries selected for this mission are packs made by Yardney/Lithion Inc., the same company that manufactured the MER batteries. An example of what the battery looks like is shown in Figure 23.

Figure 23 – Yardney/Lithion Inc. Mars 2001 Lander Battery, similar to what will be used in the Walker configuration [Yardney 2004].

The batteries selected for this vehicle are half-size Yardney NCP8-1 batteries with a specific energy of nearly 130 W-h/kg. They are made up of 8 cells, each 3.6 V and 4 A-h with a mass of 0.15 each. Two of these 28.8 batteries make up the secondary power system to be used on the mission. Each battery provides 115.2 W-h of power, totalling 230.4 W-h with a total mass of 2.44 kg [Yardney 2004].

Table 20 – Half-Size NCP8-1 Battery Characteristics Used on Walker Rover [Yardney 2004]

Half-NCP8-1	Batteries	Cells	Voltage	Current Lifetime	Mass	Energy Lifetime	Specific Energy
			(V)	(A-hr)	(kg)	(W-hr)	(W-hr/kg)
Cell	0	1	3.6	4	0.1525	14.4	94.42622951
Battery	1	8	28.8	4	1.22	115.2	94.42622951
System	2	16	28.8	8	2.44	230.4	94.42622951

This will be sufficient to power the thermal heaters during the night and provide secondary power as needed to supplement the solar arrays during the day and provide power in excess of the nominal power requirements for locomotion, science, or other unforeseen needs.

5. THERMAL

The thermal regulation of onboard equipment is essential to sustain the life of the rover because the Martian environment is very harsh. The thermal conditions are noted in Table 21.

Table 21 – Mars Thermal Conditions.

Conditions	Min T (°C)	Max T (°C)
Mars Atmosphere Extreme Temp.	-140	20
Mars Atmosphere Temp @ VL2 Site	-96	-3
Mars Surface Temp.	-99	22

All equipment and hardware on the rover has thermal constraints within which they work most efficiently and a larger range that must be sustained to ensure hardware survival. The requirements of some of the onboard equipment is as follows:

Table 22 – Thermal Constraints for Onboard Systems.

Hardware	Min T (°C)	Max T (°C)
Vitals	-40	40
Batteries	-20	40
Power (inside WEB)	-50	50
Power (outside WEB)	-105	55
RAD6000 Mainboard	-30	65
Inertial Measurement Unit (IMU)	-54	71
Motors (Locomotion)	-120	70
Thin Film Heater Around Motors	-120	115
Heater (Solar Panels)	-120	110
Motors (Instruments)	-120	85
Cameras (Operating)	-55	22
Cameras (Survival)	-120	70

VI.5.1. Thermal Control

In order to sustain these thermal ranges, there will be several systems used to regulate the conditions of the systems within the rover.

Gold Paint

To help prevent heat from escaping out of the rover body and cold air from coming inside, the outside of the rover body is painted with a gold coating. The gold coating helps reduce energy that is radiated (energy spread outward) from the rover body. The highly reflective gold finish effectively isolates the rover body from emitting heat energy out to the cold, sky temperature [Viotti 2005].

Aerogel

The rover is also kept warm by a special layer of insulation, called solid silica aerogel, which prevents heat from escaping outside of the rover body walls. Aerogel traps heat inside the rover body. It is a unique silicon-based substance nicknamed “solid smoke” because it is 99.8% air. Aerogel is one thousand times less dense than glass. Such a lightweight material

has benefits in making it much cheaper (in terms of mass penalty) to launch and fly to Mars [Viotti 2005].

Heaters

There is a combination of heaters used to thermally regulate the electronics in the WEB. First, passive heating released by onboard electronics will be utilised.

Second, Radioisotope Heater Units (RHUs) will be used to provide a constant 1-watt of heat energy. These lightweight heaters will be located throughout the rover to act as the primary form of onboard heating. RHUs help conserve nighttime battery power. While an electrical heater can be turned on or off, RHUs continuously provide about 1-watt of heat [US DOE 1998].

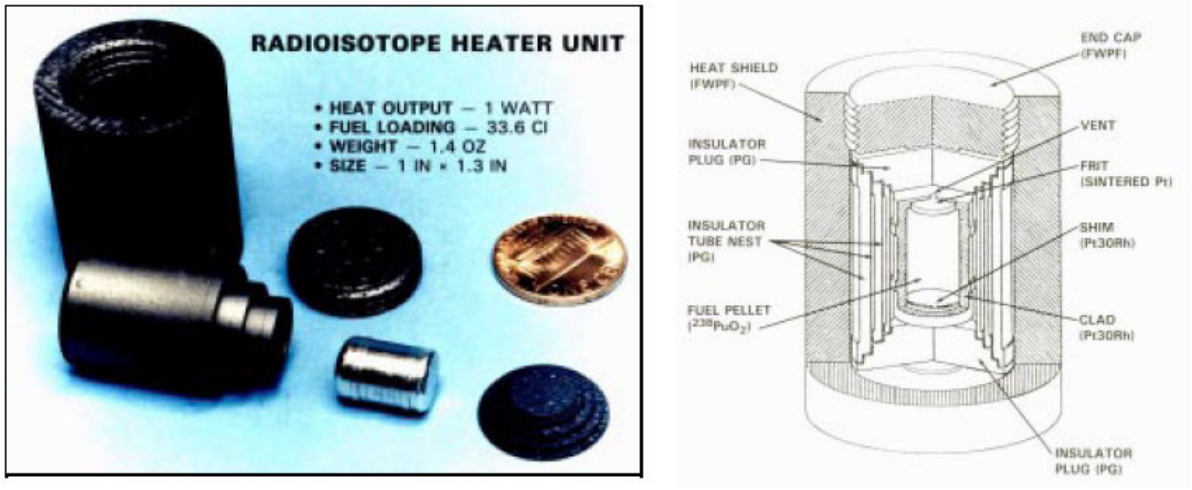

Figure 24 – RHU Image and Schematic [US DOE 1998].

Third, electrical heaters will be used as needed (usually at night) to provide additional heating when necessary to the WEB [Viotti 2005].

Thermostats

During the day, the rover actually might need to release heat if the rover electronics, electrical heaters, or RHUs generate excess heat. The rover has a "thermal switches" that turn the heaters on and off, depending on the "open" and "closed" set-points of the thermostats, which are similar to common thermostats used in homes. The thermal switches would automatically activate or deactivate heaters to maintain electronics and battery temperatures in the required range, even during the Martian night while the rover is "asleep" [Viotti 2005].

Heat Switches

The heat switch is another autonomous device that moderates a heat transfer path in order to maintain a specific battery temperature. If the batteries start to cool below -20º C, the heaters will turn on. If the temperature of the batteries approaches 20º C, the switch would increase the heat transfer path to the radiators so that the excess heater could be convected and radiated

away to the Martian environment. When the excess heat becomes necessary to maintain battery temperatures (especially during the night), the switch decreases the heat transfer path to the radiators in order to retain heat [Viotti 2005].

Heat Rejection System

An active heat rejection system will be required during transfer from Earth to Mars, however this is not a part of the study.

VI.5.2. Thermal analysis

A detailed thermal analysis would be required to accurately size each thermal system onboard; however, that is beyond the scope of this project. A simple thermal model to estimate the unassisted heat loss from the system (not including the benefits gained from any of the systems explained above) is expressed as [Fortescue and Stark 1995]:

$$Q_c = h_c A\left(T_{outside} - T_{inside}\right) \qquad (29)$$

where:

Q_c = *conductive heat transfer (W)*
h_c = *thermal conductivity (W/m^{2}K)*
A = *conductor's cross-sectional area (m^2)*
T = *temperature outside or inside the vehicle WEB*

The overall surface area of the vehicle's WEB is 1.06 m^2. Assuming the transverse thermal properties of the composite aluminium structure is the same in both the y and z directions due to the way the composite strips are laid, the thermal conductivity is 72 W/m-K over a 0.002 m thickness. In the worst-case scenario of the coldest day at the VL2 site (-96 ^{o}C) and the highest minimum hardware temperatures (the batteries at 20 ^{o}C), the total heat loss will be nearly 3 MW. This is unrealistic for a mission to Mars.

However, this does not take into account insulation such as aerogels, which will greatly reduce heat dissipation away from the vehicle. Assuming the following factors: 1) the aluminium composite outer skin retains the outside temperature perfectly, 2) the interior is completely saturated with silica aerogel, 3) the rectangular WEB is simplified to a sphere with surface area equivalent to the WEB's rectangular surface area and 4) the batteries are located at the centre of the sphere for ease of calculation, the following heat transfer equation can be considered [Fielding 2005]:

$$Q_c = \frac{KA\left(T_{outside} - T_{inside}\right)}{r} \qquad (30)$$

where:

K = thermal conductivity of aerogel [Ayers 2004] (0.017 W/m-K)
r = distance from the batteries to the outer skin (m)

With the spherical simplification in the equation, 2.2 W of heat are lost between the average 0.63 m distance from the batteries to the skin. This means that only 2.2 W of heat must be added to the centre of the system to maintain battery operation during the nighttime temperatures. Again, this oversimplifies thermal modelling of the system, but gives a relatively accurate understanding of the benefits of adding aerogel to the insulation of a system and the relative magnitude of the active heating requirements of the system. However, if the minimum distance from the centre of the vehicle thorax to the wall is used (0.075 m) with the same surface area (instead of the spherical simplification), 18.2 W of heat are lost.

The batteries inside the rover body need individual attention because they ultimately keep the rover alive. The baseline plan is to pack each battery with three RHUs (providing 3 W of thermal heat to each battery), one survival heater (to provide additional heating as needed during the night), and one heat switch that connects to separate radiators mounted on the walls of the rover body. This multi-staged heating strategy will ensure the batteries are kept in their operating thermal range.

Other forms of insulation and methods of controlling heat loss will be added make the thermal modelling more accurate as the vehicle design is further refined.

6. COMMUNICATIONS

The rover will be required to maintain contact with Earth during the 90-day missions for a number of reasons. Transferring images and scientific data collected by the cameras and payloads, relaying ground position and system health, and receiving command data to drive the vehicle are just a few examples of the importance of the communication system.

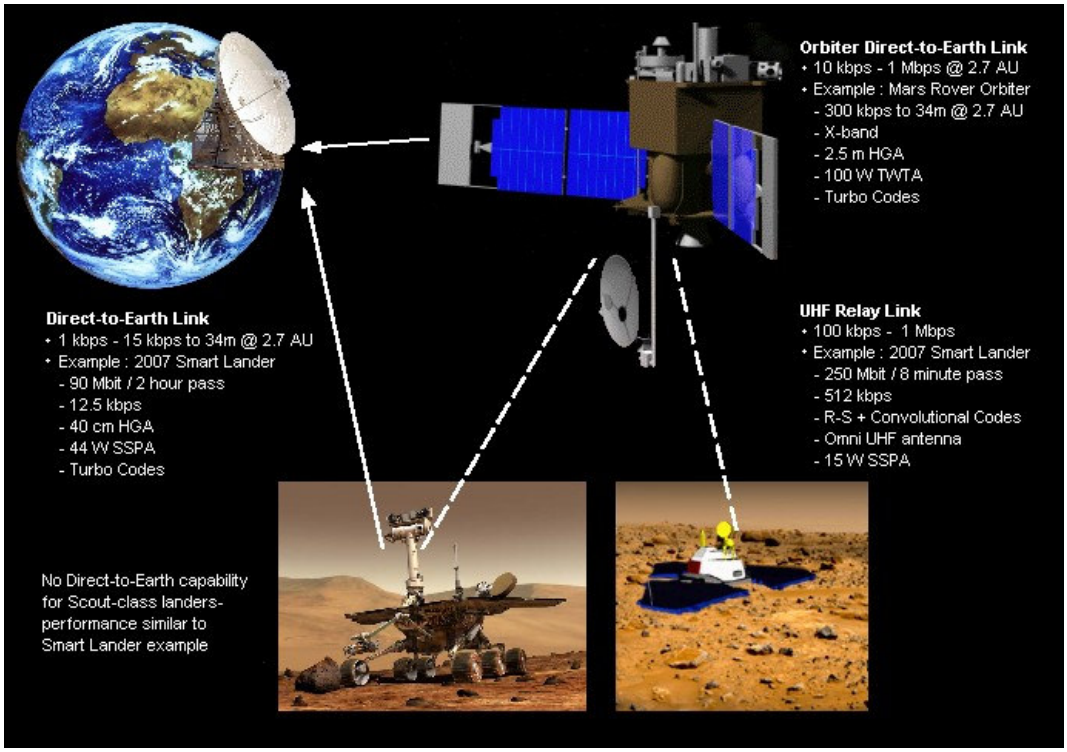

Figure 25 – How data gets from Mars to Earth [Lombry 2005].

VI.6.1. Rover Radio

The onboard radio modem works by sending and receiving data in the form of digital symbols. The radio modem transmits data packets, each consisting of 2000 eight-bit bytes, to its destination. On Mars, the data packets will transfer rover camera images and engineering telemetry detailing the operational status of the rover, as well as commands from Earth. The radio modem can either transmit or receive at any given time, with the direction of the flow of information between the rover and the intended target being controlled by the rover radio modem [Stride 1998].

There are two main parts to the radio modem: the digital portion on a single printed wiring board and the analog portion on a separate circuit board. The digital board acts as an interface between the analog board and the computer inside the rover. This digital board processes the data to be sent and received and directs the communication protocol, that is, when to transmit and when to receive. When transmitting data, the analog board turns on its 459.7 MHz UHF transmitter and sends out modulated radio waves, which correspond to the digital information formatted by the digital board. During receive, the analog board is tuned to radio waves that are the same 459.7 MHz frequency. It amplifies and filters them, and extracts (in a process called demodulation) the digital symbols in such a way that the digital board can input each information bit within a packet as it is received.

The rover radio modem also has a 0.5 W heater attached to its metal frame. This heater is used to raise the rover radio modem's temperature in the early hours of the Martian morning in preparation for the first telecommunication session of the day. This heater was added to the rover radio modem because its crystal oscillator is not temperature-compensated, allowing the transmit and receive frequency of the radio modem to change with temperature. As the radio modem temperature gets warmer, the frequencies increase; as the temperature gets colder, the frequencies decrease. The maximum permissible frequency shift is on the order of 5 kHz. Maintaining the desired temperature range will be accomplished in part by monitoring the engineering telemetry and issuing commands from Earth to control power to the rover radio modem heater [Stride 1998].

VI.6.2. Rover Antennas

All communication from the rovers will be located within the X-band frequency range. Normal X-band frequencies ranged from 7.25-7.745 GHz for downlink and 7.9-8.395 GHz signal uplink. Other commonly used communications frequencies are expressed in Table 23 [Montero 2002].

Table 23 – Commonly Used Frequency Bands in Communications [Montero 2002]

Band Name	Frequency Range
HF-band	1.8-30 MHz
VHF-band	50-146 MHz
P-band	0.230-1.000 GHz
UHF-band	0.430-1.300 GHz
L-band	1.530-2.700 GHz
FCC's digital radio	2.310-2. 360 GHz
S-band	2.700-3.500 GHz
C-band Downlink:	3.700-4.200 GHz
C-band Uplink:	5.925-6.425 GHz
X-band Downlink:	7.250-7.745 GHz
X-band Uplink:	7.900-8.395 GHz

Band Name	Frequency Range
Ku-band (Europe)	
Downlink: FSS:	10.700-11.700 GHz
Downlink: DBS:	11.700-12.500 GHz
Downlink: Telecom:	12.500-12.750 GHz
Uplink: FSS and Telecom:	14.000-14.800 GHz
Uplink: DBS:	17.300-18.100 GHz
Ku-band (America)	
Downlink: FSS:	11.700-12.200 GHz
Downlink: DBS:	12.200-12.700 GHz
Uplink: FSS:	14.000-14.500 GHz
Uplink: DBS:	17.300-17.800 GHz
Ka-band	Roughly 18-31 GHz

To accomplish the communications requirements of the rover, the radio modem will transmit information using two different antennas: a low-gain X-band antenna (LGA) for Earth-Mars limited data communication and an UHF X-band antenna to relay large amounts of data through Mars-orbiting spacecraft.

VI.6.2.1. Low-Gain Antenna

The LGA is capable of transmitting and receiving the X-band communication at a very slow rate of 600 bps. For simply transmitting position and limited system health information between Mars surface and Earth, as well as receiving commands, this is sufficient. However, transmitting images at this rate would be slow and tedious (though possible in the case of loss

of UHF signal). The LGA is a choked circular waveguide design having about a 70 degree 3 dB beamwidth pattern with ~6 dBic of peak boresite gain at 7.2 and 8.4 GHz. The height of the rover antenna when it is deployed is about 0.83 m [Maas 2004].

VI.6.2.2. Deep Space Network (DSN)

The omnidirectional LGA transmits at a low data rate directly to Earth via the Deep Space Network (DSN). The DSN is an international network of antennas that supports interplanetary spacecraft missions and currently consists of three deep-space communications facilities placed approximately 120 degrees apart around the world: at Goldstone, in California's Mojave Desert; near Madrid, Spain; and near Canberra, Australia [Wolff 2005]. DSN antennas communicate with far-flung spacecraft at frequencies of 2.2, 8.4 and 32 GHz. They consist of a collection of 34 and 70-metre radio telescopes equipped with cryogenically cooled low-noise amplifiers (approx. 20 degrees Kelvin noise temp). They operate in two microwave frequency bands, S-band (2.3 GHz) and X-band (7.2 GHz uplink, 8.4 GHz downlink) [Lombry 2005].

VI.6.2.3. UHF Antenna

The UHF antenna communicates to the Mars Odyssey and Mars Global Surveyor orbiters to relay imagery and data to the Earth. The patch antenna was designed by PSL Electromagnetics and was space qualified for use on the NASA STARDUST spacecraft. One of these antennas will be used on the walker robot for two-way communication at 7.2 GHz (receive) and 8.4 GHz (transmit). The achievable data rate to the orbiters is 128 kbps, over 200 times faster than the LGA transmission directly to Earth. More detailed electrical and mechanical information on this patch antenna can be found in Figure 26 and Figure 27 below [PSL 2005].

PSL NUMBER	MPSF62R-7180	MPSF62R-8430
Dimensions	2.0 x 2.0 x 0.2"	1.45 x 1.45 x 0.2"
Temperature	-95° C to +98° C (non-operating, acceptance) -105° C to +108° C (non-operating, protoflight) -65° C to +35° C (operating, acceptance) -75° C to +45° C (operating, protoflight)	
Thermal Interface	Internally generated heat is conducted through the ground plane of the antenna.	
Thermal Vacuum	-165° to +165° C (qualification) -34° to +71° C (acceptance)	
Vacuum Properties	Antenna is constructed of vacuum-compatible materials, but not certified with respect to CVCM.	
Magnetic Properties	No magnetic materials are used in construction	
Random Vibration	13.3 G rms. (prototype flight) 8.4 G rms. (acceptance)	
Pyro Shock	100 Hz: 65 G (prototype flight) 1000 Hz: 1750 G (prototype flight)	

Figure 26 – PSL Electromagnetics MPSF62R-8430 Patch Antenna Mechanical Properties [PSL 2005]

PSL NUMBER	MPSF62R-7180	MPSF62R-8430
Old Model Number	95.718	95.843
Band	C-Band	X-Band
Frequency (MHz)	7175.03	8400
Bandwidth	50 MHz	
VSWR	< 2:1	
Power	4 W CW	
Impedance	50 Ohms	
Pattern Shape	Cylindrically symmetric hemispherical pattern	
Gain	5.5 dBic minimum	
Polarization	RHCP (LHCP or linear available)	
Axial Ratio	< 3.0 dB on axis (θ = 0°)	
3-dB Beamwidth	approx. 120°	

Figure 27 – PSL Electromagnetics MPSF62R-8430 Patch Antenna Electrical Properties [PSL 2005]

The UHF radio signal, like all transverse electromagnetic radiation, travels at the speed of light. The rover antenna is on a mast, which deploys when the rover stands up for the first time, and is about half the length of the LGA. Once deployed, it latches into place vertically and remains that way for the duration of the mission. [Stride 1998].

VI.6.2.4. High-Gain Antenna

The use of a steerable high-gain antenna was briefly investigated in this study, but was removed due to mass concerns and unnecessary redundancy on a micro-rover class vehicle.

VI.6.3. Mars Surface to Mars Orbit Communication

VI.6.3.1. Mars Relay Requirements

The relay payload interface requirements are identical to those stated in the applicable MBR and MOC Interface Control Documents [JPL 1996].

The Mars Relay is the only payload on MGS designed not to take scientific measurements. Instead, this cylindrical-shaped antenna will focus its efforts on collecting data transmitted to Surveyor from landers on the Martian surface. After collecting the data, Surveyor will transmit the data back to Earth. The advantage of using Surveyor as a relay satellite for Mars landers is that the lander spacecraft will not need to carry a large antenna to talk with the Earth. Instead, the reduction in the weight of the lander from not carrying a large antenna can be used for more scientific instruments. The relay operates at UHF frequency and can listen to stations on the Martian surface up to 5,000 km away from Surveyor. The Centre Nationale d'Estudies Spatiales in France provided the relay antenna to NASA as part of an international cooperation toward the study of Mars [Goodall 2005].

VI.6.3.2. Communication Delay

To prepare for the worst-case scenario, there must be data storage capabilities to handle a single communication every 4 days. However, communication will nominally occur daily.

VI.6.4. Mars Orbit to Earth Communication

The Mars Global Surveyor (MGS) spacecraft will be the primary mode of relaying command and data information between the Mars walker and groundstations on Earth, however mars Odyssey can also be used as needed.

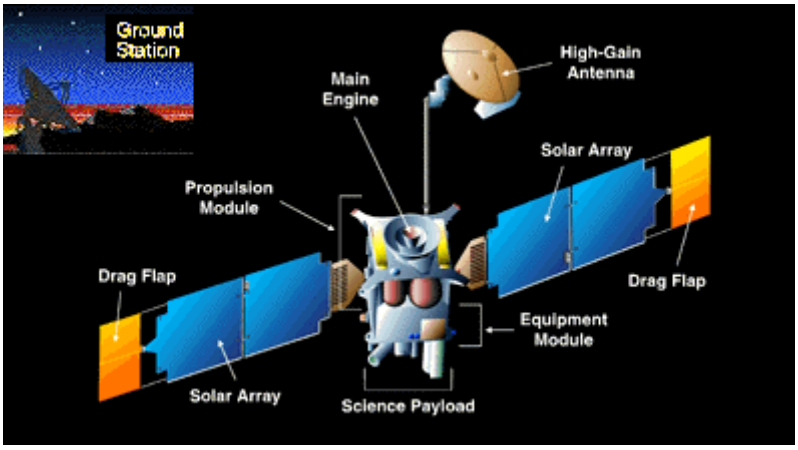

Figure 28 – Mars Global Surveyor with Subsystems Illustrated [Goodall 2005].

Surveyor takes only 118 minutes to circle Mars. When Mars is farthest from the Earth, the maximum data rate will drop as low as 21.3 kbps. When Mars is closest to the Earth, Surveyor will use a data rate of 85.3 kbps. At times in between those two extremes, Surveyor will use a medium data rate of 42.6 kbps [Goodall 2005]. In contrast, modems on modern home computers transmit data at an average speed of 56.6 kbps.

Table 24 – Mars Global Surveyor Communications Data [Goodall 2005].

Command Rate	12.5 commands per second (maximum)
Data Rate – Uplink	500 bits per second (maximum)
Data Rate – Downlink	85.3 kilobits per second (maximum)
Downlink Radio Frequency Power	26 watts
Solid State Recorders	3-gigabit capacity (total)
Solar Arrays	4 panels/ total output power 980 watts (maximum)

VI.6.5. Communication System Requirements

VI.6.5.1. Command Rate and Format.

The spacecraft bus shall be capable of accepting in- flight-switchable uplink command rates as defined in DM 514438, "Deep Space Command Detector Unit, National Aeronautics and Space Administration Design Requirement For". A low rate of 7.8125 b/s shall be used in an emergency or backup mode.

VI.6.5.2. Command Storage and Timing.

The C&DH shall be capable of storing spacecraft bus and at least 1500 PDS and science instrument commands, plus timing information for each command. The transfer of a single RTC to the PDS shall be completed within 2 seconds. The C&DH shall ensure that the transmissions of RTC and SSC contents to the PDS do not interrupt each other. The C&DH shall provide for a minimum of 5k words of memory in cruise and a minimum of 13k words of memory in mapping for storing command sequences and a script library.

VI.6.5.3. Command Error Protection.

The flight hardware and software shall be designed to preclude the unintentional execution of critical or irreversible commands. The spacecraft shall reject all invalid commands, whether they are RTCs or contained within SSCs [JPL 1996].

7. DATA

Space presents an extremely harsh operational environment for spacecraft. The Van Allen belts, solar flares and other phenomena create radiation environments that limit the on-orbit life and performance capability of key space assets. Although the effect of radiation on the Martian surface is somewhat harsh with the reduced atmosphere to obstruct radiation from the sun and deep space, the most severe impact to the rover electronics will be through ultra-violet radiation.

The requirements of future space systems are requiring higher performance, radiation-hardened electronics. Indeed, such systems require radical improvements in space electronics performance to be fielded. Through a strong focus on system needs, capabilities are added,

costs are decreased, system power/weight/size requirements are reduced, and component availability is expanded. Utilizing advances in commercial electronics will help keep hardened components for space systems affordable. Researchers are adapting commercial designs for space use with minor loss of performance and modifying commercial processes to improve the radiation tolerance of components [Shedd 2001].

One such development is the RAD6000-based CompactPCI single board computer developed by BAE Systems, shown in Figure 29. BAE Systems developed the computer hardware for numerous other space missions, most recently including the Pathfinder, Mars Odyssey orbiter, and Stardust missions. Currently, there are 145 RAD6000s running on 77 satellites in space [Fordahl 2004].

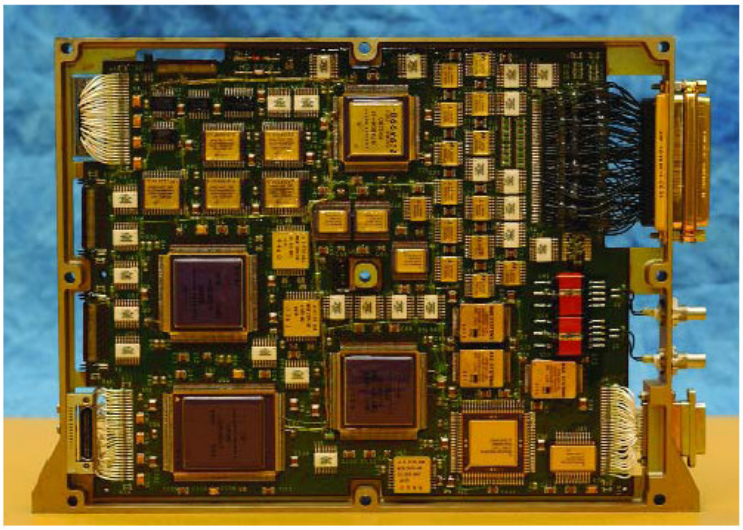

Figure 29 – RAD6000 CompactPCI Single Board Space Qualified Computer [BAE Systems 2004].

The RAD6000 has no moving parts. Data is stored on 128 megabytes of onboard memory, so there is no need for a heavy, mechanical hard drive to store data. The chip was designed in the early 1990s by International Business Machines Corp., when the BAE unit was part of IBM's Federal Systems Co. The IBM division, working with the Air Force Research Lab, developed the radiation-hardened version. The RAD6000 had 10 times better performance over previous processors qualified for space, has reduced the number of boards from five to one, and has reduced the weight and power required for the computer five fold. However, at 25 MHz, it does not even compare to today's standard 3200 MHz home PC workstations [Fordahl 2004]. The diagram in Figure 30 shows the components of the board and how they communicate with each other.

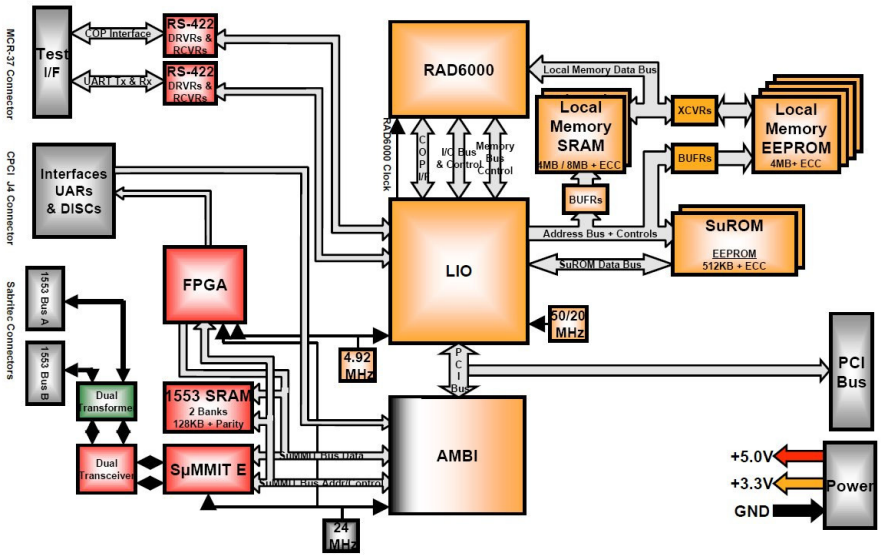

Figure 30 – Block Diagram of the RAD6000 Mainboard, Including FPGA for Navigation and Control [BAE Systems 2002].

The RAD6000 system will run the VxWorks operating system from California-based Wind River Systems Inc. The proprietary solutions previously used by NASA resulted in inconsistent performance and higher development costs, since the developers not only had to develop the mission software on schedule but also had the overhead of having to write the software platform to run these applications. With VxWorks, JPL could be assured of a powerful and lower-cost development platform right from the start – and make significant reductions to the overall development cycle. JPL has employed VxWorks to develop the intelligence of several prior missions including Mars Pathfinder, Deep Space One and other spacecraft [Stumpf 2003].

Portability was particularly important since development can take place on a variety of host systems. The 32-bit RAD6000 CPU is not commonly used outside NASA, with most commercial vendors using the PowerPC architecture. Wind River technology is highly portable with VxWorks running on more than 32 different processor families, making it the ideal choice in terms of porting to the RAD6000 [Stumpf 2003].

The onboard FPGA will be used in the development of the neural network for navigation and control algorithms described in Section VII.

VI.7.1.1. Data Streams

The spacecraft bus shall provide the following data streams:

3) S&E-1. S&E-1 is a combined science and engineering stream for recording, which is intended to permit the continuous collection of science observations. The combined data stream shall be sent to the C&DH by the PDS as a complete transfer frame that will conform to applicable CCSDS standards. The spacecraft

shall provide packetized engineering data to the PDS for insertion into the S&E-1 data stream at a rate or equivalent rate not to exceed 256 bits/second.

4) S&E-2. S&E-2 will be similar to S&E-1 except that it will utilize higher data rates and is intended for real-time transmission.

5) ENG. ENG shall be an all-spacecraft bus engineering data stream; it will be assembled by the C&DH and shall conform to the requirements of applicable CCSDS standards. The C&DH shall provide for variable rates and telemetry content as required for all spacecraft operations. An engineering dwell mode shall be provided; wherein normal telemetry is suspended while the downlinked telemetry dwells on selected points until commanded otherwise.

VI.7.1.2. Data Rates.

Science instrument data rates input to the PDS (or functional equivalent) are as defined in JPL D-4130, PDS- Instruments Interface Requirements Document. The PDS data rate outputs to the spacecraft are as defined in JPL D-3419, vol.1, Payload Data Subsystem Functional Requirements Document.

Data rates for the ENG data stream shall transmit at 10 bps and shall provide for 256 b/s and 2 kb/s data rates for normal engineering-only telemetry.

VI.7.1.3. Data Storage Capacity.

The spacecraft bus shall provide the capability both to record and to playback the S&E-1 data stream. The capacity shall be adequate to record S&E-1 data at up to 16 ks/s data rate for a minimum of 24 hours. Simultaneous record and playback operations shall be as defined in JPL D-3419, vol.1, PDS Functional Requirements Document.

8. CAMERAS

There are two kinds of cameras that are incorporated into this design: navigation and panoramic. Each camera is built to the same basic specification (see Table 25), however the lenses of each camera type is different, providing a different field of view. Using common specifications for the cameras will reduce design and integration complexity of the system, manufacturing costs, and image processing software development (as the same software can be used for all image data). Each camera has a 1024x1024 pixel image capture format, with the lenses providing the personalized touch to each one.

Table 25 – Camera Common Properties.

Parameter	Value	Units
Mass	< 0.265	kg
Volume	< 470	cm^3
Operating Power	2 3	W (Continuous) W (Peak)
Warm-Up Heater	2.7	W
Electrical Interface	LVDS	
Encoding	12	bit
Data Transfer Rate	200,000	pixels/second
Exposure Time Range	0-335	s (@ 5 sec steps)

VI.8.1. Panoramic Cameras (PanCam)

The cameras used on this mission are identical to the ones designed for the MER mission. Also, a stereoscopic head will be developed for the panoramic cameras. These cameras will provide a 360° image of its surroundings. This will help mission controllers determine where the rover will go to make closer inspections. The pair of panoramic cameras look and function like eyes. Their resolution and field of view mimic human vision, making them the most advanced colour imaging system ever sent to another planet. The Pancams can rotate in a complete circle on their long, neck-like mast and can swing up to 180° up or down. More than a dozen filters allow for imaging across every possible wavelength of light.

PanCam uses 1024 ×2048 pixel Mitel CCD array detectors developed for the MER Project. The arrays are operated in frame transfer mode, with one 1024 ×1024-pixel region constituting the active imaging area and the another adjacent 1024 ×1024 region serving as a frame transfer buffer. The frame transfer buffer has an opaque cover that prevents > 99%of light at all wavelengths from 400 to 1100 nm from being detected by this region of the CCD. The pixels are continuous, and the pitch is 12 µm in both directions. The arrays are capable of exposure times from 0 ms (to characterize the "readout smear" signal acquired during the ~5 ms required to transfer the image to the frame transfer buffer) to 30 sec [Cornell 2004].

Table 26 – Basic PanCam Facts [Planetary Society 2005].

Location	Top of mast 30 centimetres apart 1.3 meters above ground surface
Image size	1024 x 1024 pixels (images can be mosaicked into panoramas of up to 22,000 x 4000 pixels)
Field of View	16.8^o x 16.8^o 0.293 x 0.293 radians
Angular Resolution	0.0164 degrees/pixel 0.286 milliradians/pixel
Spectral Range	400-1100 nanometres

The optical design allows PanCam to maintain optimal focus from infinity to within about 1.5 metres of the cameras. At ranges closer than 1.5 metres, PanCam images suffer from some defocus blur. For example, at a range of 80 cm (the approximate distance from the PanCam calibration target), the defocus blur is about 10 pixels.

The two PanCam eyes are mounted on a mast on the rover deck. The mast is referred to as the PanCam Mast Assembly (PMA). The boresite of the PanCam cameras is approximately 1.3 m above the Martian surface once the PMA has been deployed. The cameras are moved together by ±90 °in elevation using a geared brush motor on the camera bar. The entire PMA head, including the cameras, can be rotated 360° in azimuth by a geared brush motor assembly [Cornell 2004].

The two PanCam eyes are separated by 30 cm horizontally and have a 1° toe-in. This separation and toe-in provide an adequate convergence distance for scientifically useful stereo topographic and ranging solutions to be obtained from the near-field (5-10 m) to approximately 100 m from the rover. Pointing control is < 2° in azimuth and < 1° in elevation. Pointing knowledge relative to the hardstops is 0.1° over the entire range of motion of PanCam. PanCam will operate primarily during the daytime to obtain high-quality measurements of sunlight reflected off rock and soil surfaces and airborne dust particles. Twilight or night sky or astronomical object imaging may be possible but has not been committed to by the project. The required operating temperature range for performance of PanCam within specifications is -55 °C to 0 °C [Cornell 2004].

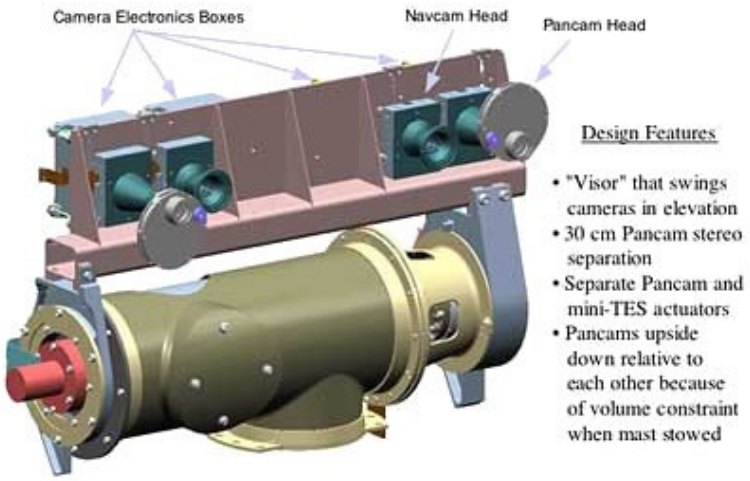

Figure 31 – PanCam and NavCam Mounted on Boom-Head [Cornell 2004].

PanCam will be commanded by and will return digital data directly to the rover computer. The computer provides the capability to perform a limited set of image processing tasks on PanCam data prior to transmission. These tasks include [Cornell 2004]:

- Bias and dark current subtraction
- Electronic shutter effect correction

- Bad pixel replacement
- Rudimentary automatic exposure control capability to maximize the signal to noise ratio, (SNR) of downlinked data while preventing data saturation
- Image subsampling and subframing
- Image compression using a JPL-developed wavelet compression algorithm called ICER.

VI.8.2. Navigation Cameras (NavCam)

One of two kinds of non-scientific panoramic cameras aboard the rover, two stereo NavCams help mission engineers back on Earth get a visual impression of the surroundings in black-and-white. With its elevated 45-degree field of view, the NavCams are designed to look at the area ahead of the rover and help plan future trajectories. The rover is designed to navigate on its own part of the time, making computer-generated decisions about where and how to move about the Martian landscape per mission control's daily set of general specifications. The NavCams provide engineers with a means of visually tuning in as the rover carries out their commands – though not in real time, because of the tens-of-minutes lag time in sending and receiving communications between Earth and Mars [Maas 2004].

Table 27 – Basic NavCam Details [Planetary Society 2005].

Location	Top of mast 20 centimetres apart 1.3 meters above ground surface
Image size	1024 x 1024 pixels
Field of View	45^{o} x 45^{o} 0.79 x 0.79 radians
Angular Resolution	0.088 degrees/pixel 0.77 milliradians/pixel
Spectral Range	400-1100 nanometres
Filters	none

VI.8.3. Hazard Avoidance Sonar

Although not as accurate as cameras, sonar will be used for hazard avoidance for many reasons. Primarily, it is a significant reduction in mass. Also, sonar is much less power and data processing intensive. Hazard avoidance techniques can be incorporated to avoid obstacles picked up on sonar signal reflects, instead of complicated image processing or human interface on Earth to recognise obstacles.

VII. BEHAVIOUR CONTROL

1. EVOLVED DYNAMICAL NEURAL NETWORKS

This part of the report details an illustrative study of the use of a particular biologically inspired method (evolved artificial neural networks) for developing a highly distributed dynamical control system of the type that could be used on a walking Mars rover. Various potential advantages over more traditional methods, including various kinds of robustness, are indicated.

Detailed background on the technique, and the field of evolutionary robotics – which utilises this methodology to develop controllers, body morphologies and other aspects of the overall robot design – was given in a previous report from this project (Technical Note 1 for the Bionics & Space Systems Design study).

Artificial neural networks have been successfully evolved to control, in real time, a physical model of a simplified walker operating in a virtual environment based loosely on Mars surface data (both of these have been constructed using the ODE physics engine [Smith 2003]). Note that this means that this section is somewhat different from the other parts of the report. It would have been far beyond the scope of the current project to have built a detailed physical model of an actual proposed walker, based on the previous design study material, and then evolved controllers for that – that would have taken much longer and required far more funds. However, instead of just doing a paper study of how to apply evolutionary robotics techniques to this problem, it was decided to perform this study on a simplified simulated walking rover as the results better illustrate the potential of the methodology.

This means that the physical design used for the walker (inspired by aspects of insect morphology and locomotion mechanisms as described in Section VII.3 below) is an illustrative design, it is not 'the' definitive design advocated by the overall study, although it is not in conflict with the more detailed design study material.

The next section provides backgrounds and context to work on the artificial evolution of walking machines. The sections following that describe the experiments done for this study.

2. EVOLVED WALKING MACHINES

This section gives a more detailed overview of evolved walking machines than was provided in the previous report (Technical Note 1 for the Bionics & Space Systems Design study). It is not exhaustive but help to set the context for the present study by indicating how the field has developed and what the current state-of-the-art is.

Over the past decade or so there has been a growing body of work on evolving controllers for various kinds of walking robots – a non-trivial sensorimotor coordination task. An evolutionary search algorithm is used to find good settings for some set of free variables that define the control systems and/or other aspects of the machine. This often entails searching a space of possible neural network controllers. In this case, the dimensions of the search space

represent the weights on connections, properties of nodes and possibly aspects of the overall neural architecture (such as number and arrangement of nodes and how they are connected to sensors and actuators). This methodology was first explored because the hand design of such architectures is extremely difficult; for more complex dynamic networks it is nigh on impossible [Husbands and Harvey 1992; Cliff *et. al.* 1993; Nolfi and Floreano 2000; Beer and Gallagher 1992].

Early work in this area concentrated on evolving dynamical network controllers for simple (abstract) simulated insects (often inspired by cockroach studies), which were required to walk in simple (flat surface) environments [e.g. de Garis 1990; Beer and Gallagher 1992]. The promising success of this work soon led to versions of this methodology being used on real robots. Probably the first success in this direction was by Lewis *et. al.* (1992, 1994) who successfully evolved a neural controller for a simple hexapod robot. All evaluations were done on the real machine (not in simulation). The key idea was to decompose the "learning to walk" into two functional stages in order to make this process feasible and not too time consuming. The robot was able to execute a simple tripod gait on flat surfaces. Gallagher *et. al.* (1996) describe experiments where neural networks controlling locomotion in an artificial insect were evolved in simulation and then successfully downloaded on a real hexapod robot. This machine was more complex than Lewis *et. al.*'s, with a greater number of degrees of freedom per leg. In this approach, each leg was controlled by a fully interconnected network of 5 Hopfield-like continuous neurons [Hopfield 1984], each receiving a weighted sensory input from that leg's angle sensor. Initially an architecture based on what is known of the neural mechanisms underlying locomotion in cockroaches was used. This produced efficient tripod gaits for walking on flat surfaces. In order to produce a wider range of gaits operating at a range of speeds such that rougher terrain could be successfully negotiated, a different distributed architecture, more inspired by stick insect studies, was found to be more successful [Beer *et. al.* 1997].

A genetic algorithm has been used by Galt *et. al.* (1997) to derive the optimal gait parameters for a Robug III robot, an 8-legged, pneumatically powered walking and climbing robot. The individual genotypes were encoded to represent the phase and duty factors, i.e. the coordinating parameters that represent each leg's support period and the timing relationships between leg movements. These parameters were inputs to a mechanistic state based pattern-generating algorithm that drove the locomotion. Such algorithms rely on relatively simple control dynamics and do not have the same potential for the kind of sophisticated multi-gait coordination that complex dynamical neural network architectures have been shown to produce. However, controllers were thus evolved that have been proved capable of deriving walking gaits that are suitably adapted to a wide range of terrains, damage or system failures (although an individual controller had to be tuned to each environment; they were not able to self adapt across a wide range of conditions). Gomi and Ide (1997) evolved the gaits of an 8-legged robot using genotypes made of 8 similarly organized sets of genes, each gene coding for leg motion characteristics such as the amount of delay after which the leg begins to move, the direction of the leg's motion, the end positions of both vertical and horizontal swings of the leg, the vertical and horizontal angular speed of the leg, etc. After a few dozen generations, a mixture of tetrapod and wave gaits is obtained. Using a developmental

approach called Cellular Encoding [Gruau 1995] – which genetically encodes a grammar-tree program that controls the division of cells growing into a discrete-time dynamical recurrent neural network of the kind used by Beer and colleagues – Gruau & Quatramaran (1997) evolved a single-leg neural controller for a walking robot which generated a smooth and fast quadripod locomotion gait. Jakobi (1998a,b) has successfully used his minimal simulation techniques (ultra-fast, ultra-minimal robot simulations that guarantee successful transfer of results from simulation to reality) to evolve controllers for the same 8-legged robot. Evolution in simulation took about 2 hours only, and then transferred successfully to the real robot. Jakobi evolved modular controllers based on Beer's continuous recurrent networks to smoothly control the robot engaged in walking about its environment avoiding obstacles and seeking out goals. The robot could smoothly change gait, move backward and forward and even turn on the spot.

Recently there has been successful work on evolving coupled oscillator style neural controllers for the highly unstable dynamic problem of biped walking. Reil and Husbands (2002) showed that accurate physics based simulations using physics-engine software could be used to develop controllers able to generate successful bipedal gaits. Reil and colleagues have now significantly developed this technology to exploits its commercial possibilities, in the animation and games industries, for the real time control of physically simulated 3D humanoid characters engaged in a variety of motor behaviours (see *www.naturalmotion.com* for further details).

Vaughan has taken related work in another direction. He has successfully applied evolutionary robotics techniques to evolve a simulation of a 3D, ten degree of freedom bipedal robot. This machine demonstrates many of the properties of human locomotion. By using passive dynamics and compliant tendons it conserves energy while walking on a flat surface. Its speed and gait can be dynamically adjusted and it is capable of adapting to discrepancies in both its environment and its bodies' construction [Vaughan *et. al.* 2004a]. The parameters of the body and continuous dynamical neural network controller were evolved. The machine started out as a passive dynamic walker [McGeer 1990] on a slope and then over many generations the slope was lowered to a flat surface. The machine demonstrated resistance to disturbance while retaining passive dynamic features such as a passive swing leg. This machine did not have a torso, but Vaughan has also successfully applied the method to a simplified 2D machine with a torso above the hips. When pushed, this dynamically stable bipedal machine walks either forward or backwards just enough to release the pressure placed on it. Just as a tango dancer uses a dance frame to control the movements of their follower, external forces are a subtle way to control the machines speed. Again, when the machine is subjected to noise in its body's size, weight, or actuators as well as external forces it demonstrates the ability to dynamically adapt its gait through feedback loops between its actuators and sensors. It took advantage of passive dynamic properties by supporting its torso on a straight leg and using a passive knee joint [Vaughan *et. al.* 2004b].

Recently McHale and Husbands (2004a,b) have compared many forms of evolved neural controllers for bipedal and quadrapedal walking machines. Recurrent dynamical continuous time networks and GasNets were shown to have advantages in most circumstances.

The vast majority of these studies were conducted for relatively benign environments. Not withstanding this observation, we can conclude from this field of research that the more complex dynamical neural network architectures, with their intricate dynamics, produce a wider range of gaits and generally produce smoother more adaptive locomotion than the more standard technique of using finite state machine based systems employing parameterised rules governing the timing and coordination of individual leg movements producing limit cycle behaviour [e.g. Laszlo 1996].

Building on this work to develop robust controllers capable of dealing with a range of more demanding terrains was one of the aims of the study reported here.

3. DESIGN

The design of the rover's control system is partly inspired by what is currently known about the nervous system of the stick insect. While a detailed understanding of its neural wiring still eludes us, it is possible to hypothesize about its internal construction by performing behavioural studies. [Cruse *et. al.* 1993] performed extensive experiments with these insects to try and understand how their gait was generated and made several models that could reproduce many of their behaviours. Specifically it was found that each leg had one or more oscillators that rhythmically lifted and extended the insect's legs. While these oscillators could step independently from each other they had some subtle influences from neighbouring legs that kept them synchronised in a walking gait. If a leg was hindered or detected a gap in the environment the leg could prevent other legs from stepping until the obstruction was avoided or a better foot placement was found. To detect if a leg is hindered these insects take advantage of sensitive hairs to trigger reflexes such as lifting the leg over small rocks or branches.

This loose coupling of the individual leg control circuits, which results in rapid overall stabilization and adaptation to the immediate terrain, is a powerful property that can be usefully incorporated into the control system for a walking machine. Beer *et. al.* (1997), among others, have demonstrated its efficacy in legged robots. In a comparative study they show that control architectures inspired by stick insects have advantages over those more closely inspired by what is known of cockroach locomotion control. Specifically, a wider range of gaits and gait speeds and better performance on rough terrain was achieved.

While there are no doubt many useful lessons that can be learned from a wide range of walking insects, for the purposes of this illustrative study, with its limited scope, we have taken inspiration from the stick insect as well as more general aspect of control that are common to most arthropods. Other potentially useful properties of stick insect locomotion control include:

- Stick insects are relatively large and designed to walk carefully in an energy efficient way. They keep their thorax off the ground, while insects such as cockroaches stay close to the ground and move very quickly. A planetary rover is likely to be required to walk carefully and efficiently to reduce energy and damage. It must keep its thorax off the ground to minimize damage to sensitive equipment.

- It is a misconception to think that the sick insect is slow moving. Cruse did experiments on treadmills with various species and demonstrated that many can run very fast [Cruse *et. al.* 1993].
- Stick insects are capable of stepping over gaps up to the full length of their bodies [Blaesing and Cruse 2004]. If the rover reaches a crack in the ground it would be ideal if they could detect and step over it.
- Stick insects have several gaits and use extensive sensor feedback with the ground to walk as smooth and efficient as possible. At slow speeds they use tetrapod gaits while at high speeds they use tripod. This increases their stability at slow speeds.
- The combination of their overall body morphology and neural control systems make stick insects extremely stable when walking or standing, something that has been noted and exploited in a number of robot studies [Beer *et. al.* 1997; Ferrell 1995]. There are obvious potential advantages in this for a rover.
- Stick insects have been heavily studied and hence a rich seam of data is available.

Stick insects have eyes but sense their environment primarily with their front legs and feelers on their head [Blaesing and Cruse 2004]. When crossing gaps blindfolded they were found to perform equally well by reaching with their feelers or front legs for the other side. If the feelers were removed the insect would rely on its front legs with nominal performance loss.

It should be noted that our interest is in taking inspiration when it proves helpful, not in slavishly modelling particular insect behaviours and morphologies (although of course that is very useful when the primary questions are biological). Hence aspects of the simplified walking rover used in this part of the study are inspired by stick insects and other arthropods; certain useful properties are adapted to our own ends in developing a walking machine.

The stick insects behaviours were evolved over millions of years. Over time structures were slowly added, each system subsuming earlier ones. New behaviours appeared, as selection pressures required them. Our approach is to evolve a Mars rover by starting with a relatively simple artificial nervous system and body inspired by the stick insect. These virtual insects are constructed and tested in a physics simulator (the ODE physics engine [Smith 2003]). Once a suitable rover is found, its design could be transferred to a physical machine. Parameters of the rovers can be found in Figure 32. To develop behaviours selection pressure is placed on the population over hundreds of generations. Specifically we demonstrate how to select for certain useful behaviours such as walking, navigation, and obstacle avoidance.

Our nervous system was constructed in four stages. In stage one we selected for straight line walking on a flat surface allowing the machine to coordinate its legs into an alternating gait. In stage two a more rugged terrain was created by adding simulated impact craters. In stage three the rover was evolved to navigate to the beacons placed in a random location. In stage four the machine was given laser based proximity sensors as feelers to avoid obstacles. This incremental approach, with each stage building on the previous results of evolution, allowed us to gradually guide the evolutionary process towards our end goal. This proved to be a highly effective strategy.

The initial nervous system for straight line walking on a flat surface was composed of six bilaterally symmetric continuous time neural recurrent networks (CTRNN) each in charge of controlling a single leg (Figure 33). Networks were loosely connected to their neighbouring oscillators to create synchronising influences. Unlike traditional neural networks, a CTRNN uses time constants to allow neurons to activate in real time and out of phase with each other. For a detailed analysis of this kind of network refer to Beer (1995).

The state of a single neuron was computed by the following equation:

$$\tau_i \dot{y}_i = -y_i + \sum_{j=1}^{N} w_{ji}\sigma(g_j(y_j + \theta_j)) + I_i \qquad i = 1,...,N \tag{31}$$

$$\sigma(y) = \frac{1}{1+\exp(-y)} \tag{32}$$

where:

y = *the state of each neuron*
τ = *The time constant*
w = *The weight of an incoming axon*
σ = *The sigmoid activation function*
g = *The gain*
θ = *A bias*
I = *an external input*
N = the number of nodes in the network

The state of each neuron was integrated with a time step of 0.2 using the Euler method. In our model the network variables were encoded in the artificial genome as a vector of real values with τ and g in the range [1, 20] while connection weights and biases were encoded with real values in the range [-20, +20].

The initial biases at the start of an evolutionary run were calculated as follows:

$$\theta_i = \frac{-\sum_{j=1}^{N} w_{ji}}{2} \tag{33}$$

Mathayomchan and Beer (2002) refer to networks with this modification as centre-crossing CTRNNs. They suggest that population seeded with centre-crossing networks may be more likely to yield a wider range of dynamics than a population with purely random biases.

The body of the rover was composed of a thorax, six tibias, and six femurs, as shown in Figure 32. Antagonist muscles were placed around each degree of freedom and connected to their respective motor neurons.

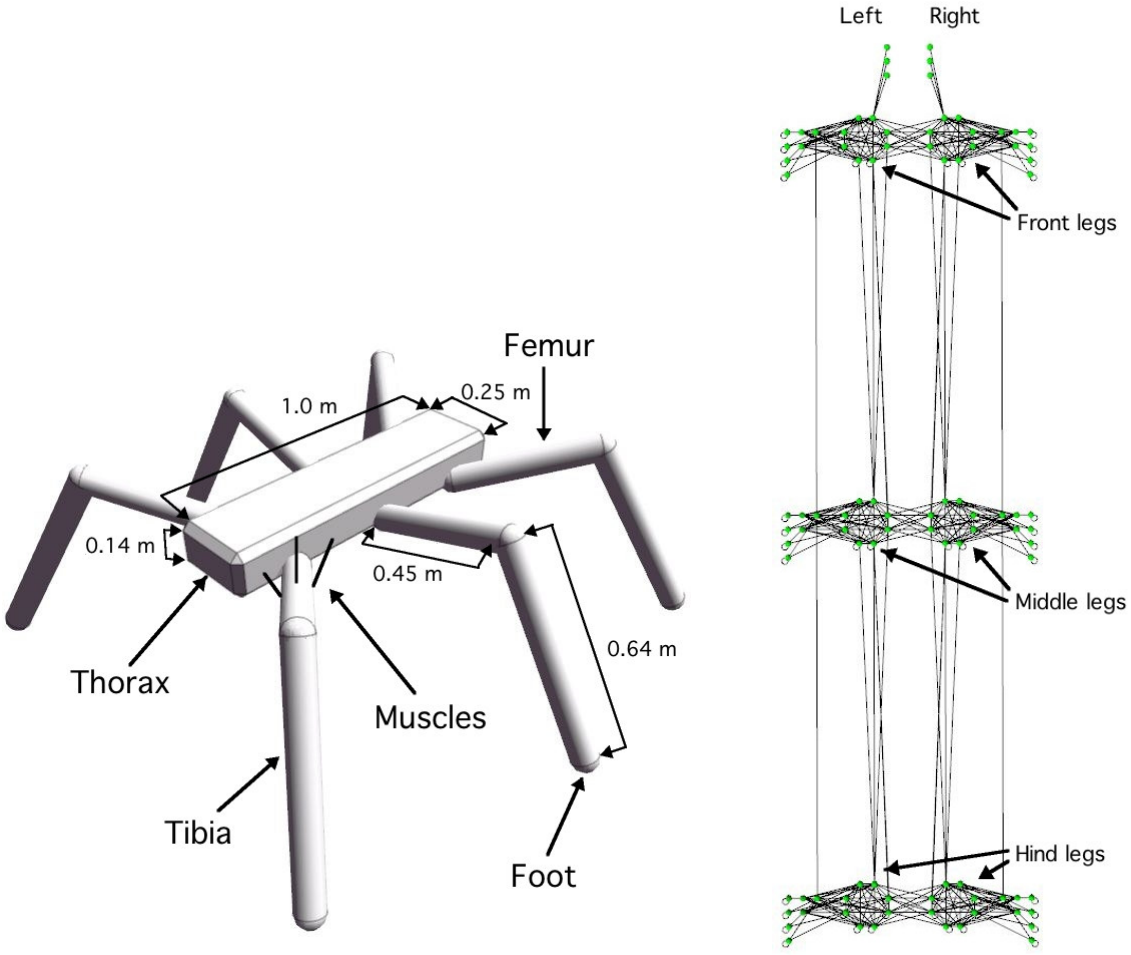

Figure 32 – a) The body of the rover and b) the rover's nervous system composed of six bilaterally symmetric continuous time neural networks. Networks on the right side are mirror images of the left. Initially front, middle, and rear networks are wired identically.

The body and legs were modelled in ODE [Smith 2003] using appropriate rigid body primitives (cylinders and boxes). The total mass of the machine is 17.2 kg (thorax = 10 kg, each leg = 1.2 kg). The radii of the tibia and femur are both 0.04 m. The hip joint is modelled using universal joints and has two degrees of freedom (up-down and side-to-side), each with a range of -1 to +1 radians. The knee joint have one degree of freedom and are modelled as hinges (also with an angular range of -1 to +1 radians). The way in which ODE motor components were used to power joints is explained in Section VII.3. Friction between the feet and the ground was handled using a Coulomb friction model.

The neural architecture for stage one of the evolutionary process (straight line walking on flat surface) is shown in Figure 32 and Figure 33. Each pair of legs is connected to a dedicated bilaterally symmetric continuous time recurrent neural network (CTRNN), which is composed of two mirror image sub-networks. Each sub-network comprises a fully connected network of

8 nodes (the ring of nodes in the centre of Figure 33). Four motor neurons are used to control the hip joint. One neuron from the fully connected sub-network (neuron 8) operates (via a pair of oppositely signed connections) the forward and back motor neurons, and another (neuron 15) the lift and lower motor neurons. Two further motor neurons (not shown) are used to control the knee joints. To decrease the search space the motor neurons in the knee joints were left disconnected. By default these neurons emit a constant output of 0.5 causing each muscle to pull slightly against each other. This gave the knees a compliant spring-loaded property. Two angle sensor neurons (connected to angle sensors in the hip joint) are each connected to every node in the 8 node fully connected sub-network.

Inter-leg influences as observed in the stick insect were implemented by randomly connecting axons to nearby neurons from each posterior network to their anterior network as well as the reverse. Collateral influences were created following the same procedure between networks laterally along the body with a higher a probability of inhibitory connections (Figure 33).

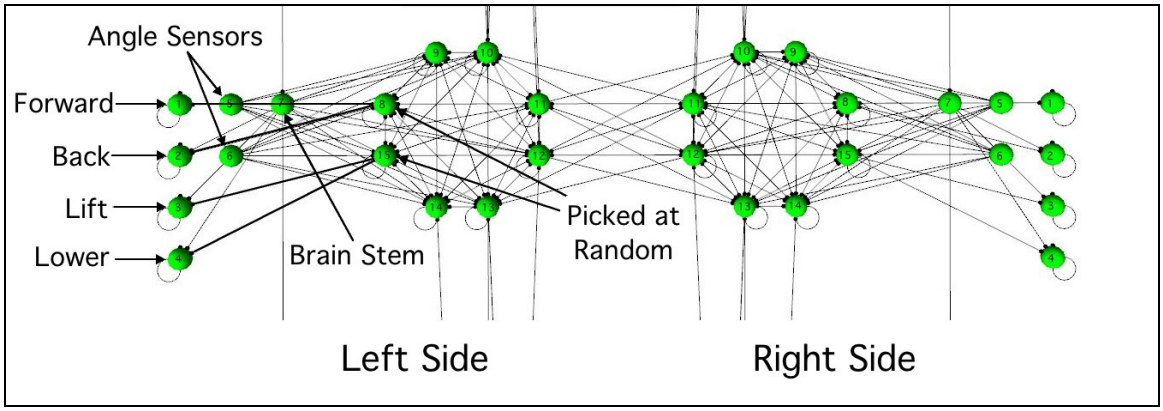

Figure 33 – Two bilaterally symmetric networks for controlling the left and right middle legs.

Figure 33 shows that neurons 1-4 are motors neurons for rotating the hip around the x and y-axis. Neurons 5 and 6 are angle sensors for detecting the current angle of the joint around x and y. Neurons 8 and 15 initially power the motor neurons. Neurons with the same number had identical bias, time constant, and connections weights.

Following experience with previous evolved walkers [Vaughan 2004a,b], the overall design of the machine deliberately incorporated features that would allow the exploitation of passive dynamics [Pratt and Pratt 1999]. As described in more detail in Section VII.7, this helped to produce very efficient gaits in the rover.

In the initial population connection weights and neuron properties (time constants, biases, gains) were set randomly (except the pairs of connection from neurons 8 and 15 to the motor neurons which were set to -2 and +2 in order to bias the initial motor behaviours to something vaguely sensible). The evolutionary search algorithm, described in the next section, was then free to change these values until a control system capable of generating the desired behaviour was found. The next section gives further details on how this was achieved and then

subsequent sections explain how evolutionary search was used in an incremental way to build more and more complex behaviours.

4. WALKING

The most basic behaviour we wish to evolve is walking. As discussed earlier in this report, insects walk with many different gaits depending on terrain. To allow evolution to decide the proper gait we used a very simple fitness function to evaluate individuals. Fitness is to be maximized.

$$fitness = G(d)*G(x)*G(y)*G(e) \quad (34)$$

where:

$$G(x) = \frac{1}{1+x}$$

d = absolute distance to beacon at end of trial
x = average change in rotation of body about x axis
y = average change in rotation of body about y axis
e = average energy used

This function encourages maximising distance moved while minimising x, y and e which will encourage the machine to walk as far as possible using as stable and efficient gaits as possible.

The Open Dynamics Engine physics (ODE) simulator [Smith 2003] was used to evaluate the rover's body and control system. It provided a stable system for simulating rigid body dynamics as well as simple motor models for powering joints. To integrate with ODE's motor system the following simplified muscle model was used:

$$p = f-e \quad (35)$$

$$s = f+e \quad (36)$$

$$v = (p - a)*s*vg \quad (37)$$

$$t = |(p - a)*s|*tg \quad (38)$$

where:

f = Activation of flexor motor neuron
e = Activation of extensor motor neuron
p = Desired position of joint
s = Stiffness of joint
v = Desired velocity of joint
t = Maximum torque used to achieve desired velocity v
vg, tg = gains

Where *v* and *t* were provided directly to ODE to power and control the motors around each joint.

To find a rover that could achieve the desired behaviour a geographically distributed genetic algorithm [Husbands 1994] was used with a population of 25 individuals. Each individual was constructed with random axonic weights, biases, and time constants. The following procedure was used to evolve and evaluate them:

1) Each individual was constructed and placed in the simulator.
2) A beacon was dropped 15 metres directly in front of the individual
3) The simulation was allowed to run for one minute.
4) At the end of the run (or once the beacon had been reached, if sooner) the fitness was computed using the function detailed earlier.
5) Individuals with a higher fitness had a greater probability of generating offspring.

In more detail the evolutionary algorithm works as follows. The population of individual are spread out over a 2D 5x5 grid. Two individuals are chosen at random, the best of these is selected. An offspring is created by 'mating' this individual with the fittest other individual in its immediate neighbourhood on the grid (the surrounding 8 cells). Crossover and creep mutation (at a probability of 0.01 per gene) are used [Michalewicz and Fogel 2004]. Two members of the neighbourhood are chosen at random; the less fit of these is replaced with the newly created offspring. These steps are repeated until success has been achieved. This process was implemented in a fully distributed way over a grid of 20 Macintosh computers (many with dual processors). For a discussion of the advantages of this kind of distributed parallel algorithms see Husbands (1994).

After 100 generations an individual was found that could reach the beacon using an efficient coordinated tripod gait.

5. ROUGH TERRAIN

In the next stage of evolution the population of rovers were tasked with walking over rougher terrain containing randomly placed impact craters as illustrated in Figure 34. The incremental approach taken here meant that this more sophisticated behaviour was built on top of the walking behaviour achieved in the first stage. A new population was created by making mutated copies of the best individual from the previous stage evolutionary run. The architecture was augmented as described below and the evolutionary algorithm was run again with the same fitness function until a machine capable of walking to the beacon over rough terrain emerged.

To aid the rovers, they were given more axonic connections as well as touch sensors on each foot and the knees were now powered. The following connections were added to the networks depicted in Figure 33. The initial weight values were set at 0 but could be changed by the

evolutionary algorithm. This allowed a gradual exploration of the affect of these connections. If they had been initially set at random values most of these would have had destructive influences and the walking behaviour already achieved would have been badly compromised.

1) Each network was fully connected to its respective motor neurons.

2) Touch sensors were fully connected to each network.

3) Each network was fully connected to its knee's motor neurons.

4) Additional connections from the homing neuron we used to modulate the weights of connections between the network and its motor neurons (as described for navigation in Section VII.6)

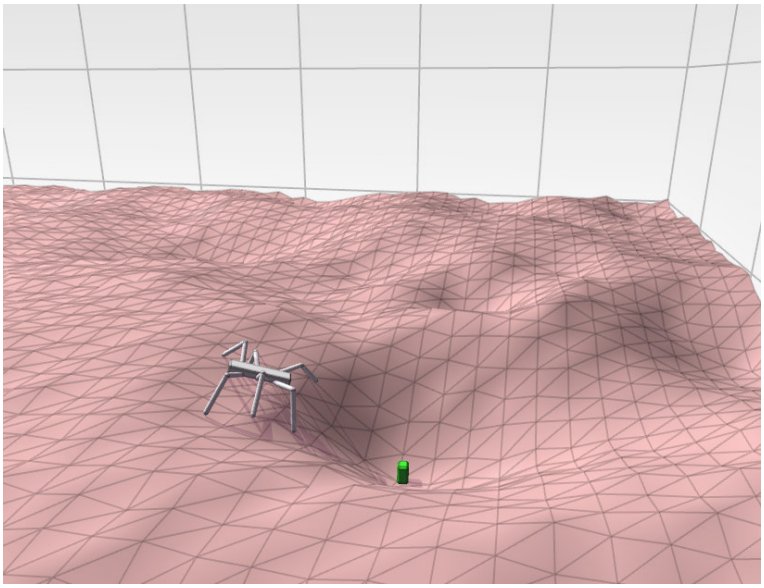

Figure 34 – Rover entering an impact crater to reach a beacon.

After further evolution, in which the search algorithm was free to change values for both the original and additional neurons and connections, the resulting rover demonstrated the ability to keep its thorax relatively still while walking in and out of steep craters and on uneven ground. If the machine became stuck it varied its foot placement to get additional traction and could consistently free itself. This demonstrates that legs can provide a stable platform on rough terrain that could insolate sensitive electronics from excessive vibration.

6. NAVIGATION

A useful trick that many insects have been shown to use for navigation is *path integration*, or 'dead reckoning' [Collett *et. al.* 1998]. For instance, by continuously monitoring information on orientation (using some form of compass) and distance travelled, an insect foraging for food is able to keep track of the distance and direction to its nest. As Collett and Collett

(2000) point out, at the core of path integration is an accumulator. This is set to an initial state at the nest, or starting place, and is updated as the insect moves so that it always reports the insect's current position relative to the nest. Navigation that uses path integration requires, in addition, a way of storing states of the accumulator at significant places for subsequent recall in relation to specific goals, and a means of computing the direction to such goals. Although finding the biological basis of such mechanisms is highly non-trivial, the basic idea is relatively easily implemented on a mobile robot [Lambrinos *et. al.* 2000]. Accumulated noise can reduce the reliability of this method so in nature it is nearly always used in conjunction with other mechanisms, such as visual landmark navigation, which are often also used to help keep it calibrated [Srinivasan 1998; Srinivasan *et. al.* 1997; Judd and Collett 1998].

Path integration provides a good solution for navigation in the rover. If it is explicitly given a home vector it will walk to that location even if obstacles create extensive detours along the way. While the equations as well as neural implementations of path integration are known [Vickerstaff 2003; Vickerstaff and Di Paolo (Forthcoming)], so that an integrated distributed path integration systems could be implemented, that is out of the scope of this case study. Instead we have assumed the output of a path integration system, which is a vector that always points to the desired target, in our case a homing beacon.

This third stage of behaviour was developed in an incremental way much as the second stage was built on the first – a new population was constructed from mutated copies of the best individual from the second stage and the artificial nervous system was provided with some potentially useful enhancements. The evolutionary algorithm was then free to search this new space of distributed control systems until the desired behaviour was found.

To make the rover responsive to the homing vector the brain stem (previously unconnected) was fully connected into nearby leg networks (Figure 35). As in our previous modifications, their axonic weights were initially set to zero. Additional axons from the homing neuron we used to modulate the connection between the network and its motor neurons (Figure 36). The modified axon's weight was computed by the following equation:

$$w_m = w_o * (\frac{1}{\sigma(wa_h)}) * c \qquad (39)$$

$$\mathrm{wa_h} = w_h * a_h \qquad (40)$$

where:

$\mathrm{w_m}$ = *the modified weight value*
$\mathrm{w_o}$ = *the original weight value*
$\mathrm{w_h}$ = *weight of the homing axon*
$\mathrm{a_h}$ = *activation of the homing neuron*

Initially the modulating axons from the homing neuron were made inhibitory. This provided a control system similar to a tank. Increasing both homing neurons caused the machine to walk faster, decreasing them caused it to walk slower. Strengthening one and weakening the other caused it to turn.

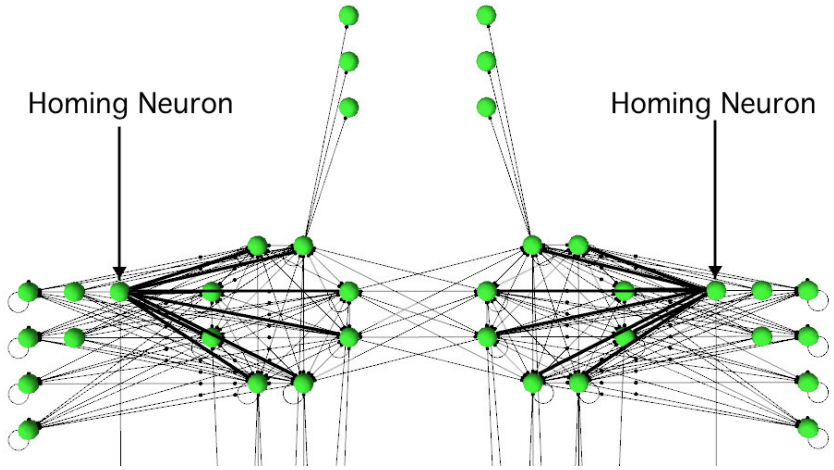

Figure 35 – Addition of symmetric homing sensory neurons to the front legs.

In Figure 35, their output is fully connected to their respective networks. These signals are propagated down the brain stem to the homing neuron in the next network and the pattern repeated for each set of legs. If the beacon is to the rover's left the right homing neuron receives a positive signal that is the angle between the heading and the beacon. The right homing neuron receives the same signal but with the opposite sign.

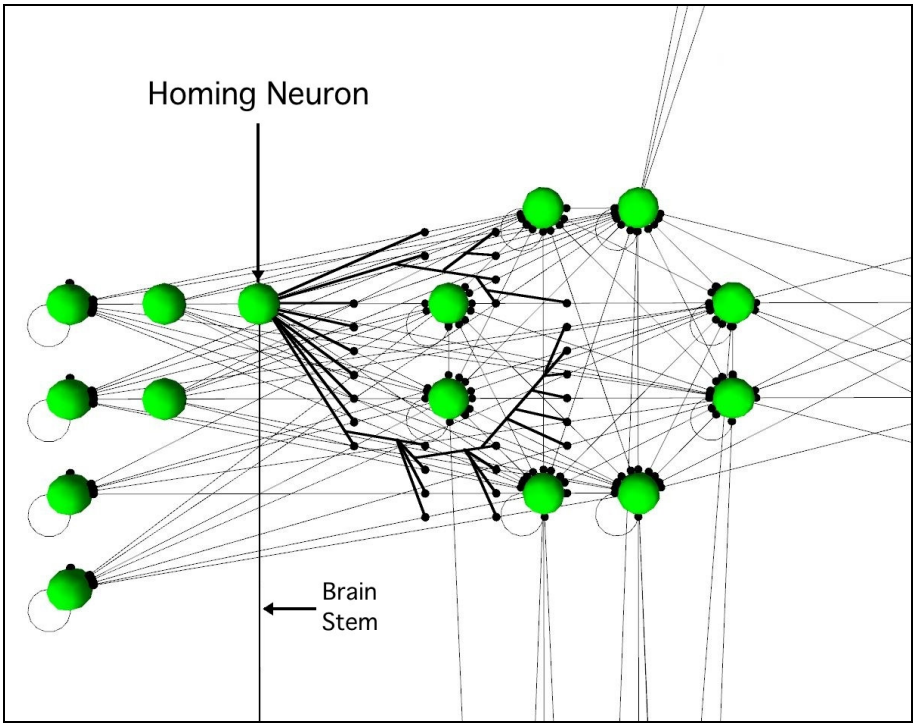

Figure 36 – Homing neurons also modulate the axons between network neurons and motor neurons.

As in Figure 36, when inhibited the homing neuron magnifies axonic connections between the network and their motor neurons causing the machine to take larger steps. When stimulated it weakens connections causing the machine to take smaller steps. By manipulating the activity of these neurons steering can be achieved.

To find a beacon the brain stem neurons on the front two legs were adjusted with the following equations:

$$als = \left(\frac{al}{\frac{\pi}{2}}\right) - 1.0 \qquad ars = -\left(\frac{ar}{\frac{\pi}{2}}\right) - 1.0 \qquad (41)$$

where:

als = *The value to add to the left sensor neuron*
al = *The angle between the machines heading and the beacon*
ars = *The value to add to the right sensor neuron*
ar = *The angle between the machines heading and the beacon*

In order to reflect the new behaviour goal of this stage of evolution, the fitness function from the previous stages was modified to be the product of fitnesses of five separate trials where beacons are placed at different locations spread out over an angular range of $\pm\frac{\pi}{2}$ as shown in Figure 37.

$$Fitness = f(0)*f(1)*f(2)*f(3)*f(4)$$

where:

$f(t) = G(d)*G(x)*G(y)*G(e)*G(h)$
$h = |ba - ha|$
ba = Angle to beacon
ha = Angle of heading
t = Index to beacon placements over a range of $\frac{\pi}{2}$ *as illustrated in Figure 37*

The other symbols have the same meaning as in the previous fitness function. This new fitness function requires the rover to robustly navigate to a beacon wherever it is placed, as it must achieve high fitness on all trials in order to get a good overall fitness. After 100 generations a rover was found that could successfully reach the beacon placed in any of the 5 locations, as shown in Figure 37.

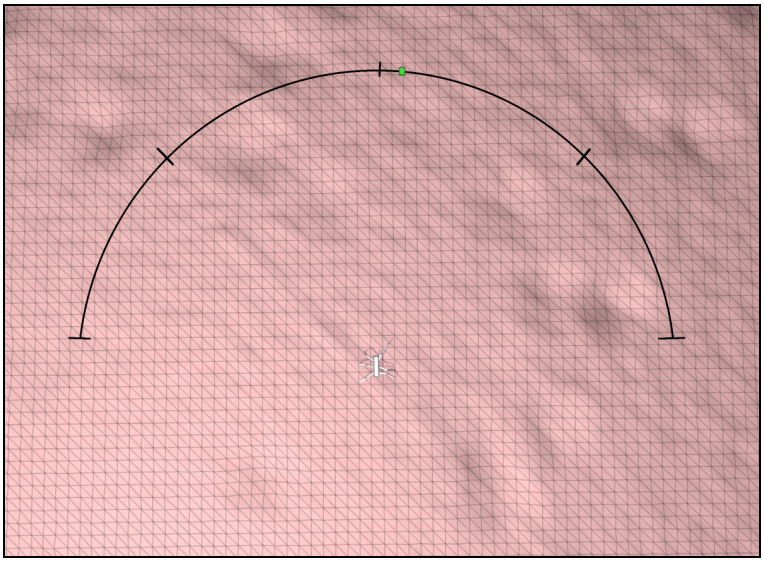

Figure 37 – Illustration showing the five beacon locations.

As shown in Figure 37, on each evaluation the beacon was placed on each tick and then randomly moved by an offset in the range of $[-\frac{\pi}{5}*0.5, +\frac{\pi}{5}*0.5]$.

7. OBSTACLE AVOIDANCE

To avoid obstacles and navigate over rough terrain stick insects use two feelers as well as their front legs to actively probe their environment. The feelers on the rover were implemented by using two actively controlled laser proximity sensors rather than mechanical feelers (Figure 38). While physically embodied feelers would be more biologically accurate, they add an increasing complexity and may also be prone to being stuck or damaged as they look for obstructions.

To implement feelers, an additional two networks were connected directly to the muscles that guide the proximity sensors and their weights initially set to 0. Using an approach popularised by Braitenberg (1984), axons connecting each feelers sensor was connected to the network on the opposite side the body. When a feeler detected an obstacle the legs on that side were inhibited proportionally to the distance of the object. This created a natural feedback system that gently steered the rover away from obstacles that touched it's feelers. However, in many insects feelers are very specialised and capable of localizing obstacles, following wall, etc. To allow the rover the possibility of these behaviours, the new networks were allowed to evolve independently subsuming the built in Braitenberg behaviour.

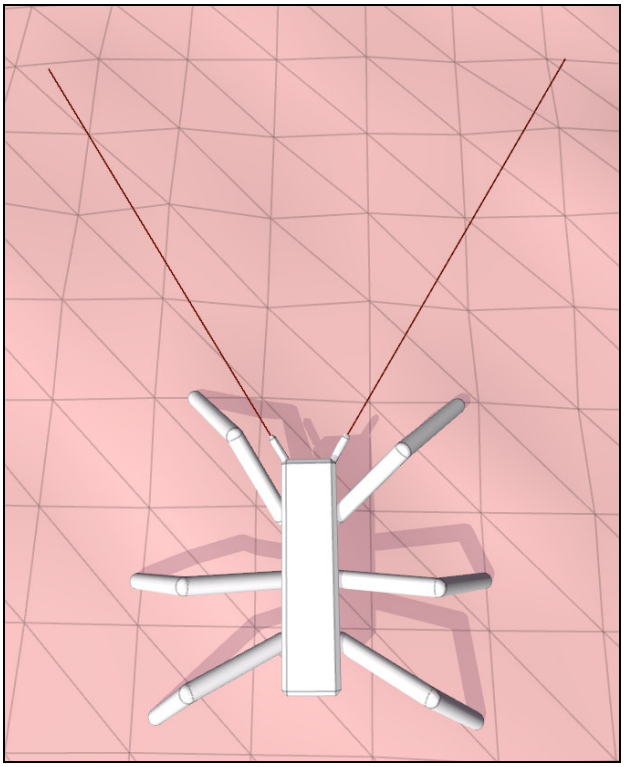

Figure 38 – The rover with active 'laser' feelers.

Stick insects actively scan with their feelers by constantly moving and tapping their environment. If the feeler were to stay fixed and not allowed to move the rover would have large blind spots in its vision. A primary example is directly in front of the machine. To address these issues the feeler networks were initially wired with the following simple algorithm:

1) Wave the feelers back and forth across the field of vision

2) If an obstacle is detected remember it momentary so when the feeler loses contact during the sweep the machine won't just forget and turn right into it.

The wiring of the algorithm is quite simple as is illustrated in Figure 39. When the proximity sensor detects an object less than two metres from the machine it stimulates the feeler neuron proportionally to distance. The closer the object the more stimulated it becomes. These neurons are wired by a positively weighted axon to a randomly picked neuron in the feeler network named *memory* for convenience. The *memory* neurons are given a time constant of 50 and a recurrent connection of 2. This creates a neuron that when stimulated charges up quickly but decays very slowly giving it a small short-term memory. A final positive connection is made to the homing neuron. To create a simple waving motion, two different neurons were picked from the feeler networks that were observed to oscillate in reponse to incoming connection from the leg network. These were then connected in the motor neurons for the feelers.

The same incremental methodology was used as at the previous stages and the new population evolved using the same fitness function as at the previous stage but in a more challenging environment including large obstacles.

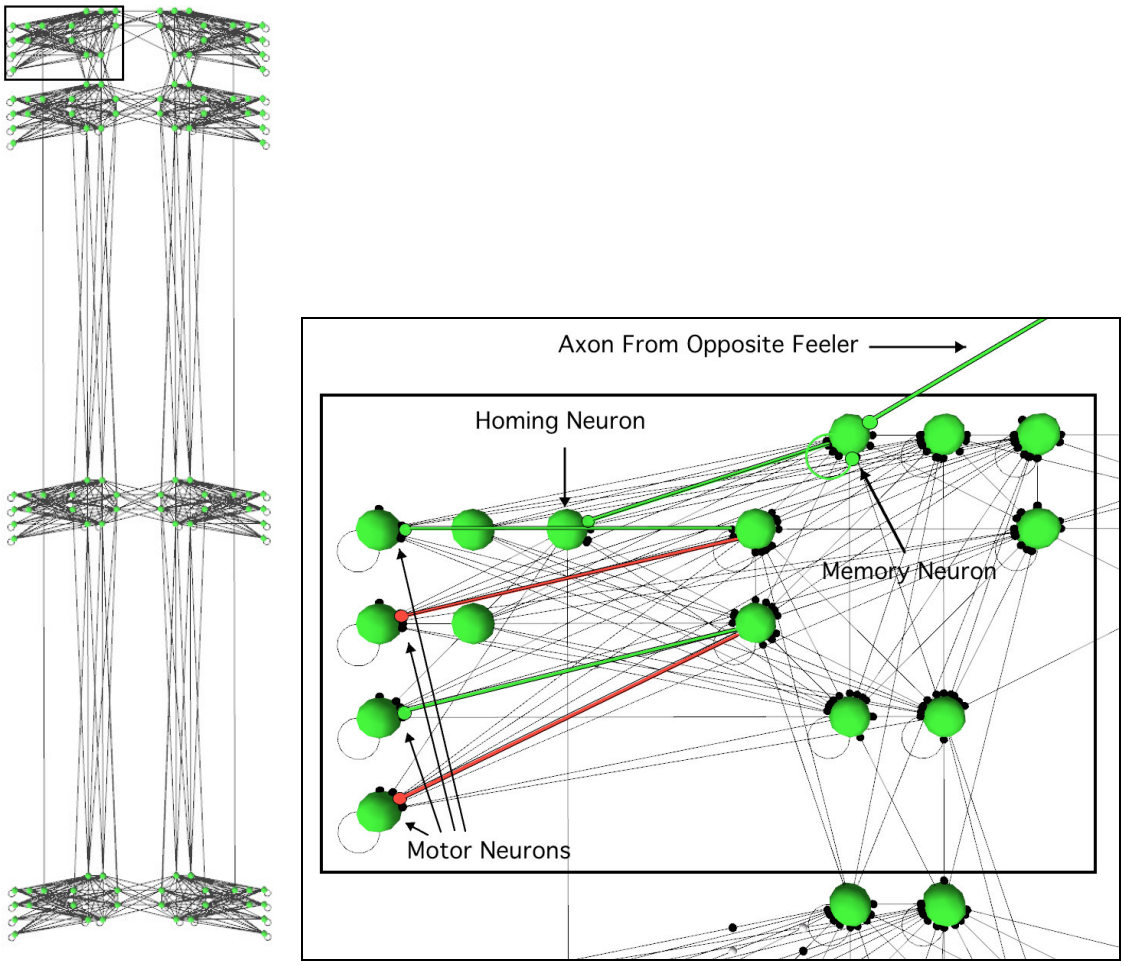

Figure 39 – a) full nervous system with feeler network added and b) close up of network connectivity.

In Figure 39, the opposite feeler stimulates the memory neuron who intern stimulated the homing neuron. A recurrent connection and large time constant in the memory neuron allow it to hold its state acting a short-term memory. A simple waving movement it achieved by making positive and negative connection from two arbitrarily assigned neurons in the network to the feeler's motor neurons.

To test these modifications the environment was changed to have randomly placed rocks protruding from the ground, at spacings based on Mars surface data (Figure 40), and the population evolved for an additional 100 generations. The resulting machine learned to use its laser feelers to actively avoid large rocks in the terrain and still arrive at its beacon. Figure 41 shows the path of a rover as it moves around an obstacle.

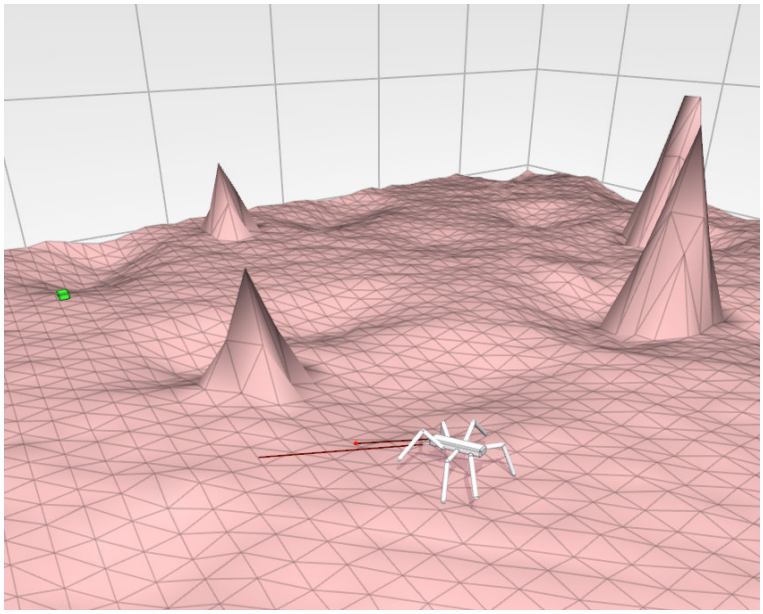

Figure 40 – Terrain with obstacles protruding from the surface. The rover must navigate to its beacon on the left while using its feelers to detect obstructions and avoid them.

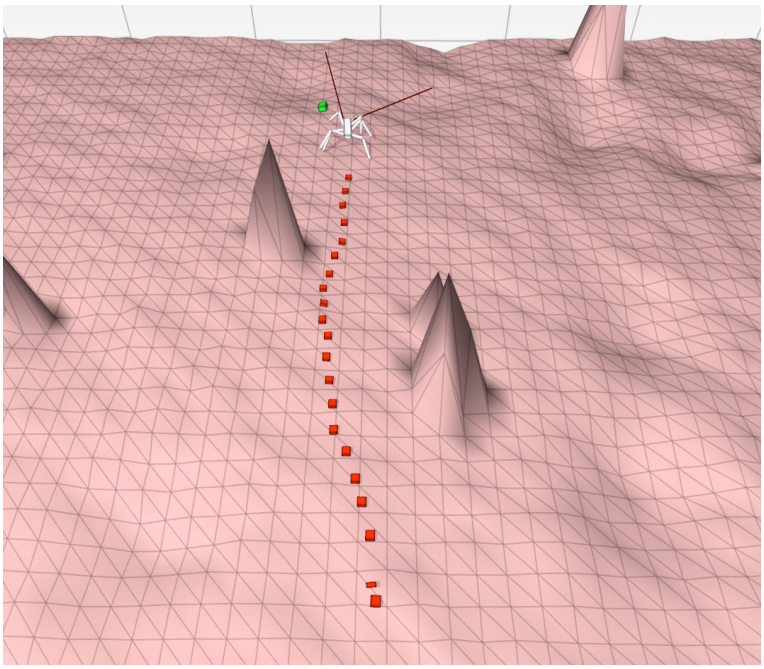

Figure 41 – The path taken by a rover through obstacle on the way to the beacon.

8. EFFICIENCY

Regardless of the type of power supply used by the rover: batteries, solar, etc., minimising energy is a priority. The rover should be able to achieve its goal while at the same time use as little energy as possible. In most animals including humans, passive dynamics are exploited to reduce energy by taking advantage the physics of the body. Instead of powering each movement, muscles initiate and guide the legs and allow them to swing naturally. Researchers combining passive dynamic walking and neural networks have realized efficient walking algorithms [Vaughan *et. al.* 2004; Pratt and Pratt 1999].

Our fitness function has consistently placed pressure on the machine to move in an efficient way. Its muscle model has allowed it to apply gentle forces and take advantage of passive dynamics within the body. The amount of energy required is based heavily on the type of actuator used. Actuators that can take advantage of passive dynamics will have increase efficiency.

In simulation, the average speed of a typical rover was found to be 0.26 m/s. When walking 13 metres on rugged terrain the machine uses a total of 5.26 N-m of torque.

9. ROBUSTNESS

VII.9.1. Damage

Insects are very robust to physical damage. Even with the loss of legs, eyes, feelers, or even neural tissue they can continue to successfully navigate and survive. These properties are the result of a redundant and adaptive design. By using an evolved neural network based nervous system our design has similar properties. To illustrate the extent of these properties in our rover the population was evolved for an additional 100 generations in which damage occurred during it's lifetime. The following procedure was used each time a rover was constructed:

1) Each motor was damaged by a factor of 5% by multiplying their desired velocity and maximum torque by a randomly picked gain. If the gains were low this approximated power loss due to worn motors or friction building up in joints. If the gain was high this indicated excessive power possibly due to electrical problems.

2) 5% of all network parameters: axonic weights, biases, and time constants were damaged by adding in a random error to them. This approximated damage to the nervous system during construction or exposure to radiation.

The following equations were to add damage:

$$g_v = \begin{cases} \phi(1) < p & 1.0 + (\phi() - 0.5) * 2.0 * e \\ \phi(1) \geq p & 1.0 \end{cases} \qquad (42)$$

$$g_v = \begin{cases} \phi(1) < p & 1.0 + (\phi() - 0.5) * 2.0 * e \\ \phi(1) \geq p & 1.0 \end{cases} \quad (43)$$

$$v_n = \begin{cases} \phi(1) < p & v_o + v_o * (\phi() - 0.5) * 2.0 * e \\ \phi(1) \geq p & v_o \end{cases} \quad (44)$$

where:

g_v = *A gain that is multiplied by the ODE motor's desired velocity each time step*
g_t = *A gain that is multiplied by the ODE motor's maximum torque each time step*
v_n = *The new value of a parameter such as: axon, bias, or time constant*
v_o = *Original value of a parameter such as: axon, bias, or time constant*
e = *0.05 (5% error)*
$\phi(x)$ = *A random number between 0 and* x

During each rover's evaluation the pre-computed gains and skewed parameters were applied. After evolving for 100 generations a rover was found that was resilient to damage as illustrated in Figure 42. Even after 30% of damage was applied the machine was still able to find its target 75% of the time.

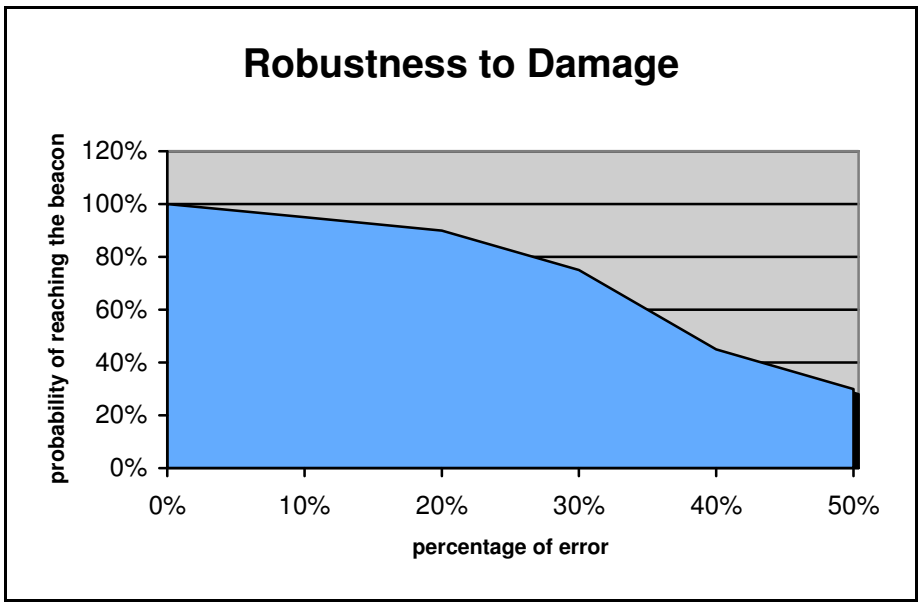

Figure 42 – A graph showing the rover's ability walk to a beacon after being damaged.

Figure 42 shows that as the damage increases from 0% to 50%, the probability that the machine will reach its target slowly degrades. Even after the machine has incurred 30% damage it can still reach the beacon 75% of the time. The probability of a machine reaching the beacon was computed by constructing the rover 20 times, counting the number of times it reaches the beacon and taking the average.

Robustness to damage of the rovers neuro-controller can be extensively leveraged when physically building them for space exploration. The nervous system could be implemented in parallel distributed hardware such as FPGAs or custom analogy circuits allowing it to absorb unforeseen damage from radiation or impact.

VII.9.2. Motor Failure

A primary concern with any mobile machine is motor failure. If such a fault occurs the machine may lose traction, the ability to turn, or both. Insects address this problem by adapting their gait and gracefully degrade in performance as additional muscles fail. Our rover having a parallel, evolved, control system is no exception. Following a similar procedure as our previous experiment the population was evolved for additional generations in which:

1) Upon construction one out of the 18 motors (there are three per leg) actuating the machine was completely disabled allowing the joint rotate freely.

2) After 100 generations an individual in the population was found that could consistently reach its target on average 75% of the time when tested over 20 trials (Figure 43). When two motors were damage the machine could still reach its target 35% of the time.

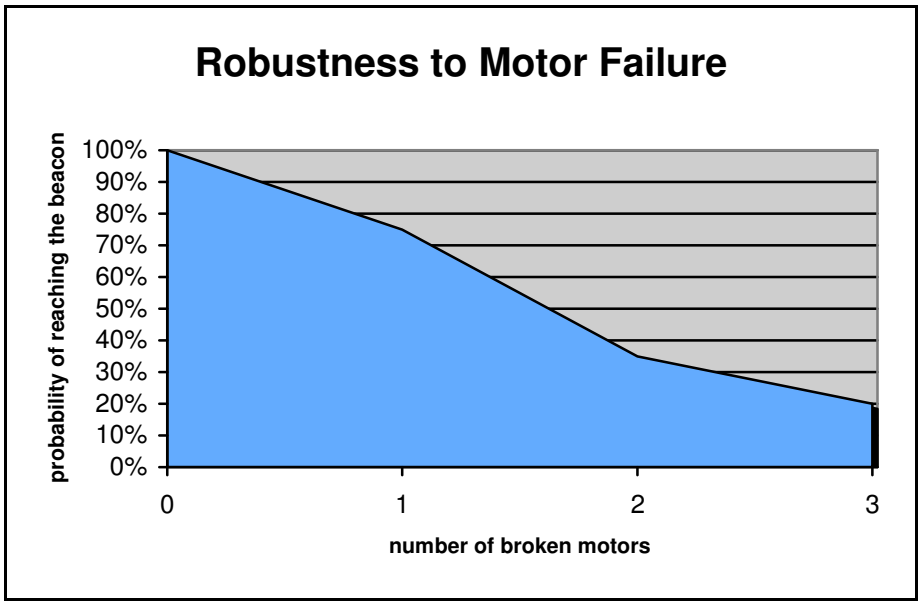

Figure 43 – Graph illustrating robustness to motor damage.

When tested in environments different from the one they were evolved in, including with different gravity, the walkers were able to operate extremely well.

These preliminary results are very encouraging and suggest that with more time it should be relatively easy to evolve extremely robust machines able to cope with a wide range of damage and failure.

10. CONTROL SYSTEM SUMMARY

This study has illustrated that artificial evolution can be successfully used to produce a robust distributed control system, based on continuous time recurrent neural networks, capable of generating efficient walking behaviours in a physically simulated hexapod rover.

The use of a careful incremental approach has resulted in walkers that successfully coordinate a number of behaviour to generate efficient navigation across rough terrain cluttered with obstacles. Previous studies have not dealt with such demanding terrain or such complex network-based control systems. Hence, as well as indicating the potential for this methodology in a more detailed walker project, this study has extended the state-of-the-art in this branch of evolutionary robotics.

A more detailed evolutionary robotics study would look at more complex actuator models and body morphologies (in particular, the legs could be more functionally specialised with different designs for each pair, as is common in the insect world). Parameters determining these aspects of the rover could also be put under evolutionary control.

Movies demonstrating a wide range of evolved walker behaviours can be found at the following urls:

Walking in different situations:

http://www.informatics.sussex.ac.uk/users/ev25/projects/mars/movies/avoid.mov
http://www.informatics.sussex.ac.uk/users/ev25/projects/mars/movies/lessenergy.mov
http://www.informatics.sussex.ac.uk/users/ev25/projects/mars/movies/craters.mov
http://www.informatics.sussex.ac.uk/users/ev25/projects/mars/movies/craters2.mov
http://www.informatics.sussex.ac.uk/users/ev25/projects/mars/movies/edge.mov
http://www.informatics.sussex.ac.uk/users/ev25/projects/mars/movies/verysmooth.mov

Tests when motors are damage:

http://www.informatics.sussex.ac.uk/users/ev25/projects/mars/movies/brokenmidkneeandhiplifter.mov
http://www.informatics.sussex.ac.uk/users/ev25/projects/mars/movies/brokenrearforwardback.mov
http://www.informatics.sussex.ac.uk/users/ev25/projects/mars/movies/brokenrearlifter.mov
http://www.informatics.sussex.ac.uk/users/ev25/projects/mars/movies/brokenrightfrontknee.mov
http://www.informatics.sussex.ac.uk/users/ev25/projects/mars/movies/brokenrightmidknee.mov
http://www.informatics.sussex.ac.uk/users/ev25/projects/mars/movies/brokenrightrearleg.mov
http://www.informatics.sussex.ac.uk/users/ev25/projects/mars/movies/brokenrightrearleg2.mov

VIII. CONCLUSIONS

It has been shown through the above design that a near-20 kg biomimetic walking vehicle for Mars exploration is a viable mission. The required hardware exists and can be incorporated into a space-ready vehicle. A further, more comprehensive investigation into the impact of thermal constraints on a more detailed rover design would be required to ensure the survivability of the vehicle on the harsh Martian environment. Table 28 below shows the complete system mass requirements of all subsystems, and shows the total mass of this viable walking Mars explorer to under 24 kg.

Additionally, a control system can be designed to learn and adapt under Mars-like conditions to traverse a vehicle across the rugged Martian terrain. However, a fully integrated control system design would need to be implemented on the final vehicle design in order to measure the benefits of vertebrate-like muscle compliance on drawbar pull, mean free path determination, and obstacle negotiation capability.

Table 28 – Complete System Mass Requirements

Item	Unit Mass	Q	Total Mass	Subsystem Mass
	(kg)		(kg)	(kg)
Instruments			**1**	**3.840**
Payload – Raman	1.00	1	1	
Payload – Enose	0.75	2	1.5	
Image/Sci Cams	0.27	2	0.54	
Nav Cams	0.30	2	0.6	
Haz Sonar	0.05	4	0.2	
Structure			**1**	**3.664**
Shell Mass	2.66352	1	2.66352	
Supp. Structure	1	1	1.000	
3DOF Leg			**6**	**8.158**
Motor	0.346	3	1.038	
Pre-Femur		1	0.032	
Femur		1	0.129	
Tibia		1	0.161	
Communications			**1**	**0.665**
LG Antenna	0.2	1	0.2	
UHF Antenna	0.2	1	0.2	
Radio Modem	0.265	1	0.265	
Onboard Computing			**1**	**1.749**
Main Board	0.849	1	0.849	
Image Board	0.3	1	0.3	
Batt. Charge Board	0.1	1	0.1	
Other Boards	0.4	1	0.4	
Wires	0.1	1	0.1	
Power			**1**	**3.663**
Batteries	1.22	2	2.44	
Solar Cells	0.00068	255	0.1734	
Cell Backboard	2500	0.00042	1.05	
Thermal			**1**	**2.148**
Batt RHUs	0.04	6	0.24	
Other RHUs	0.04	6	0.24	
Gold Foil	19320	0.0000035	0.068	
Radio Heater	0.4	1	0.4	
Batt Heaters	0.4	2	0.8	
Other Heaters	0.4	1	0.4	
TOTAL				**23.887**